Aus der Medizinischen Klinik für Endokrinologie und Stoffwechselmedizin
der Medizinischen Fakultät Charité – Universitätsmedizin Berlin

DISSERTATION

The mammalian citrate transporter $_{m}$INDY (I'm not dead yet) and its protective role in hepatic metabolism

zur Erlangung des akademischen Grades
Doctor medicinae (Dr. med.)

vorgelegt der Medizinischen Fakultät
Charité – Universitätsmedizin Berlin

von

Martin André Daniels

aus Köln

Datum der Promotion: 05.03.2021

Table of contents

1. Directory of tables and figures

Abbreviations (in alphabetical order)

ACADM	medium-chain acyl-CoA dehydrogenase
ACC2	serine-phosphorylated acetyl coenzyme A carboxylase 2
AGI	alpha-glucosidase inhibitor
ASO	antisense oligonucleotide
AUC	area under the curve
BAT	brown adipose tissue
BCA	bicinchoninic acid assay
BW	body weight
cAMP	cyclic adenosine monophosphate
cDNA	complementary deoxyribonucleic acid
CI	confidence interval
CNS	central nervous system
Cre	cre recombinase
CPT1A	carnitine palmitoyl transferase I
CREBP	cAMP responsive element binding protein
DAG	diacylglycerol
DIO	diet-induced obesity
DM	diabetes mellitus
DMEM	Dulbecco's modified Eagle's medium
DNA	deoxyribonucleic acid
DNAJB9	DnaJ heat shock protein family (Hsp40) member B9
dNTP	deoxynucleoside triphosphate
DPP-4	dipeptidyl peptidase-4
EE	energy expenditure
ELISA	enzyme-linked immunosorbent asay
ETC	electron transport chain
FFA	free fatty acid

GEE	generalized estimated equation
GIR	glucose infusion rate
GLP-1	glucagon-like peptide-1
HE-clamp	hyperinsulinemic-euglycemic clamp
HEK-293	human embryonic kidney 293 cells
HET	heterozygous
HFD	high-fat diet
HFD+S	high-fat diet plus 5% saccharose in drinking water
HGO	hepatic glucose output
HOMA-IR	homeostasis model assessment of insulin resistance
IC_{50}	concentration of inhibitor causing 50% carrier inhibition
IL6	interleukin-6
INDY	I'm not dead yet; sodium-coupled citrate transporter
$_{m}$INDY	see INDY; mammalian orthologue
$_{vc}$INDY	see INDY; prokaryotic orthologue (Vibrio cholerae)
INKO	whole-body knockout of $_{m}$INDY orthologue in mice
IPC	internal positive control
ipGTT	intraperitoneal glucose tolerance test
i.v.	intravenous
KO	knockout
LINKO	liver-specific knockout of $_{m}$INDY orthologue in mice
loxP	locus of X-over P1; recombination site for Cre recombinase
NaCT	sodium-coupled citrate transporter, see INDY
NaDC1	sodium-coupled dicarboxylate transporter 1
NaDC3	sodium-coupled dicarboxylate transporter 3
NAFLD	nonalcoholic fatty liver disease
NaS1	sodium-coupled sulfate transporter 1
NaS2	sodium-coupled sulfate transporter 2

NCD	normal chow diet
nPKC	novel protein kinase C
NRF1	nuclear respiratory factor 1
pAMPK	phospho-adenosine-monophosphate-activated protein kinase
PBS	phosphate-buffered saline
PCR	polymerase chain reaction
PKC	protein kinase C
PPARGC1A	peroxisome proliferator-activated receptor-γ coactivator 1α
qPCR	quantitative polymerase chain reaction
RCF	relative centrifugal force
RER	respiratory exchange ratio
RNA	ribonucleic acid
RT	room temperature
SD	standard deviation
SE	standard error
SGLT-2	sodium-dependent glucose transporter 2
siRNA	small inhibitory ribonucleic acid
SIRT1	sirtuin 1
SLC13A	family of sodium-coupled di- and tri-carboxylate/sulfate transporters
SREBF1	sterol regulatory element-binding transcription factor 1
TCA cycle	tricarboxylic acid cycle, Krebs cycle
TD-^{1}H-NMR	time-domain-^{1}H-nuclear magnetic resonance
T2DM	type 2 diabetes mellitus
UV	ultraviolet
UPR	unfolded protein response
WT	wildtype
XBP1	x-box binding protein 1
2-DG	2-deoxy-D-[1-^{14}C]-glucose

As with all knowledge, once you knew it, you couldn't imagine how it was that you hadn't known it before.

Margaret Atwood, The Year of the Flood

2. Abstract

a. English

The soaring global prevalence of metabolic disease including obesity, type 2 diabetes mellitus and NAFLD warrants the search for novel pharmacological targets. Across species, decreased function of the transmembrane carboxylate transporter mINDY (I'm not dead yet) confers a metabolic phenotype akin to caloric restriction, including protection against diet-induced obesity, insulin resistance, and hepatic steatosis. However, the underlying mechanism is not fully understood. Based on mINDY's high expression levels in mammalian livers, we examined to what extent liver-specific deletion of mINDY contributes to the protective phenotype observed in the whole-body mINDY knockout (INKO) model.

We were the first to establish a liver-specific conditional mINDY knockout (LINKO) mouse. We performed comprehensive metabolic phenotyping, including body composition, glucose disposal, gas exchange and insulin sensitivity over 16 weeks across three dietary regimens of differing caloric density: Normal chow diet (NCD), high-fat diet (HFD) and high-fat diet with sucrose-enriched water (HFD+S). We assessed capacity for glucose production in LINKO primary hepatocytes and screened for gene expression changes in LINKO liver samples.

When compared to WT controls, LINKO mice did not show differences in body weight and length, body composition and response to intraperitoneal glucose tolerance tests. In hyperinsulinemic-euglycemic clamps, glucose infusion rates did not differ between the groups; however, we observed suppressed glycolysis and increases in clamp glucose clearance and glycogen synthesis in HFD-fed LINKO mice, relative to WT controls. Respirometry yielded conflicting results, with LINKO mice in the HFD cohort showing slightly increased energy expenditure relative to WT controls, but the opposite effect occurring in the HFD+S-cohort. Respiratory exchange ratio was significantly elevated in HFD-fed LINKO homozygotes compared to WT controls, indicating a shift towards carbohydrate catabolism. LINKO primary hepatocytes showed increased capacity for glucose production compared to

WT controls. Lastly, LINKO livers showed increased expression of genes implicated in mitochondrial function and unfolded protein response, but no differences in genes related to lipid or glucose metabolism and inflammation.

Our data show that liver-specific deletion of mINDY improved whole body glucose clearance and energy expenditure in HFD-fed mice, but did not reduce body weight. Thus, the LINKO model did not fully replicate the phenotype seen previously in the INKO model. These data suggest that other organs than the liver also contribute to that phenotype; more studies in different organ systems are needed for a comprehensive understanding of mINDY's role in metabolism and in order to pave the way towards novel treatments of metabolic disease.

b. German

Die global steigende Prävalenz metabolischer Erkrankungen, darunter das metabolische Syndrom, Diabetes mellitus Typ 2 und die nichtalkoholische Fettleberkrankheit, vermittelt einen Bedarf nach neuen und effektiveren pharmakologischen Ansatzpunkten. In verschiedenen Tiermodellen wurde eine verringerte Funktion des Transmembran-Carboxylat-Transportproteins mINDY (Säugetierhomolog, „I'm not dead yet") mit einem der kalorischen Restriktion ähnelnden metabolischen Phänotypen assoziiert, charakterisiert durch Schutz gegen diätbedingte Fettleibigkeit, Insulinresistenz und hepatische Steatose. INDYs Substratpräferenz für Citrat sowie die hohe Expressionsdichte in murinen Hepatozyten legen nahe, dass INDY's Einfluss auf die Energiehomöostase auf einer Schlüsselrolle im Intermediärstoffwechsel beruhen könnte. Wir untersuchten daher, ob die Abwesenheit von mINDY in der Leber einen ähnlich ausgeprägten metabolischen Phänotypen wie das Ganzkörperknockoutmodell erzeugen kann.

Erstmals etablierten wir eine leberspezifische konditionelle mINDY Knockout- (LINKO-) Maus und charakterisierten umfassend deren Stoffwechsel. Wir bestimmten Körpermaße und -zusammensetzung, Glukosetoleranz, Gasaustausch sowie Insulinsensitivität über einen 16-wöchigen Zeitraum unter drei Diätinterventionen unterschiedlicher kalorischer Dichte: Normal chow diet (NCD), Hochfettdiät (HFD) und Hochfettdiät mit Sucrose-angereichertem Trinkwasser (HFD+S). Zudem bestimmten wir die Kapazität für glukagonstimulierte Glukoseproduktion in LINKO-Primärhepatozyten und führten ein Screening auf genetische Expressionsänderungen in LINKO-Leberproben durch.

LINKO-Mäuse und Wildtyp-Kontrollen unterschieden sich nicht in Körpermaßen, Körperzusammensetzung und Glukosetoleranz. Im hyperinsulinämisch-euglykämischen Clamp zeigte sich kein Unterschied in den Glukoseinfusionsraten; LINKO-Mäuse in der HFD-Kohorte wiesen aber relativ zu Wildtyp-Mäusen eine gesteigerte Glukose-Clearance und Glykogensynthese sowie eine verringerte Glykolyse auf. Respirometrisch zeigte sich ein gesteigerter Energieverbrauch in LINKO-Mäusen auf HFD, aber der gegenteilige Trend in den Mäusen der HFD+S-Kohorte. Das Gasaustauschverhältnis war in LINKO-Mäusen der HFD-Kohorte geringfügig, aber signifikant erhöht, was auf eine erhöhte Neigung zum Katabolismus von Kohlenhydraten hindeutet. LINKO-Primärhepatozyten zeigten im Vergleich mit Wildtyp-Kontrollen eine gesteigerte Kapazität zur Produktion von Glukose unter Stimulation durch Glukagon. Zuletzt wiesen LINKO-Leberproben eine gesteigerte Expression von Genen der mitochondrialen Funktion und ER-Stressantwort auf, jedoch keine Expressionsunterschiede in Genen des Fett-, sowie Glukosestoffwechsels oder der Inflammation.

Zusammenfassend zeigten sich im LINKO-Mausmodell zwar leichte metabolische Effekte, diese waren jedoch deutlich schwächer ausgeprägt als die Befunde im $_{m}$INDY-Ganzkörperknockoutmodell. Da neuere Studien durch interventionelle Methoden der leberspezifischen Inhibition von $_{m}$INDY jedoch stärkere Phänotypen erzeugen konnten, stellt der Transporter weiterhin einen vielversprechenden pharmakologischen Ansatzpunkt dar. Weitere Studien in verschiedenen Organsystemen sind notwendig, um ein besseres Verständnis der Rolle des Citrat-Transporters im Energiehaushalt zu ermöglichen und einen möglichen neuen therapeutischen Ansatz metabolischer Erkrankungen weiter zu erschließen.

3. Introduction

a. Diabetes mellitus

Diabetes mellitus (DM) is a group of metabolic disorders characterized by hyperglycemia induced by insulin resistance and/or deficiency; in type II diabetes mellitus (T2DM), insulin resistance accompanied by a relative insulin deficit is the predominant causative factor.[1] A range of potentially severe complications are associated with T2DM, including non-alcoholic steatohepatitis (NASH), angiopathy and cardiovascular disease, nephropathy, retinopathy, neuropathy and others.[2] Despite the onset of T2DM being delayed or even prevented through reduced caloric intake or increased physical activity, its global health burden is significant: In 2014, T2DM affected nearly every tenth adult (8.5%) worldwide, and DM and elevated blood glucose together caused 3.7 million deaths.[3] With a fast-growing T2DM pandemic affecting especially low- and middle-income countries, new insights into pathophysiological and protective factors of T2DM are needed in order to capacitate better strategies of prevention and clinical treatment.[1,3,4]

In the complex pathophysiology of T2DM, insulin resistance plays a central role.[1] This suppression of insulin signalling in response to physiological stimuli has been linked to disturbances of intracellular energy homeostasis. Several specific ectopic lipid species are thought to act as inhibitors of intracellular insulin signalling: Increased levels of intracellular diacylglycerol (DAG) activate novel protein kinases C (nPKC), which in turn inactivate the insulin receptor substrates 1 and 2 (IRS1/2) and thus suppress insulin signalling.[5,6] Ceramides represent another intracellular lipid species thought to impede the insulin signalling pathway. The proposed mechanism is the prevention of Akt2-activation by IRS1/2.[7]

In a context where abundancy of certain intracellular lipid species plays a central role in the pathogenesis of insulin resistance and hence T2DM, the nutritional dimension of the disease should be highlighted. In accordance with the hypotheses proposed above, lowered calorie intake leads to a catabolic metabolic state, which in turn mediates lipolysis and lipid oxidation instead of de-novo lipogenesis. Nutritional restriction and physical activity can reverse insulin resistance, but show limited effectiveness in real-world settings.[8–11]

b. Research directions for novel treatment options

With ample evidence supporting the role of lifestyle factors in the etiology of T2DM, a relevant genetic susceptibility has been suggested by family studies indicating heritability between 20% and 80% as well as a high concordance rate between monozygotic twins of about 70%.[12–15] Indeed, more recent genomic studies in large cohorts have identified a growing number of common genetic loci associated with T2DM.[16–18] However, their cumulative contribution to this risk tends to be limited to around 10%.[19,20] While striving for a comprehensive genetic understanding of a disease of T2DM's global dimensions is important, it has so far – while indeed providing new pathophysiological insights – not yielded effective treatment strategies.[21]

Pharmacological approaches to the treatment of T2DM have hence built their antidiabetic properties on intervention with key regulators of glucose metabolism and thus, energy homeostasis. While some were developed based on accidental findings (biguanides, sulfonylureas), others were designed specifically to target known physiological pathways, such as enhance insulin secretion (Glinides), curb glucose (re-) absorption (SGLT-2 inhibitors, AGIs) or promote the incretin system (GLP-1 receptor agonists, DPP-4 inhibitors).[22] Considering their varying profiles of effectiveness and unwanted drug effects as well as a growing group of genetic polymorphisms known to affect their therapeutic outcomes in the individual, research towards novel pharmacological strategies targeting energy homeostasis is still warranted.[23]

c. A new target: INDY (I'm Not Dead Yet)

Since its initial characterization in the fruit fly, the INDY gene has been subject to growing interest in metabolic research, having been associated with strong beneficial effects on the metabolic and aging phenotype in several animal models when downregulated.[24]

The INDY gene encodes a Na^+-dependent carboxylate-transporter, orthologues of which are found in prokaryotes, non-vertebrate and vertebrate eukaryotes.[25] The most notable effects of INDY's orthologues observed throughout different animal models are decreased body size, body weight and relative fat mass, as well as increased insulin sensitivity and significantly extended life span, together building a beneficial metabolic phenotype similar to that of caloric restriction.[24,26–29]

i. The SLC13 transporter family

The mammalian INDY orthologue SLC13A5 ($_m$INDY) is classified into the SLC13A family of Na^+-sulfate/carboxylate cotransporters. This family comprises five members with high structural homology that all mediate Na^+-coupled anion uptake but differ in substrate specificity and sites of expression (**Table 1**). They can be divided into two functionally distinct groups: The Na^+-dependent sulfate transporters SLC13A1 and SLC13A4 (NaS1 and NaS2 resp.) that transport mainly sulfate, selenite and thiosulfate and the Na^+-dependent carboxylate transporters SLC13A2, A3 and A5 (NaC1, NaC3 and NaCT, resp.) specific for carboxylates of different valences with functional roles as Krebs-cycle intermediates.[25] SLC13A5 is the newest-found member of the SLC13 family and the first transmembrane carrier with specificity for citrate.

Table 1: The SLC13 family of Na^+-sulfate/carboxylate cotransporters (adapted from Hediger et al., 2013).[25]

Gene name	***Protein name***	***Aliases***	***Substrates***	***Expression sites***
SLC13A1	NaS1	Na-sulfate, NaSi-1	Sulfate, selenate, thiosulfate	Kidney
SLC13A2	NaC1	SDCT1, NaDC-2, NaDC1	Succinate, citrate, α-ketoglutarate	Kidney, intestine
SLC13A3	NaC3	NaDC3, NaC3, SDCT2	Succinate, citrate, α-ketoglutarate, NALA, glutarate and its derivatives	Kidney, liver, pancreas, brain, placenta
SLC13A4	NaS2	SUT1	Sulfate, oxyanions selenium and chromium	Placenta, tonsillae, testes, heart
SLC13A5	NaC2	NaCT, INDY	Citrate, succinate, pyruvate	Liver, brain, testes

ii. Genetic architecture

Following INDY's initial characterization in *D. melanogaster*, mammalian orthologues in rat, human and mouse were identified in 2002, 2002 and 2004 respectively.[30–32] The SLC13A5 genetic sequence is highly conserved in mammals: In rodents, the gene is ~23 kb long and comprises 12 exons. The cDNA length is 3.254 bp containing an open reading frame of 1.719 bp. Human SLC13A5 is larger counting ~30 kb, but also comprises 12 exons. CDNA and open reading frame are slightly shorter than in rodents, with 3.207 and 1.707 bp respectively, accounting for a shorter gene product in humans.[30–32] Several splice variants of differing transport functionality have been described, but their physiological roles have not been studied in detail.[33,34]

iii. Protein structure

A comparison between the amino acid sequences of mouse, rat and human $_{m}$INDY showed a high level of identity: Mouse $_{m}$INDY was 86% and 74% identical with the rat and human orthologues, respectively. Taking into account conserved amino acid exchanges as well, mouse $_{m}$INDY shares 93% and 85% of its primary structure with rat and human $_{m}$INDY, respectively.[32] Examining sequence homology within the SLC13A family by comparing mouse $_{m}$INDY with NaC1, NaC3, NaS1 and NaS2 revealed much lower levels of identity: $_{m}$INDY was 50% and 44% identical with NaC1 and NaC3 respectively, and 40% and 39% identical with NaS1 and NaS2. Analysis of identity within the rat SLC13 family showed similar results. A comparison of mouse and rat $_{m}$INDY with their *Drosophila* orthologue revealed 33% and 34% identity, respectively.[30,32] All five family members, however, share a highly conserved sequence motif as well as a number of consensus phosphorylation and myristoylation sites of yet unclear functional role.[35]

The first high-resolution structural data on INDY was derived from X-ray-crystallography of the prokaryotic $_{Vc}$INDY (*Vibrio cholerae* INDY), co-crystallized with Na^+, Li^+ and citrate.[36] The transporter occurs as a homodimer, each protomer being built up of 11 transmembrane α-helices. The amino terminus lies in the cytosol, whereas the carboxy terminus points into the extracellular space (**Figure 1**).[36,37]

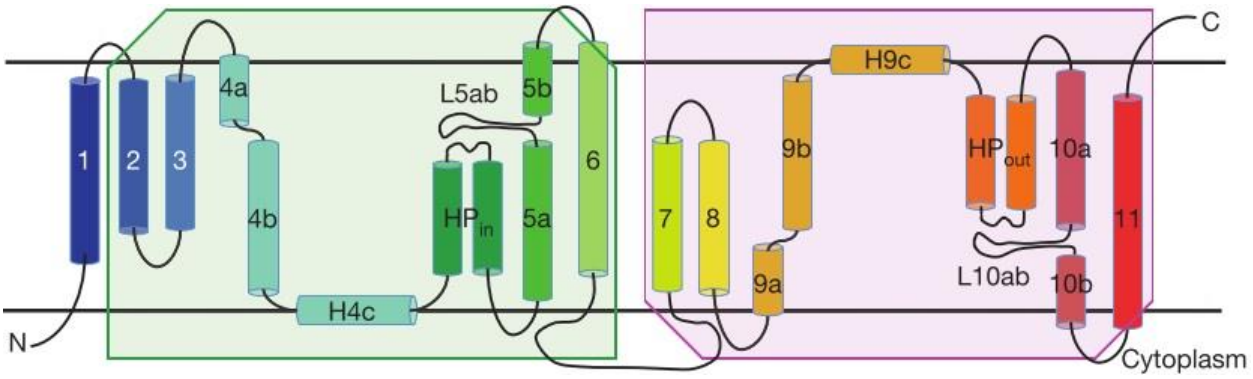

Figure 1: Transmembrane topology of $_{Vc}$INDY. The two halves of the protein, transmembrane domains 2–6 and transmembrane domains 7–11, are related by a repeat in amino acid sequence, resulting in an inverted two-fold symmetry (adapted from Mancusso et al., 2012 under Springer Nature license no. 4825450278300).[36]

Two intramembrane hairpin motifs (HP_{in} between helices 4 and 5 and HP_{out} between helices 9 and 10) have been shown to be highly conserved within the SLC13 families of several species, including *Vibrio cholerae*, fly, mouse, rat and human. They are thought to play a key role in transport mechanics (**Figure 2A**).[36] In the crystal structure, the protein shows an inward-facing conformation with citrate and Na^+ binding on the cytosolic side. The proposed Na^+ binding sites lie within the hydrophilic dimer basin. A citrate binding site with strong net positive charge lies centrally in between the two Na^+- binding sites and is framed by several amino acid residues (**Figure 2B-D**).[36] The proposed binding mechanism follows an induced-fit model, stating that binding of Na^+ in the first place alters the binding site and enables citrate to bind. Additionally, a change in secondary conformation was hypothesized, suggesting a shift between two conformational states during the transport process.[38]

A homology model of the human $_{m}$INDY orthologue was created recently using an in-silico-approach, based on the known crystal structure of $_{Vc}$INDY. Here too, two conformational states ($NaCT_{inward}$ and $NaCT_{outward}$) were modelled, suggesting changes in secondary structure during the transport process. Two helical hairpin-motifs gate the substrate-binding site on each side of the channel. Conformational changes between these central hairpin motifs and their highly conserved residues modulate affinity for citrate, enabling substrate binding and release depending on the present secondary structure confirmation.

Interestingly, the possibility for allosteric inhibition was suggested based on two residues that are located outside of the citrate binding site, but influence transport activity.[34]

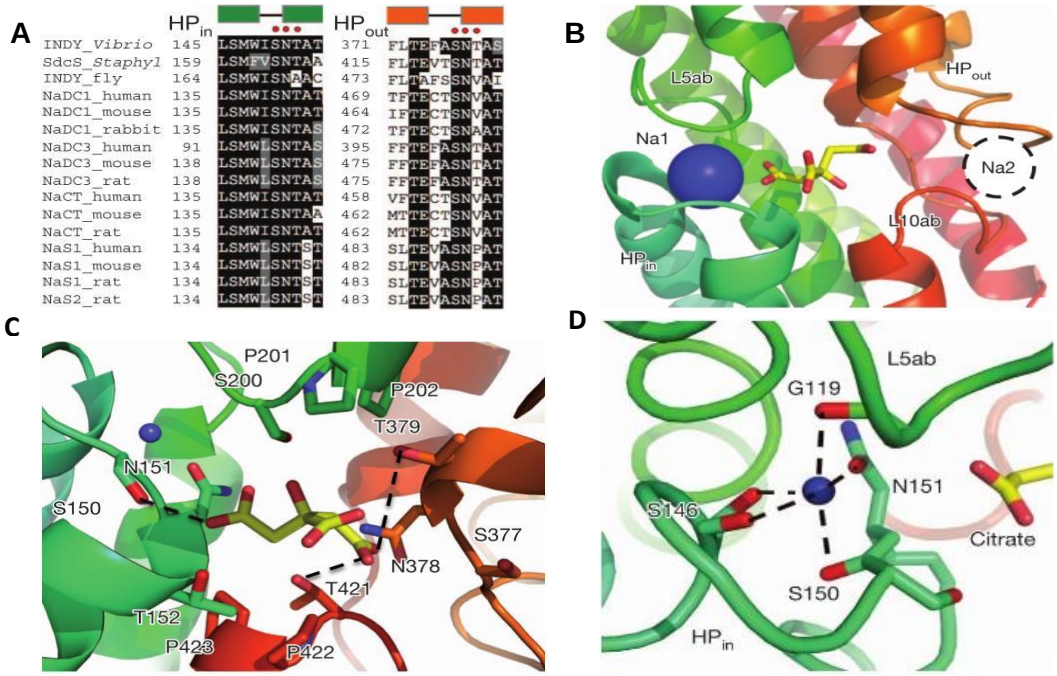

Figure 2: INDY citrate binding site. **A:** Amino acid sequence alignment of $_{Vc}$INDY and its homologues, showing the two SNT carboxylate-binding motifs. **B:** Structure of the Na1-binding site (Na1) formed by the tip of HP_{in} and the L5ab loop. A second, putative Na1-binding site (Na2), is suggested to be located between the tip of HP_{out} and the L10ab loop. **C:** Structure of the substrate-binding site with a citrate bound, showing the coordination of the substrate analogue. Hydrogen bonds are indicated by dashed lines. **D:** Coordination of the Na1 ion at the Na1 site. Both side chains of amino acid residues and backbone carboxyl oxygen atoms are involved in the Na1 coordination (adapted from Mancusso et al., 2012 under Springer Nature license no. 4825450278300).[36]

iv. Expression

$_{m}$INDY expression levels in rodents and humans are highest in the liver, where it occurs in the sinusoidal membrane of hepatocytes as shown by immune staining in human and rat livers.[31,37,39] Moderate expression levels were also detected in testes and the central nervous system: *In situ* hybridization in mouse brain showed expression of $_{m}$INDY in the cerebral cortex, hippocampus, olfactory bulb and cerebellum, where it is expressed in neurons and,

potentially, in glial cells.[25,30,40,41] Low expression levels were seen in mouse kidney, brown adipose tissue (BAT), skeletal muscle and pancreas.[27] These data are in accordance with initial findings in *D. melanogaster*, where INDY expression was highest in fat body, midgut and oenocytes, all three known to be sites of liver-like functions such as intermediary metabolism, absorption and metabolic storage.[24]

v. Substrate specificity and transport kinetics

The transport characteristics of rat, mouse and human mINDY have been studied in human retinal pigment epithelium (HRPE-) and human embryonic kidney (HEK-293) cell lines. Additionally, mouse and rat mINDY were expressed in *X. laevis* oocytes for voltage clamp studies, together portraying mINDY as a high-affinity and high-capacity transporter of cytosolic citrate into the cytoplasm.[27,30–32]

Transport function for citrate, succinate and pyruvate was evaluated in rat mINDY: Citrate uptake was, relative to the control, increased 90-fold. Succinate and pyruvate uptake were increased 7-fold and 3-fold respectively, indicating high affinity of mINDY toward citrate.[31] Mouse mINDY showed a similar trend, with citrate and succinate uptake being 20-fold and 8-fold higher than in controls.[32] Lastly, the expression of mouse mINDY in human HEK293-cells showed a similar ratio between the two substrates at physiological concentrations, and a ~8.5-fold higher uptake capacity for citrate than for succinate.[27] These results are somewhat surprising when taking into account that NaDC1 and NaDC3 both have succinate as their preferred substrate, despite their high structural homology.[42]

Competitive inhibition studies using several tri- and dicarboxylates assessed mINDY's substrate affinity: At supraphysiological concentrations, citrate and succinate competed most potently with [^{14}C] - labeled citrate for uptake into the cell, marking a 6-fold higher affinity of mINDY for citrate relative to succinate. At physiological substrate concentrations, this difference was more pronounced, with citrate being almost 50-fold more potent than succinate at competing against labeled citrate.[30] Taken together, these data show a strong substrate preference of mINDY for citrate, distinguishing it functionally from NaDC1 and NaDC3.

The citrate transport via $_m$INDY is strongly dependent on Na^+ in the pericellular fluid: When Na^+Cl^- in the uptake medium was replaced by other solutes, uptake of citrate ceased almost completely.[30] This finding supports the later-proposed transport mechanism (see **3.c.iii**), according to which the presence of Na^+ ions is a necessary condition for structural changes that allow for the binding of a substrate molecule.[36] The transport of citrate was also shown to be electrogenic, with a Na^+ : citrate stoichiometry of 4 : 1. With citrate occurring mostly in its tervalent form at a physiological pH, each transport event will bring one net positive charge into the cell.[30] Transport rates were highest at a pH between 7.0 and 7.5, which is close to physiological blood pH levels.[30,32]

vi. INDY modulates energy homeostasis

INDY's role in mammalian metabolism was investigated comprehensively in one study. A whole-body $_m$INDY knockout (INKO) mouse model was created using the Cre-loxP system in a C57Bl/6J background, and its metabolic phenotype was characterized.[27]

Firstly, body weight and body length were seen to be significantly decreased in INKO mice that were fed a normal chow diet, relative to WT controls. Additionally, INKO mice showed increased basal energy expenditure that was independent of locomotor activity, even though the latter was also increased. These findings reflect the initial findings in *D. melanogaster* in that they resembled a fasted phenotype.[24,43] INKO mice were also protected from obesity caused by high-calorie diet and aging, as shown by a strong reduction in body weight and body fat content as well as increased plasma markers for hepatic lipid oxidation relative to controls, the effect size increasing with age.[27]

Fittingly, hepatic steatosis was reduced in INKO mice on HFD as compared to wildtype controls: electron and light microscopy showed a marked decrease in density of intracellular lipid droplets. Also, triglyceride content and, more markedly, DAG content were decreased in liver tissue by 20% and 40%, respectively, with PKCε being reduced in the cytoplasmic membrane.[27] These observations go in accordance with the DAG hypothesis (see **3.a**) and may therefore cause a protection of INKO mice against insulin resistance and, subsequently, T2DM. Supportive of these molecular findings, increased insulin sensitivity and peripheral glucose uptake as well as decreased basal and clamp hepatic glucose output in INKO mice

were observed in HE-clamp experiments. With increasing age, these effects became more pronounced.[27]

The knockout of mINDY accounted for further changes in hepatocyte subcellular anatomy as well as intracellular signaling: Electron microscopy of liver cells revealed a strong increase in mitochondrial density. A hepatic gene set enrichment analysis revealed an upregulation especially in genes that are involved in mitochondrial regulation and the electron transport chain (ETC). Following analysis of key genes from this finding revealed an intracellular increase of the regulatory protein phospho-AMP-activated protein kinase (pAMPK) and its two downstream targets, peroxisome proliferator-activated receptor-γ coactivator 1α (PGPARGC1A) and serine-phosphorylated acetyl coenzyme A carboxylase 2 (ACC2). PPARGC1A accounts for the upregulation of mitochondrial biogenesis and ACC2 is normally responsible for the initiation of de-novo-lipogenesis, but is inhibited via serine-phosphorylation by p-AMPK.[27] INKO hepatocytes hence show characteristics of a catabolic metabolism despite identical feeding conditions.

vii. Regulation and pathophysiology

To date, regulatory factors for mINDY expression and activity are only partly understood. Experiments in rat primary hepatocytes have found the transporter to be regulated by glucagon signaling. In the presence of glucagon, mINDY expression and transport activity increased. A downstream effector of the glucagon receptor and PGC-1α signaling, cAMP responsive element binding protein (CREBP), was found to bind specifically to a CREBP-binding site within INDY's promoter sequence. Inactivation of CREBP abolished mINDY induction. Surprisingly, mINDY was upregulated in fasted as well as in artificially induced diabetic rats, suggesting yet unknown regulatory elements.[44]

Another putative regulatory mechanism accesses interleukin-6 (IL6) signaling: mINDY expression levels in liver probes correlated positively with whole body fat content and hepatic steatosis in a study on obese, insulin resistant patients with NAFLD. A study with rhesus monkeys supported this finding by showing an increase in mINDY expression after a two-year long HFD+S intervention. In the same study, IL6 was found to stimulate mINDY expression through the IL6-Stat3 signaling pathway in human primary hepatocytes, leading

to increased citrate uptake and hepatic lipogenesis – an effect that was abolished in the absence of mINDY.[45] The pro-inflammatory cytokine IL6 is secreted by adipose tissue macrophages as part of the low-grade inflammatory response to increased body fat content.[46] Projecting these results to the pathogenesis of obesity and consequent insulin resistance, mINDY might be one actor in a vicious cycle: Increased body fat leads to stimulation of mINDY-expression via IL6 signaling, which in turn mediates increased citrate uptake into cells, resulting in further accumulation of lipids. However, a full picture of mINDY's role in the pathophysiology of metabolic disease does not exist yet.

d. Scientific question

Research on the INKO model has shown that restricted transport of mINDY's substrates, most notably of the intermediary metabolite citrate, into cells of all tissues is associated with a protective metabolic phenotype akin to caloric restriction. In line with hypotheses linking T2DM to the intracellular abundance of energy substrates, the INKO model has therefore opened a new field of questions regarding mINDY's possible consequences for future strategies to counter T2DM and associated metabolic conditions. The liver being a central organ of mammalian intermediary metabolism as well as one of mINDY's main sites of expression, this work was conducted to answer the question to what extent suppression of mINDY in the liver alone can reproduce the INKO model's metabolic phenotype. Further, we asked whether metabolic effects of a liver-specific suppression of mINDY are especially pronounced under adipogenic stress, as seen in the INKO model. Finally, we attempted to elucidate the contradictory interplay between mINDY and hepatic glucose production, as well as liver-specific effects of our model on mRNA expression.

4. Materials and Methods

a. Mice

i. Animal Rights

We conducted all procedures of animal care and testing in accordance with institutional guidelines at Charité University School of Medicine, Berlin, as well as national (TierSchVersV 01.08.2013, BGBl. I S. 3125, 3126) and international (Directive 2010/63/EU on the protection of animals used for scientific purposes with effect from 1 January 2013) guidelines. All experimental protocols were approved by the ethics committee at Charité University School Berlin prior to their execution.

ii. Transgenic mice

To establish a liver-specific conditional knockout model using the Cre-loxP system, $_{m}$INDY-floxed C57Bl/6J mice were created as described previously,[27] and mated with transgenic mice from the same background carrying Cre-recombinase under the control of the albumin promoter (B6.Cg-Speer6-ps1Tg(Alb-cre)21Mgn/J, the Jackson Laboratory).

Mice were genotyped at the beginning of week 3. Tissue from ear punching was lysed using a proteinase K-based tissue lysis buffer. DNA was precipitated from lysates following standard protocols for isopropanol precipitation and ethanol wash. DNA yield was assessed through peak absorbance at 260nm in a NanoDrop 2000 spectrophotometer (ThermoFisher Scientific, CAT ND-2000). DNA samples were stored at -20°C.

For PCR, we used GoTaq DNA polymerase and chemicals by Promega Corp. (CAT M3001, CAT C1141, CAT A3511 and CAT P1193). DNA templates were added at <0.2 µg DNA / 25 µl reaction buffer. Standard protocols were used for PCR, with annealing temperatures of 49.5°C for $_{m}$INDY WT and floxed, and 51.7°C for Cre and IPC. Primers for PCR of the loxP-sites were 5’-GAGCTGACTGTACAGGAATC-3’ (forward) and 5’-TTACCAACCACCTCGCTAGT-3’ (reverse), with amplicon lengths of 301 bp for wildtype and 371 bp for floxed $_{m}$INDY gene.

Primers used for Cre recombinase detection were 5'-GCGGTCTGGCAGTAAAAACTATC-3' (forward) and 5'-GTCAAACAGCATTGCTGTCACTT -3' (reverse), creating a 100bp amplicon, and 5'-CTAGGCCACAGAATTGAAAGATCT-3' (forward) and 5'-

GTAGGTGGAAATTCTAGCATCATCC-3' (reverse) for internal positive control, creating a 324 bp amplicon. Gel electrophoresis was carried out in TAE-buffer using 2% and 3% (w/v) agarose gels stained with SYBR Safe (Invitrogen, CAT S33102) for loxP, and for Cre and IPC detection, respectively. Gels were loaded with 100bp DNA ladder (Invitrogen, CAT 15628019) and DNA templates from one known positive control, one known negative control and one sample of buffer without DNA template.

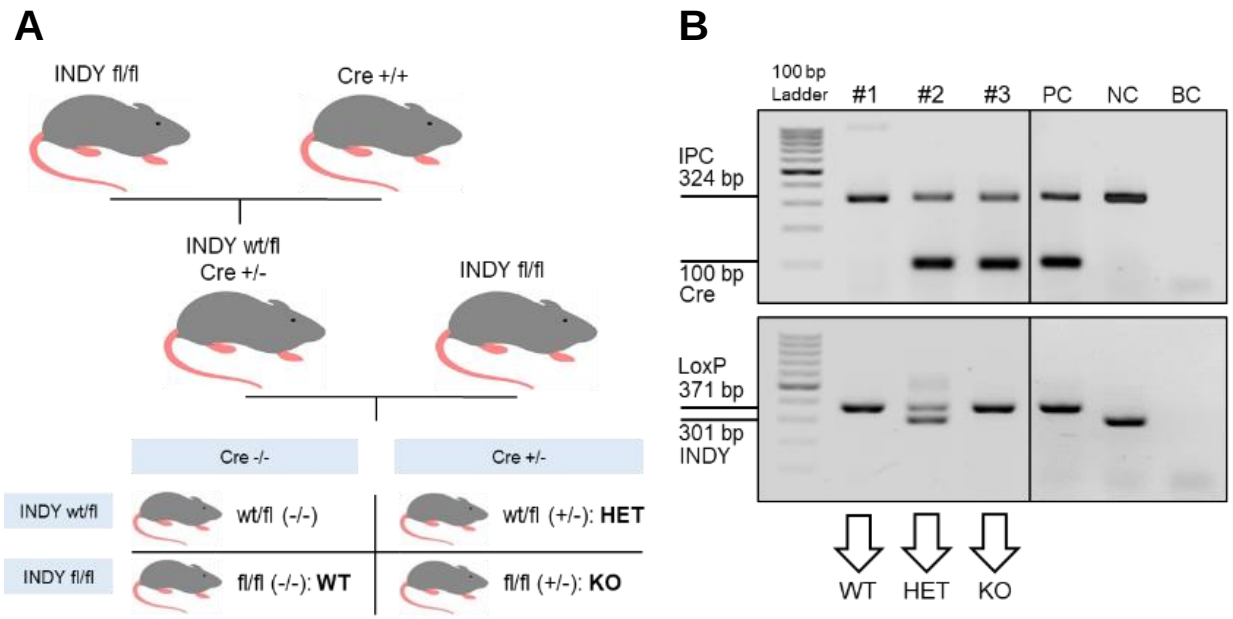

Figure 3: A: LINKO mice breeding strategy. **B:** Gel electrophoresis for Abumin-Cre and LoxP PCR gel electrophoresis (exemplary). BC: Buffer control (no DNA template). Bp: Base pairs. Cre: Albumin Cre recombinase. LoxP: $_{m}$INDY floxed. HET: $_{m}$INDY heterozygous. IPC: Internal positive control. KO: $_{m}$INDY conditional knockout. PC: Known positive control. NC: Known negative control. INDY: $_{m}$INDY non-floxed. WT: $_{m}$INDY wildtype.

iii. Housing and Diets

Mice were held on a 12-hour light/dark cycle (lights on 07:00 - 19:00). Temperature and relative humidity were controlled at 22 ± 1 °C) and 50 - 70 %, respectively. Littermates were housed together where possible in individually ventilated cages with *ad libitum* supply of food and water. Mice were identified by ear punch numbering.

After weaning, mice were fed on normal chow diet containing 15% kcal from fat, 24% kcal from protein, and 61% kcal from carbohydrates at a physiological fuel value of 3386 kcal/kg (1320M, Altromin) until they reached 28 ± 3 days of age, and then cluster-randomized into three diet groups: normal chow diet + water (NCD); high fat diet + water (HFD), or high fat diet + water with 5% saccharose w/v (HFD+S). The high fat diet contained 60% kcal from fat, 20% protein and 20% carbohydrates at a physiological fuel value of 5150 kcal/kg (E15742-30, Ssniff Spezialdiäten, Germany). For all mice receiving HFD or HFD+S, the diet intervention was introduced over 3 days through a balanced mixture of HFD and NCD pellets.

b. Metabolic phenotyping

All experiments were carried out in age-matched males. Body weight (BW) was measured weekly, starting at day 21 ± 3. At weeks 3, 9 and 15, mice underwent NMR spectroscopy to determine body composition. Functional metabolic phenotyping was initiated at week 12 by the assessment of glucose tolerance through an intraperitoneal glucose tolerance test (ipGTT). At week 14, mice underwent indirect calorimetry (IC) in respiration chambers. At week 16, insulin sensitivity was assessed using hyperinsulinemic-euglycemic clamp (HE-clamp). Mice were sacrificed immediately after the HE-clamp or, if not having undergone HE-clamp, at week 16, and organs harvested for analysis. A random subset was maintained for continued body weight and body composition measurements through week 20.

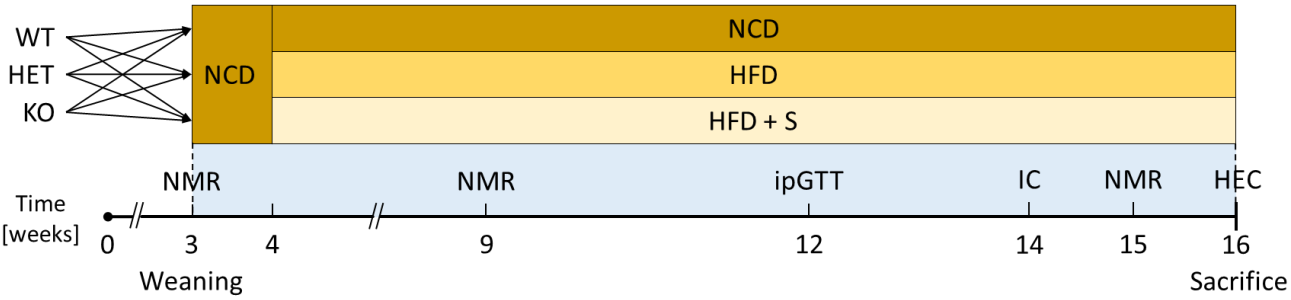

Figure 4: Metabolic phenotyping schedule. Mice were cluster-randomized into one of three diet groups of differing adipogenic stress and underwent a 16-week-long schedule of metabolic phenotyping. HEC: Hyperinsulinemic-euglycemic clamp. HET: $_{m}$INDY liver-specific conditional knockout heterozygous. HFD: High fat diet. HFD+S: High fat diet + 5% sucrose. IC: Indirect calorimetry. IpGTT: Intraperitoneal glucose tolerance test. KO: $_{m}$INDY liver-specific conditional knockout homozygous. WT: $_{m}$INDY wildtype homozygous.

i. Body weight, size and composition

Body weight was measured weekly using a benchtop scale with two decimal places accuracy. Animal size was determined as the linear distance between nose and tail root in prone position with 1 mm accuracy after mice were euthanized at week 16. Body composition was monitored using a benchtop time-domain ^{1}H-nuclear magnetic resonance (TD-^{1}H-NMR) spectrometer (MiniSpec LF50, Bruker BioSpin, Billerica, USA). The manufacturer's software was used for data collection. The spectrometer was calibrated according to the manufacturer's instructions and checked daily for proper calibration. For outlier detection, maximal mahalanobis distance was set at 0.77 for fat mass, 1.203 for free fluid mass and 0.422 for lean mass. Outliers were excluded from the analysis. To minimize metabolic strain, mice were not fasted prior to measurements. Each NMR recording was preceded by a measurement of BW.

ii. Intraperitoneal glucose tolerance test

For 16h prior to the ipGTT (18:00 to 10:00), mice were housed individually and fasted of their respective diet, with water ad libitum. Water and nesting materials were removed from the cages for the duration of the ipGTT, and the experiment was carried out in silence in a dedicated room separate from the breeding facility. BW was measured and intraperitoneal injections prepared for a final concentration of 1 g/kg, using a 10% stock solution of D-glucose (Sigma Aldrich, St Louis, MO). After mice were fixed using standard plexiglas mouse restrainers (diameter: 34mm, LabArt UG & Co. KG), blood samples of <5µL were collected from the tail vein and blood glucose was measured using a glucometer kit (Bayer Contour XT) at baseline (0 min) and at 15, 30, 60 and 120 min. For plasma insulin measurements, we collected blood samples of 30µL at each time point in heparinized capillaries (Servoprax Cat# 537-1010013), centrifuged them for 500 RCF for 5 minutes at 4°C, and analyzed them using a mouse insulin ELISA (Crystal Chem, Cat# 90080). Homeostasis model assessment of insulin resistance (HOMA-IR) was calculated from fasted baseline plasma glucose and insulin levels as described elsewhere.[47]

iii. Indirect calorimetry

We measured energy expenditure, respiratory exchange ratio and locomotion using computer-controlled, open-circuit respiration chambers (PhenoMaster / LabMaster, TSE Systems, Bad Homburg, Germany). Mice were single-housed in light- and sound-proof respiration chambers under their standard environmental and dietary conditions (see Fehler! Verweisquelle konnte nicht gefunden werden.). An acclimatization period of 48h was followed by a continuous measurement over 24h. All recordings were preceded by measuring body weights and body composition through ^{1}H-NMR. Calibrations according to the manufacturer's instructions were carried out before each cohort measurement. Data were recorded using the PhenoMaster software (TSE Systems, Bad Homburg, Germany). Locomotion was recorded by a three-dimensional array of infrared light beams, in which horizontal locomotor activity was approximated by the total amount of beam breaks in the X and Y plane. Caloric intake was approximated by continuous weight measurements of food and water consumed by the animals. Energy expenditure was measured continuously in terms of gas exchange, recorded every 5 min, calculated through abbreviated Weir formula under omission of protein metabolism, and expressed as kcal/h per cage.[48] Resting energy expenditure was approximated through the lowest EE measurement during resting period. The contribution of covariates was analyzed statistically *a posteriori* by including them in a mathematical model (see **5.e**).[49]

iv. Hyperinsulinemic-euglycemic clamp

One week prior to the HE-clamp, mice were implanted with a silicone catheter (diameter 0.012 in, wall thickness 0.006 in, Dow Corning Corporation, CAT 2415496) in the right jugular vein under deep isoflurane anesthesia. Immediately after surgery, mice were injected subcutaneously with 0.5 ml of 20% D-glucose solution and 0.5 ml isotonic NaCl solution and placed under a red light for one hour to dampen effects of energy, fluid and heat loss. Analgesia with Metamizole was given from one day before surgery until the end of the recovery period one week after surgery. Mice were fasted overnight (16h) before the HE-clamp. They were placed into plexiglas mouse restrainers (diameter: 34mm, LabArt UG & Co. KG) and shielded from their visible light spectrum using a cover of red plexiglas. The

tail tip was cut for blood sampling and covered with a sterile gauze 2h prior to the experiment.

A continuous infusion of 0.05 µCi/min [3-^{3}H]-D-glucose (PerkinElmer) over 120 min into the i. v. catheter for determination of basal glucose metabolism was followed by a priming bolus infusion of 21 mU/kg insulin and 0.72µCi/min [3-^{3}H]-D-glucose over 3 min, a continuous infusion of 3 mU/kg/min insulin (NovoNordisk), and a variable infusion of 20%-D-glucose over 140 min in order to maintain blood glucose around 120 mg/dL. To assess total glucose uptake and suppression of hepatic glucose output, these infusions were accompanied by a continuous infusion of 0.1 µCi/min [3-^{3}H]-D-glucose. To counter blood loss, artificial plasma was continuously infused at a rate of 4.2 µl/min as described elsewhere.[50] Upon reaching steady state at 85min, mice received a bolus infusion of 10 µCi 2-deoxy-D-[1-^{14}C]-glucose (2-DG) to assess insulin-mediated organ-specific glucose uptake. Blood samples were taken at 0, 30, 50, 65, 80, 100, 110, 120, 130, and 140 min.

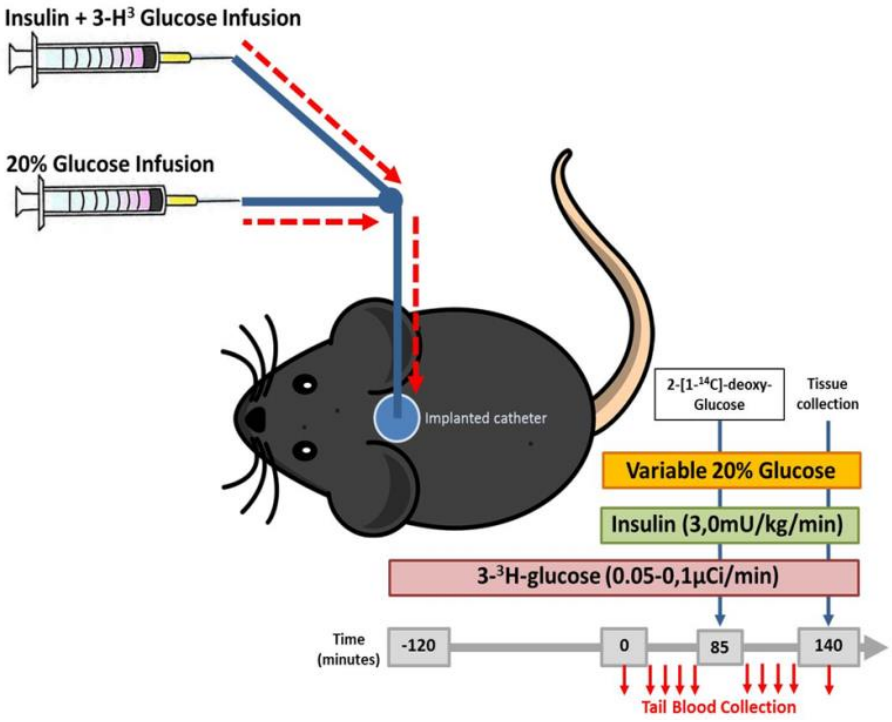

Figure 5: Schematic representation of the HE-clamp procedure

After completion of the clamp infusions, mice were sacrificed by cervical dislocation and organs (skeletal muscle, abdominal adipose tissue, brown adipose tissue, heart, liver and blood) were swiftly collected and flash-frozen in liquid nitrogen within 3 min. Plasma [^{3}H]-D-glucose was measured by dry scintillation counting of $ZnSO_4$-$Ba(OH)_2$-deproteinized serum. Blood glucose concentration was measured using a glucose oxidase analyzer (Beckman Coulter Inc.). Plasma insulin concentrations were measured using a mouse insulin ELISA Kit (Crystal Chem, Cat# 90080). Plasma free fatty acid concentrations were measured using an acyl-CoA oxidase–based colorimetric kit (Wako Chemicals USA, Inc).

c. Glucose production in LINKO primary hepatocytes

12-week-old LINKO mice on HFD were deeply anesthetized by intraperitoneal injection of Ketamin 200mg/kg (Pfizer Inc., PZN 3151811) / Xylazine 30mL/kg (Bayer AG, PZN 1320422), and absence of reflexes was confirmed. The abdomen was sterilized with 70% ethanol and incised from the suprapubic abdominal wall bilaterally extending towards the rib cage. A peripheral venous cannula (Braun GmbH, CAT 4268113B) was placed into the inferior *Vena cava*. Retrograde perfusion with 20 ml clearance buffer at 4 °C was initiated at 4 ml/min flow rate using a peristaltic pump, and the hepatic portal vein was cut open for blood drainage. Perfusion was continued with 50 ml digestion buffer at the same flow rate. Liver lobes were transferred into tissue culture and disrupted in standard medium at 4°C using cell scrapers. The resulting suspension was passed through a 70µm cell strainer (Corning CAT 352350) and remaining tissue debris was filtered out by centrifugation in a density separation gradient solution (Biochrom CAT L6145). After 3 washing steps, cells were resuspended in standard medium. Following Trypan blue staining, viable cells were counted in a hemocytometer. Cell yields with >80% viability were cultivated in standard medium in monolayers at a density of 300.000 cells / well in collagen I-coated 12-well-plates (Sigma-Aldrich, CAT C3867). Cells were maintained in a humidified atmosphere at 37°C and 5% CO2 and underwent medium changes every 48 h.

To stimulate glucose production through glucose starvation, 24- to 48-hour-old cells at ~80% confluency were washed with PBS and incubated with DMEM-O for 60 minutes. After another wash with PBS, cells were incubated for 3 h with 1 ml/well DMEM-O or one of three glucose production media, each containing different combinations of the catabolic hormone

glucagon (Sigma, CAT G2044) and gluconeogenesis substrates Na^+-glutamate (Sigma, CAT 144660) and Na^+-pyruvate (Sigma, CAT P5280).

After incubation, supernatants were aspirated, cleared of cellular debris by centrifugation, and stored at -80°C until analysis. Cells were immersed in TRIzol 500µL / well, disrupted using a cell scraper and frozen at -80 °C until protein measurement. Cell lysates were analyzed for protein content using a BCA protein assay (Pierce, CAT 23227) with a bovine serum albumin (BSA) standard and colorimetry at wavelength 562 nm. Supernatants were analyzed for glucose concentration using a glucose assay (Abcam, CAT ab65333) with a glucose standard curve and colorimetry at wavelength 570 nm. Glucose concentration was normalized to protein count per well. The experiment was carried out in biological triplicates, and cell stimulation as well as glucose and protein assay measurements were carried out in technical triplicates.

Table 2: Media and Buffers used for primary hepatocyte culture and experiments

Medium / Buffer	**Contents**
Clearance buffer	EBSS w/o $CaCl_2$ w/o $MgCl_2$ (Sigma-Aldrich, CAT E6267) + 10% EGTA 50mM (Alfa Aesar, CAT 67-42-5)
Digestion buffer	HBSS (Gibco, CAT 14025092) + Collagenase I 0.3 mg/ml (Sigma-Aldrich, CAT C5894)
Standard Medium	DMEM (Gibco, CAT 11965118) + 10% FBS (Corning, CAT 35011CV) + 1% Penicillin / Streptomycin 10000 U/mL (Gibco, CAT 15140163).
DMEM-O	DMEM w/o glucose, w/o phenol red, w/o pyruvate, w/o L-glutamine, w/o bicarbonate (Sigma, CAT 5030) + 3.7 g/L sodium bicarbonate.
GG	DMEM-O + glucagon 100nM + glutamate 10mM
GP	DMEM-O + glucagon 100nM + pyruvate 10mM
GGP	DMEM-O + glucagon 100nM + pyruvate 10mM + glutamate 10mM

d. Gene expression in LINKO liver samples

For gene expression analyses, we extracted RNA from samples using the phenol-$CHCl_3$ extraction method[51,52] and performed RealTime quantitative PCR (qPCR). Liver samples from HFD-fed LINKO mice were transferred to liquid nitrogen immediately after harvest and stored at -80°C. For tissue disruption and denaturation, 50-100 µg organ pieces were cut under liquid nitrogen, placed in tubes containing 500 µl of TRIzol reagent and 500 µg of zirconium oxide beads (MP Biomedicals, CAT 116540438), and homogenized at -20°C in a bead mill homogenizer (Analytik Jena AG, CAT AJ 845-00007-2). For RNA extraction, we followed standard protocols for phenol-$CHCl_3$ phase separation and alcohol precipitation. Samples were resuspended in nuclease-free water and measured for nucleic acid quantity and purity using peak absorbance at 260 nm wavelength and the A260/A280 ratio in a Nanodrop 2000 spectrophotometer (ThermoFisher Scientific, CAT ND-2000). For DNase digest and reverse transcription, we used established kits (Thermo Scientific, CAT EN0521 and K1622, respectively) and strictly followed the manufacturer's protocols. Samples were stored at -20°C for maximally two weeks before qPCR. For qPCR, we used Power SYBR Green PCR Master Mix (Applied Biosystems, CAT 4367659). Master mixes were prepared for every gene. Each reaction included 10 ng of cDNA template in a 96 Multiply PCR Plate (Sarstedt, CAT 72.1979.102), and was run on a standard protocol for SYBR green (denaturation: 94°C, annealing: 60°C) in a 7300 Real Time PCR System (Applied Biosystems). Reactions were measured in technical triplicates, controlled for cross-contamination by including buffer controls and normalized to two reference genes, GAPDH and HPRT.

Table 3: RealTime-qPCR primers

Gene	Sense	Antisense
GAPDH	CTCCACTCACGGCAAATTCA	ATGGGCTTCCCGTTGATGA
HPRT	CACAGGACTAGAACACCTGC	GCTGGTGAAAAGGACCTCT
ACACA	GCCATTGGTATTGGGGCTTAC	CCCGACCAAGGACTTTGTTG
ACADM	AGGGTTTAGTTTTGAGTTGACGG	CCCCGCTTTTGTCATATTCCG
ACOX	AGCTCCGATCAGCCAGACAT	TTCTTGAAACAGAGCCCAGAATG
CPT1A	TTGCACGAGGGAAAATAAGC	CCAACGTCACGAAGAACGC
CREB1	AGCAGCTCATGCAACATCATC	AGTCCTTACAGGAAGACTGAACT
DDIT3	CTGGAAGCCTGGTATGAGGAT	CAGGGTCAAGAGTAGTGAAGGT
DNAJ B9	CTCCACAGTCAGTTTTCGTCTT	GGCCTTTTTGATTTGTCGCTC
FASN	GGAGGTGGTGATAGCCGGTAT	TGGGTAATCCATAGAGCCCAG
G6PC	CAGGAGGACTACCGGACTTAC	TCAACTGAAACCAAAGTGGGAA
GCK	AGGAGGCCAGTGTAAAGATGT	CTCCCAGGTCTAAGGAGAGAAA
HSPA5	ACTTGGGGACCACCTATTCCT	ATCGCCAATCAGACGCTCC
IL1B	GCAACTGTTCCTGAACTCAACT	ATCTTTTGGGGTCCGTCAACT
IL6	TAGTCCTTCCTACCCCAATTTCC	TTGGTCCTTAGCCACTCCTTC
NRF1	GACAAGATCATCAACCTGCCTGTAG	GCTCACTTCCTCCGGTCCTTTG
PC	CTGAAGTTCCAAACAGTTCGAGG	CGCACGAAACACTCGGATG
PCK1	AGCATTCAACGCCAGGTTC	CGAGTCTGTCAGTTCAATACCAA
PPARA	AACATCGAGTGTCGAATATGTGG	CCGAATAGTTCGCCGAAAGAA
PPARG	GGAAGACCACTCGCATTCCTT	GTAATCAGCAACCATTGGGTCA
PPARGC1A	GAAAGGGCCAAACAGAGAGA	ACTGCCTATGAGCACTTCAC
SAA3	AGAGAGGCTGTTCAGAAGTTCA	AGCAGGTCGGAAGTGGTTG
SIRT1	GCTGACGACTTCGACGACG	TCGGTCAACAGGAGGTTGTCT
SLC13A3	GGAAGGCCGATGCCTCTATG	GGAAGTTGGTGTCGAGGAAGT
SLC13A5	GGCACCACACTTCTACAATG	GGGGTGTTGAAGGTCTCAAAC
SLC25A20	GACGAGCCGAAACCCATCAG	AGTCGGACCTTGACCGTGT
SREBF1	GATGTGCGAACTGGACACAG	CATAGGGGGCGTCAAACAG
TFAM	ATTCCGAAGTGTTTTTCCAGCA	TCTGAAAGTTTTGCATCTGGGT
TNF	GGTGCCTATGTCTCAGCCTCTT	GCCATAGAACTGATGAGAGGGAG
XBP1	AGCAGCAAGTGGTGGATTTG	GAGTTTTCTCCCGTAAAAGCTGA

e. Statistics

Data were collected and pooled in Microsoft Office Excel 2013 (Microsoft Corp., USA). Statistical analyses and graphing were carried out using SPSS Statistics Version 25 (IBM Corp., USA). Unless otherwise indicated, individual data points were pooled by genotype. Missing data points were excluded from the analysis. Error bars indicate one standard deviation. Outliers are displayed as circles and were not excluded from the analysis.

Parametric assumptions: Normality of residuals was tested by calculating a univariate linear regression with genotype as independent variable, plotting the regression standardized residuals in a probability-probability-plot, and assessing the distribution around the interpolation line. Mean, median, standard deviation, skewness and kurtosis were also assessed for every dataset. Homoscedasticity was assessed using a scatterplot of standardized residuals against standardized predicted values, and Levene statistic.

Analysis of variance: Where appropriate, statistical significance of variance between groups was assessed using single-factor analysis of variance (ANOVA) with correction for multiple testing using the Holm-Sidak method. Where assumptions of normality or homoscedasticity were violated, Kruskal-Wallis-test or Welch statistic were used, respectively. In all longitudinal datasets (i.e., BW, BC, EE and RER during indirect calorimetry, glucose and insulin excursions during ipGTT, blood glucose concentration and glucose infusion rate during HE-clamp), generalized estimated equations (GEEs) were fitted to the unweighted data. Logarithmic or linear link functions were used, respectively, depending on whether the data violated assumptions of normality and homoscedasticity or not. Model effects were analyzed using Type III Wald χ^2 statistics. For hypothesis tests regarding the independent variable and covariates, type I Wald χ^2 statistic was used. Goodness of fit was evaluated according to the log quasi-likelihood function, and the best fit selected for analysis. IpGTT results were also analyzed by calculating the area under the curve (AUC) under the assumption of a 1-compartment model, using the log-linear trapezoidal method for glucose, and the linear trapezoidal method for insulin curves.[49] For all variance analyses, significance was set at $\alpha = 0.05$.

5. Results

a. Metabolic phenotyping

i. Body weight and size

Over 20 weeks, no differences in body weight could be seen between LINKO homozygotes and WT controls in all diet groups, using a GEE model with linear link function. However, LINKO heterozygotes showed a slight, but statistically significant attenuation of DIO in the HFD group. In the HFD+S group, this was contradicted by a near significant, more pronounced DIO phenotype (**Figure 6A-C, Table 4**). Of note, both the HFD and the HFD+S intervention induced DIO, but the HFD was more effective than the HFD+S (**Figure 6D, Table 4**). A body length measurement at week 16 yielded no difference between the genotypes using one-way ANOVA and Holm-Sidak correction. (**Figure 6E)**.

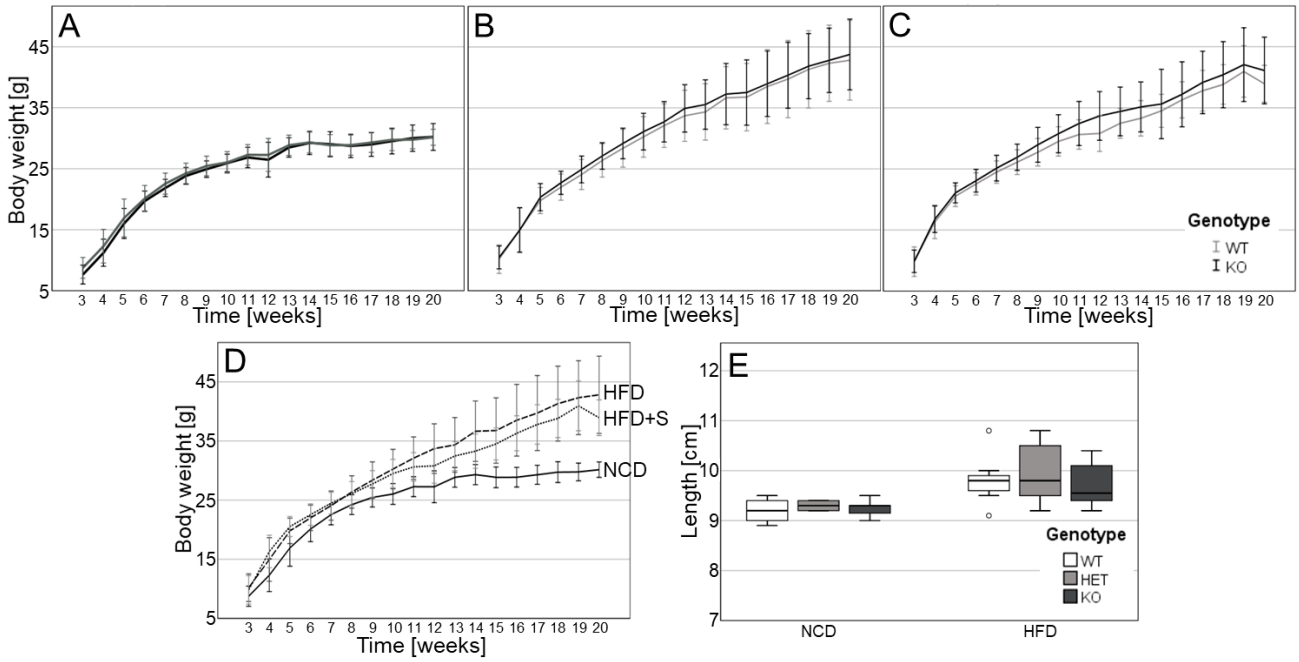

Figure 6: Body weight over time under different levels of adipogenic diet. **A:** NCD. **B:** HFD. **C:** HFD+S. WT: n = 7-8, 15-29, and 8-14; KO: n = 14-15 ,14-23, and 11-15 for NCD, HFD, and HFD+S, respectively. **D:** Comparison of body weights between diets in WT mice. **E:** Body length from nose to tail root at week 16. WT: n = 4 and 11, KO: n = 8 and 10 for NCD and HFD, respectively.

Table 4: Body weight over time: GEE parameter estimates. Linear link function. WT is expressed through the intercept, KO and HET are expressed as deviations from the intercept. This applies to all following GEE models. B: parameter vector. SE: Standard error. CI: Confidence interval. Df: Degrees of freedom.

				95% Wald CI		Hypothesis Test		
	Parameter	**B**	**SE**	**Lower Bound**	**Upper Bound**	**Wald χ^2**	**df**	**P**
NCD	Intercept	3.206	0.0201	3.167	3.246	25472.375	1	0.000
	KO	-0.014	0.0265	-0.066	0.038	0.273	1	0.601
	HET	-0.015	0.0348	-0.084	0.053	0.198	1	0.656
	Scale	0.077						
HFD	Intercept	3.451	0.0274	3.397	3.505	15825.067	1	0.000
	KO	0.008	0.0388	-0.068	0.084	0.040	1	0.841
	HET	-0.114	0.0440	-0.200	-0.028	6.688	1	**0.010**
	Scale	0.096						
HFD+S	Intercept	3.370	0.0209	3.329	3.411	25994.392	1	0.000
	KO	0.046	0.0331	-0.019	0.111	1.910	1	0.167
	HET	0.064	0.0361	-0.007	0.135	3.120	1	0.077
	Scale	0.090						

ii. Body composition

All mice developed an increasing fat proportion and a decreasing lean mass proportion over time, with stable free fluid percentage. We observed no differences over time in compartment shifts between the genotypes, using GEEs with logarithmic link functions (**Figure 7**, **Table 5**). Of note, the HFD+S intervention did not create a stronger compositional shift towards the body fat compartment than HFD alone. Therefore, the measurement during week 20 was not carried out in that group.

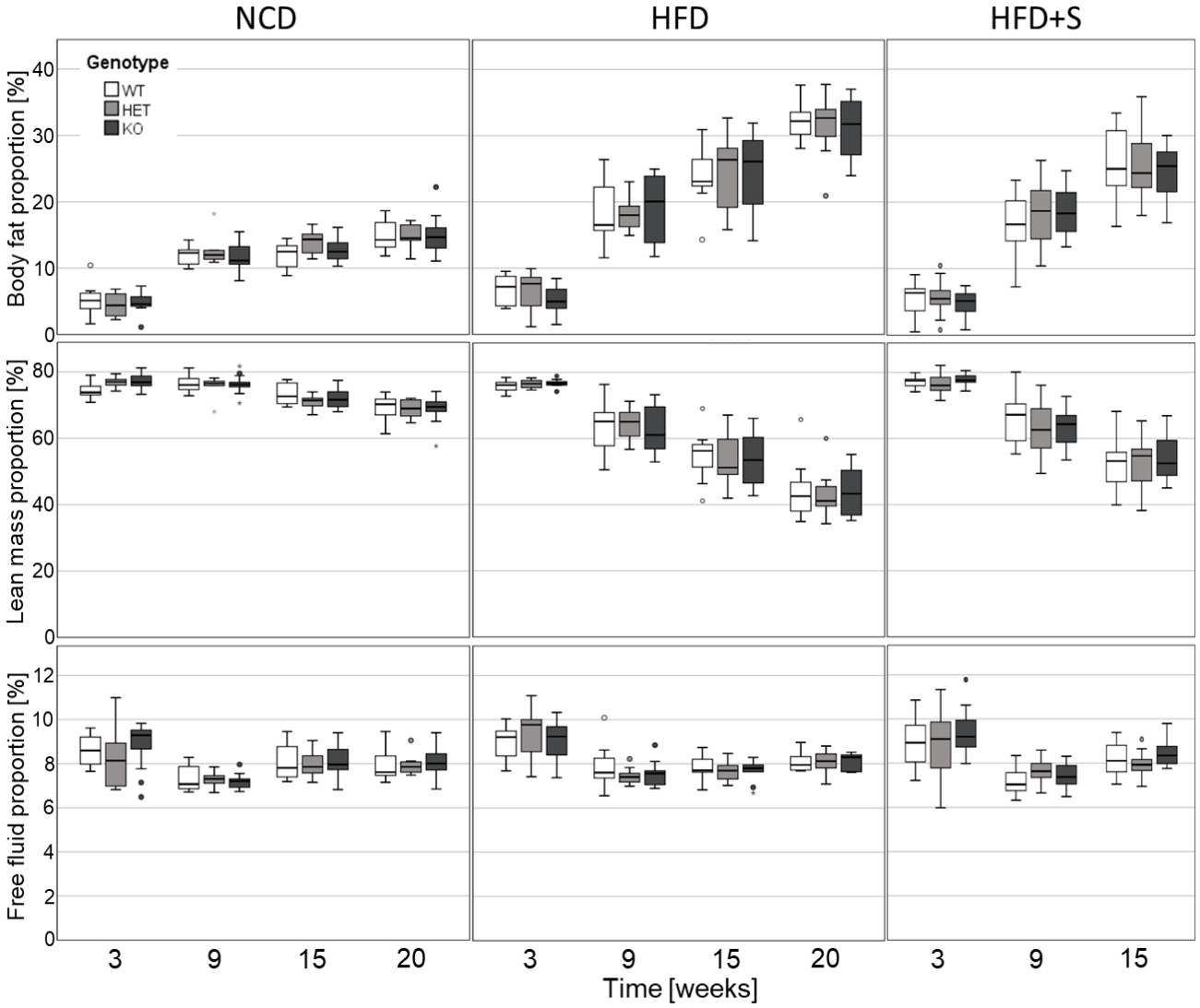

Figure 7: Body composition over time. WT: n = 7-8, 11-13, and 17-21; HET: n = 6-7, 9-14, and 13-17; KO: n = 12-15 ,10-14, and 10-15 for NCD, HFD, and HFD+S, respectively.

Table 5: Body composition over time: GEE parameter estimates. Logarithmic link function.

					95% Wald CI		Hypothesis Test		
Component	**Diet**	**Parameter**	**B**	**Std. Error**	**Lower**	**Upper**	**Wald χ^2**	**df**	**P**
Lean mass	**NCD**	Intercept	4.294	0.0094	4.275	4.312	207427.974	1	0.000
		KO	0.007	0.0108	-0.014	0.028	0.418	1	0.518
		HET	-0.004	0.0111	-0.026	0.017	0.154	1	0.695
		Scale	0.003						
	HFD	Intercept	4.101	0.0255	4.051	4.150	25929.647	1	0.000
		KO	-0.001	0.0395	-0.078	0.076	0.001	1	0.980
		HET	0.023	0.0369	-0.049	0.096	0.404	1	0.525
		Scale	0.049						
	HFD+S	Intercept	4.187	0.0185	4.150	4.223	51316.949	1	0.000
		KO	0.001	0.0254	-0.049	0.050	0.001	1	0.980
		HET	-0.016	0.0274	-0.070	0.037	0.362	1	0.548
		Scale	0.030						
Fat mass	**NCD**	Intercept	2.413	0.0490	2.317	2.509	2428.993	1	0.000
		KO	0.047	0.0618	-0.074	0.168	0.578	1	0.447
		HET	0.101	0.0635	-0.023	0.226	2.536	1	0.111
		Scale	0.125						
	HFD	Intercept	2.984	0.0403	2.905	3.063	5475.738	1	0.000
		KO	-0.021	0.0750	-0.168	0.126	0.079	1	0.779
		HET	-0.064	0.0781	-0.217	0.089	0.670	1	0.413
		Scale	0.279						
	HFD+S	Intercept	2.739	0.0548	2.631	2.846	2495.589	1	0.000
		KO	0.042	0.0765	-0.108	0.192	0.303	1	0.582
		HET	0.037	0.0751	-0.110	0.184	0.247	1	0.619
		Scale	0.314						
Free fluid	**NCD**	Intercept	2.081	0.0227	2.037	2.126	8393.304	1	0.000
		KO	0.003	0.0256	-0.047	0.053	0.016	1	0.899
		HET	-0.015	0.0308	-0.075	0.046	0.232	1	0.630
		Scale	0.013						
	HFD	Intercept	2.113	0.0248	2.065	2.162	7249.276	1	0.000
		KO	-0.023	0.0286	-0.079	0.033	0.655	1	0.418
		HET	-0.010	0.0276	-0.064	0.044	0.128	1	0.721
		Scale	0.016						
	HFD+S	Intercept	2.090	0.0149	2.061	2.119	19559.957	1	0.000
		KO	0.040	0.0239	-0.007	0.087	2.777	1	0.096
		HET	0.009	0.0215	-0.033	0.051	0.184	1	0.668
		Scale	0.018						

iii. Intraperitoneal glucose tolerance test

In ipGTTs, LINKO mice showed no differing blood glucose and plasma insulin excursions relative to WT controls, using GEE models with logarithmic link functions including baseline glucose and baseline insulin concentration as covariates (**Figure 8A-B, Table 6**), as well as using baseline-adjusted AUC (**Figure 8C-D**, statistics not shown). Insulin resistance as approximated by HOMA-IR similarly did not differ between the groups using one-way ANOVA and Holm-Sidak correction (**Figure 8E, Table 7**).

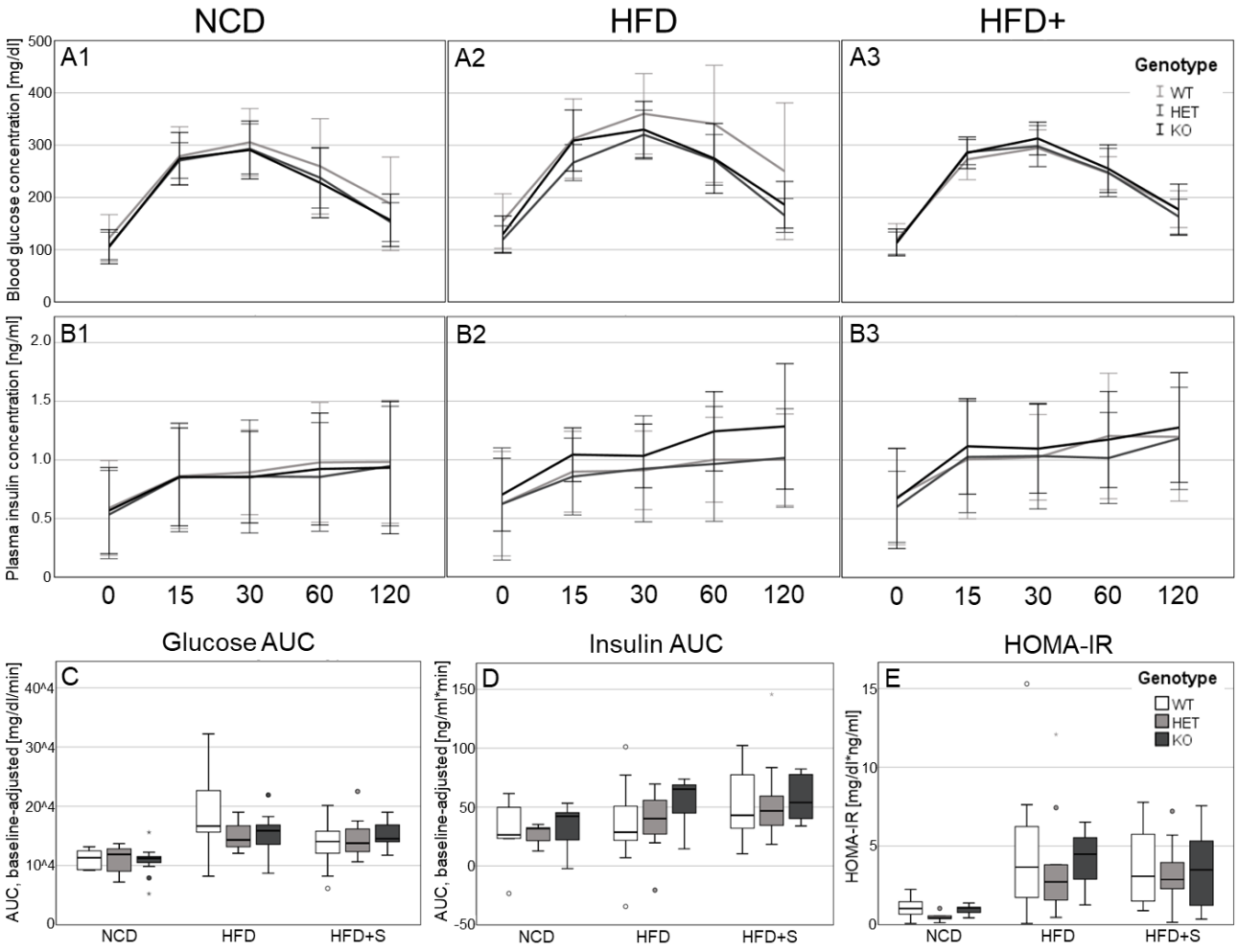

Figure 8: IpGTT: Glucose and insulin response. **A1-3:** Absolute blood glucose concentration in NCD, HFD and HFD+S. **B1-3:** Absolute plasma insulin concentrations in NCD, HFD and HFD+S. **C and D:** Baseline-adjusted AUC for blood glucose and plasma insulin, respectively. **E:** HOMA-IR in NCD, HFD and HFD+S. WT: n = 8, 13, and 21; HET: n = 7, 10, and 19; KO: n = 15, 12, and 15 for NCD, HFD, and HFD+S, respectively.

Table 6: IpGTT: GEE parameter estimates for plasma glucose and insulin response. Logarithmic link function. Glc: Blood glucose level. Ins: Plasma insulin level.

					95% Wald CI		Hypothesis Test		
Parameter	**Diet**	**Parameter**	**B**	**SE**	**Lower**	**Upper**	**Wald χ^2**	**df**	**P**
Glucose	**NCD**	Intercept	5.094	0.1862	4.730	5.459	748.678	1	0.000
		KO	-0.016	0.0316	-0.078	0.046	0.254	1	0.614
		HET	-0.029	0.0341	-0.095	0.038	0.700	1	0.403
		Glc-Baseline [mg/dl]	0.000	0.0024	-0.004	0.005	0.023	1	0.879
		Scale	0.175						
	HFD	Intercept	4.815	0.0834	4.651	4.978	3331.467	1	0.000
		KO	0.009	0.0413	-0.072	0.090	0.043	1	0.835
		HET	-0.005	0.0415	-0.086	0.076	0.014	1	0.907
		Glc-Baseline [mg/dl]	0.005	0.0004	0.004	0.006	135.880	1	0.000
		Scale	0.116						
	HFD+S	Intercept	4.971	0.0483	4.876	5.065	10604.372	1	0.000
		KO	0.044	0.0229	-0.001	0.089	3.714	1	0.054
		HET	0.020	0.0253	-0.029	0.070	0.641	1	0.423
		Glc-Baseline [mg/dl]	0.004	0.0004	0.003	0.004	71.905	1	0.000
		Scale	0.117						
Insulin	**NCD**	Intercept	-1.011	0.1436	-1.292	-0.729	49.548	1	0.000
		KO	0.031	0.1153	-0.195	0.256	0.070	1	0.791
		HET	-0.238	0.1635	-0.559	0.082	2.123	1	0.145
		Ins-Baseline [ng/ml]	1.217	0.4131	0.407	2.027	8.678	1	0.003
		Scale	0.200						
	HFD	Intercept	-0.637	0.0947	-0.823	-0.451	45.214	1	0.000
		KO	0.141	0.0803	-0.016	0.299	3.105	1	0.078
		HET	-0.032	0.0846	-0.198	0.134	0.142	1	0.706
		Ins-Baseline [ng/ml]	0.751	0.0978	0.559	0.943	58.984	1	0.000
		Scale	0.106						
	HFD+S	Intercept	-0.742	0.1050	-0.947	-0.536	49.855	1	0.000
		KO	0.073	0.0720	-0.068	0.215	1.038	1	0.308
		HET	0.054	0.0839	-0.111	0.218	0.412	1	0.521
		Ins-Baseline [ng/ml]	1.005	0.0898	0.829	1.181	125.181	1	0.000
		Scale	0.123						

Table 7: IpGTT: Statistics of fasted HOMA-IR. Baseline-adjusted AUC, one-way ANOVA or Kruskal-Wallis Test (KW), and Holm-Sidak correction.

					95% CI		ANOVA	
Diet	**Genotype**	**N**	**Mean**	**SD**	**Lower Bound**	**Upper Bound**	**F**	**P**
NCD	WT	7	1.085	0.745	0.395	1.774	2.032	0.162
	HET	5	0.503	0.335	0.086	0.919		
	KO	8	0.960	0.299	0.710	1.210		
HFD	WT	10	4.677	4.399	1.53	7.824	0.157	0.627
	HET	9	3.728	3.74	0.853	6.603		KW
	KO	7	4.153	2.145	2.169	6.137		
HFD+S	WT	16	3.645	2.385	1.977	5.178	0.293	0.866
	HET	16	3.085	1.794	2.129	4.041		KW
	KO	12	3.578	2.518	2.374	4.916		

iv. Indirect calorimetry

Using one-way ANOVA and Holm-Sidak correction, no significant differences between genotypes were seen in the covariates lean mass, fat mass, locomotion and resting energy expenditure, which were included into GEE models with linear link functions (**Figure 9**, **Table 8**).

We observed no differences in EE or RER in the NCD group. Within the HFD cohort, RER as well as EE tended to be higher in LINKO mice relative to WT, the difference being more pronounced during the lights-off period. In the HFD+S cohort, this observation was juxtaposed by a lowered EE but higher RER in LINKO mice relative to WT (**Figure 10, Table 9, Table 10**).

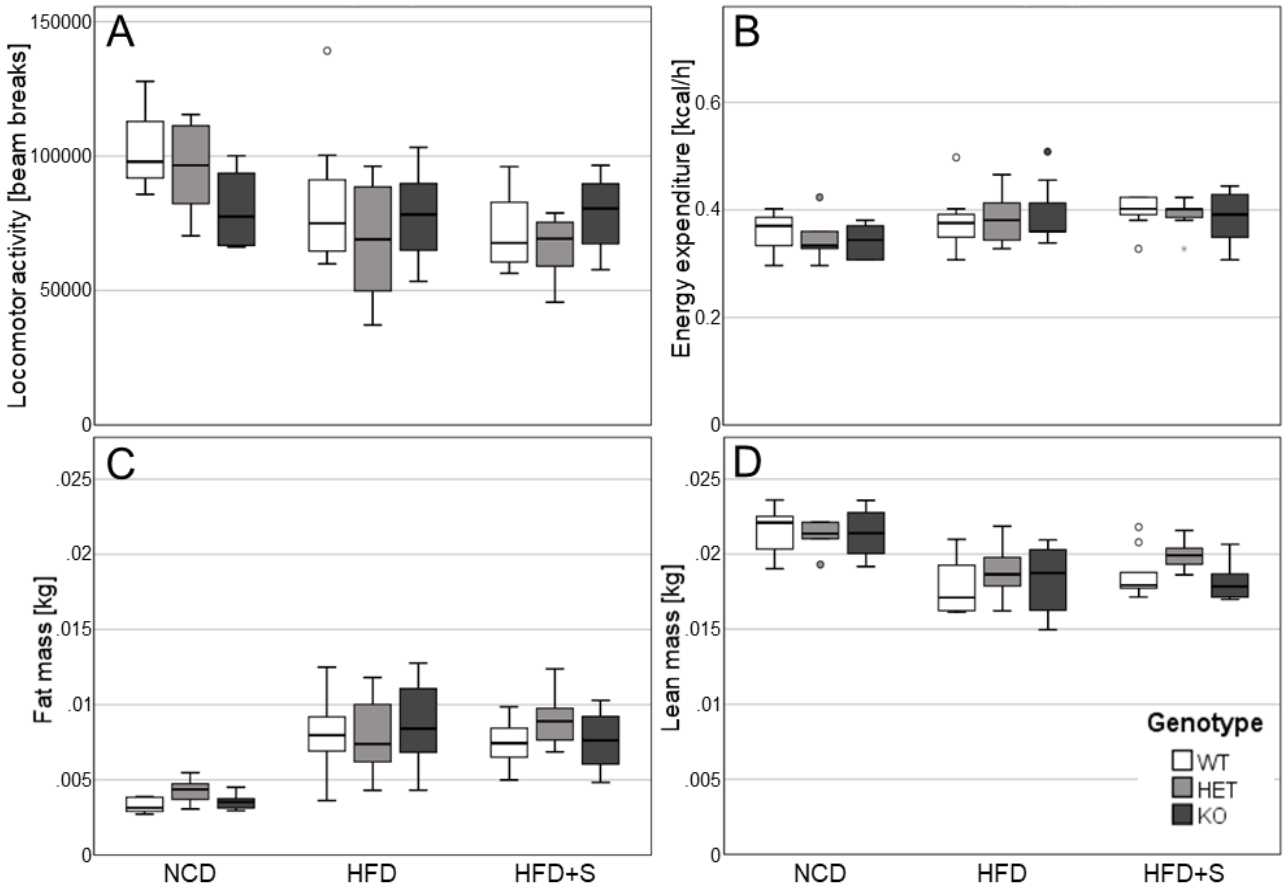

Figure 9: Indirect calorimetry: Covariates. **A:** Locomotor activity (total number of beam breaks). **B:** Resting energy expenditure. **C:** Fat mass. **D:** Lean mass. WT: n = 8, 13, and 21; HET: n = 7, 10, and 19; KO: n = 15, 12, and 15 for NCD, HFD, and HFD+S, respectively.

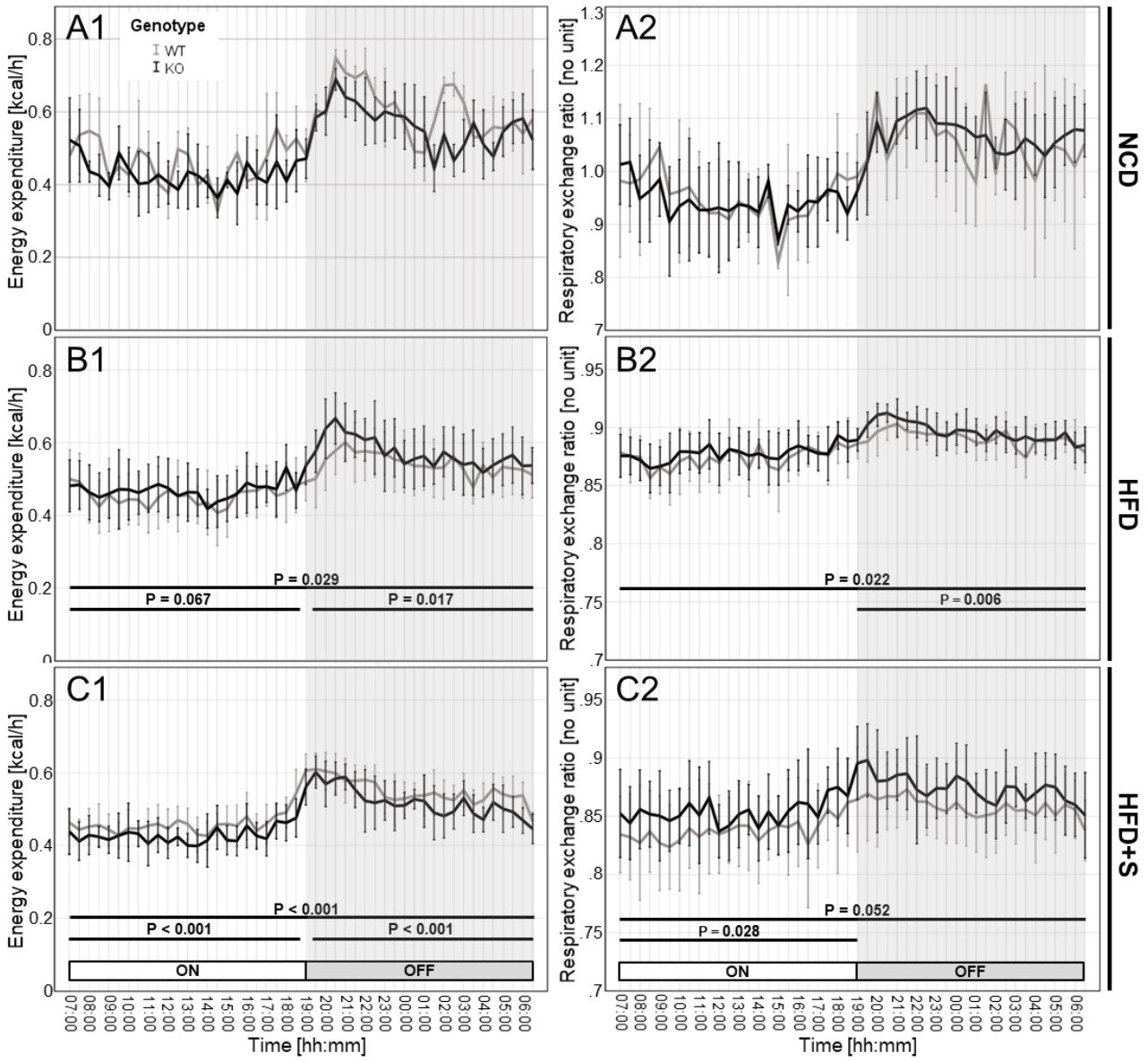

Figure 10: Indirect calorimetry: RER and EE over time. **A1** and **A2**: EE and RER in NCD, respectively. **B1** and **B2:** EE and RER in HFD, respectively. **C1** and **C2:** EE and RER in HFD+S, respectively. WT: n = 8, 13, and 21; HET: n = 7, 10, and 19; KO: n = 15, 12, and 15 for NCD, HFD, and HFD+S, respectively.

Table 8: Indirect calorimetry: Statistics for covariates. One-way ANOVA or Kruskal-Wallis Test (KW) and Holm-Sidak correction. Lean: Lean body mass. Fat: Fat body mass. REE: Resting energy expenditure. XTYT24: Locomotor activity over 24h.

Diet	Measure	Genotype	N	Mean	SD	95% CI		ANOVA	
						Lower	Upper	F	P
NCD	**LEAN [kg]**	KO	8	0.0214	0.0016	0.0201	0.0227	0.108	0.898
		HET	6	0.0212	0.0010	0.0201	0.0223		
		WT	6	0.0216	0.0017	0.0199	0.0234		
	FAT [kg]	KO	8	0.0035	0.0005	0.0031	0.0040	4.427	0.028
		HET	6	0.0043	0.0008	0.0034	0.0052		
		WT	6	0.0033	0.0005	0.0028	0.0038		
	REE [kcal/h]	KO	6	0.3423	0.0325	0.3082	0.3764	0.117	0.890
		HET	6	0.3460	0.0431	0.3007	0.3912		
		WT	3	0.3563	0.0540	0.2222	0.4905		
	XTYT24 [counts]	KO	6	80312.0	13950.1	65672.3	94951.7	2.253	0.148
		HET	6	95445.8	17648.9	76924.4	113967.3		
		WT	3	103881.7	21635.3	50136.7	157626.7		
HFD	**LEAN [kg]**	KO	10	0.0183	0.0023	0.0167	0.0200	0.681	0.515
		HET	8	0.0188	0.0017	0.0174	0.0203		
		WT	10	0.0178	0.0017	0.0165	0.0190		
	FAT [kg]	KO	10	0.0087	0.0027	0.0068	0.0106	0.255	0.777
		HET	8	0.0079	0.0026	0.0058	0.0101		
		WT	10	0.0080	0.0024	0.0063	0.0097		
	REE [kcal/h]	KO	10	0.3905	0.0546	0.3515	0.4296	0.176	0.935 KW
		HET	8	0.3836	0.0477	0.3437	0.4235		
		WT	10	0.3767	0.0524	0.3392	0.4142		
	XTYT24 [counts]	KO	10	77364.0	16252.7	65737.5	88990.5	0.823	0.534 KW
		HET	8	68558.3	22036.1	50135.6	86980.9		
		WT	10	81164.8	24202.7	63851.3	98478.3		
HFD+S	**LEAN [kg]**	KO	8	0.0181	0.0012	0.0171	0.0192	3.644	0.837 KW
		HET	7	0.0199	0.0010	0.0190	0.0208		
		WT	9	0.0186	0.0016	0.0174	0.0199		
	FAT [kg]	KO	8	0.0076	0.0020	0.0060	0.0093	1.772	0.194
		HET	7	0.0090	0.0019	0.0072	0.0107		
		WT	9	0.0074	0.0014	0.0063	0.0085		
	REE [kcal/h]	KO	8	0.3650	0.0416	0.3302	0.3997	5.089	0.214
		HET	7	0.4172	0.0229	0.3960	0.4384		
		WT	9	0.3937	0.0275	0.3726	0.4148		
	XTYT24 [counts]	KO	8	78703.8	13627.0	67311.3	90096.2	1.487	0.249
		HET	7	66111.6	12941.6	54142.6	78080.6		
		WT	9	73594.0	15409.9	61748.9	85439.1		

Table 9: Indirect calorimetry: GEE parameter estimates for RER. Linear link function.

					95% Wald CI		Hypothesis Test		
Interval	**Diet**	**Parameter**	**B**	**SE**	**Lower**	**Upper**	**Wald χ^2**	**df**	**P**
24h	**NCD**	Intercept	1.275	0.1253	1.029	1.520	103.546	1	0.000
		KO	-0.031	0.0231	-0.076	0.014	1.821	1	0.177
		HET	-0.015	0.0248	-0.064	0.033	0.388	1	0.534
		LEAN [kg]	-10.158	7.0977	-24.069	3.753	2.048	1	0.152
		FAT [kg]	41.676	12.9878	16.221	67.132	10.297	1	0.001
		REE [kcal/h]	-0.640	0.3069	-1.242	-0.038	4.346	1	0.037
		XTYT24 [Cnts]	1.483E-08	6.0047E-07	-1.162E-06	1.192E-06	0.001	1	0.980
		Scale	0.008						
	HFD	Intercept	0.780	0.0082	0.764	0.796	9152.807	1	0.000
		KO	0.003	0.0013	0.000	0.006	5.266	1	0.022
		HET	0.000	0.0016	-0.003	0.003	0.035	1	0.852
		LEAN [kg]	1.296	0.5825	0.154	2.438	4.951	1	0.026
		FAT [kg]	2.073	0.4169	1.256	2.890	24.726	1	0.000
		REE [kcal/h]	0.137	0.0189	0.100	0.174	52.420	1	0.000
		XTYT24 [Cnts]	6.031E-06	3.6775E-07	5.310E-06	6.752E-06	268.967	1	0.000
		Scale	0.000						
	HFD+S	Intercept	0.440	0.0569	0.329	0.552	59.750	1	0.000
		KO	0.022	0.0114	0.000	0.045	3.780	1	0.052
		HET	-0.010	0.0116	-0.033	0.012	0.798	1	0.372
		LEAN [kg]	15.975	3.8638	8.402	23.548	17.095	1	0.000
		FAT [kg]	7.282	3.2764	0.860	13.703	4.940	1	0.026
		REE [kcal/h]	0.120	0.1534	-0.180	0.421	0.617	1	0.432
		XTYT24 [Cnts]	9.372E-06	9.8817E-07	7.435E-06	1.131E-05	89.950	1	0.000
		Scale	0.001						
ON	**NCD**	Intercept	1.279	0.1605	0.964	1.593	63.519	1	0.000
		KO	-0.042	0.0339	-0.108	0.024	1.537	1	0.215
		HET	-0.048	0.0331	-0.113	0.017	2.093	1	0.148
		LEAN [kg]	-23.852	9.2846	-42.050	-5.655	6.600	1	0.010
		FAT [kg]	54.292	16.5432	21.868	86.716	10.770	1	0.001
		REE [kcal/h]	-0.246	0.4363	-1.101	0.609	0.317	1	0.573
		XTYT24 [Cnts]	7.646E-07	8.3548E-07	-8.729E-07	2.402E-06	0.838	1	0.360
		Scale	0.004						
	HFD	Intercept	0.763	0.0142	0.736	0.791	2900.613	1	0.000
		KO	0.002	0.0020	-0.002	0.006	1.408	1	0.235
		HET	0.001	0.0027	-0.005	0.006	0.069	1	0.793
		LEAN [kg]	0.645	0.9222	-1.163	2.452	0.489	1	0.485
		FAT [kg]	2.127	0.6212	0.909	3.344	11.721	1	0.001
		REE [kcal/h]	0.197	0.0279	0.142	0.251	49.589	1	0.000
		XTYT24 [Cnts]	7.442E-06	5.9176E-07	6.282E-06	8.602E-06	158.158	1	0.000
		Scale	0.000						
	HFD+S	Intercept	-0.720	0.0749	-0.867	-0.573	92.288	1	0.000
		KO	0.033	0.0149	0.003	0.062	4.814	1	0.028
		HET	-0.014	0.0144	-0.042	0.015	0.893	1	0.345
		LEAN [kg]	21.383	5.1586	11.272	31.493	17.182	1	0.000
		FAT [kg]	8.871	4.2440	0.553	17.190	4.369	1	0.037
		REE [kcal/h]	0.182	0.2029	-0.215	0.580	0.808	1	0.369
		XTYT24 [Cnts]	1.284E-05	1.1105E-06	1.066E-05	1.502E-05	133.655	1	0.000
		Scale	0.001						

OFF	**NCD**	Intercept	1.271	0.1448	0.987	1.554	76.983	1	0.000
		KO	-0.020	0.0249	-0.069	0.028	0.667	1	0.414
		HET	0.017	0.0283	-0.038	0.072	0.362	1	0.547
		LEAN [kg]	3.536	8.5055	-13.134	20.207	0.173	1	0.678
		FAT [kg]	29.061	12.7144	4.141	53.981	5.224	1	0.022
		REE [kcal/h]	-1.034	0.2892	-1.601	-0.467	12.787	1	0.000
		XTYT24 [Cnts]	-7.350E-07	5.4411E-07	-1.801E-06	3.315E-07	1.825	1	0.177
		Scale	0.004						
	HFD	Intercept	0.807	0.0057	0.796	0.818	20105.550	1	0.000
		KO	0.004	0.0014	0.001	0.007	7.547	1	0.006
		HET	-0.001	0.0019	-0.005	0.003	0.295	1	0.587
		LEAN [kg]	1.919	0.6377	0.669	3.169	9.055	1	0.003
		FAT [kg]	1.648	0.3798	0.903	2.392	18.813	1	0.000
		REE [kcal/h]	0.071	0.0248	0.023	0.120	8.239	1	0.004
		XTYT24 [Cnts]	3.948E-06	3.1702E-07	3.326E-06	4.569E-06	155.070	1	0.000
		Scale	0.000						
	HFD+S	Intercept	-0.579	0.0607	-0.698	-0.460	90.905	1	0.000
		KO	0.019	0.0114	-0.003	0.041	2.762	1	0.097
		HET	-0.012	0.0125	-0.037	0.012	0.959	1	0.327
		LEAN [kg]	15.798	3.9368	8.082	23.514	16.104	1	0.000
		FAT [kg]	7.885	3.3770	1.266	14.503	5.451	1	0.020
		REE [kcal/h]	0.153	0.1541	-0.149	0.456	0.992	1	0.319
		XTYT24 [Cnts]	8.551E-06	1.1994E-06	6.200E-06	1.090E-05	50.825	1	0.000
		Scale	0.001						

Table 10: Indirect calorimetry: GEE parameter estimates for EE. Linear link function.

					95% Wald CI		Hypothesis Test		
Interval	**Diet**	**Parameter**	**B**	**SE**	**Lower**	**Upper**	**Wald χ^2**	**df**	**P**
24h	**NCD**	Intercept	0.024	0.0697	-0.112	0.161	0.122	1	0.727
		KO	-0.011	0.0095	-0.029	0.008	1.247	1	0.264
		HET	0.002	0.0124	-0.022	0.027	0.038	1	0.846
		LEAN [kg]	14.129	3.6507	6.974	21.284	14.979	1	0.000
		FAT [kg]	-5.055	6.1059	-17.022	6.913	0.685	1	0.408
		REE [kcal/h]	0.593	0.1161	0.366	0.821	26.111	1	0.000
		XTYT24 [Cnts]	-9.882E-08	1.7907E-07	-4.498E-07	2.522E-07	0.305	1	0.581
		Scale	0.009						
	HFD	Intercept	-0.044	0.0268	-0.097	0.008	2.749	1	0.097
		KO	0.015	0.0069	0.002	0.028	4.778	1	0.029
		HET	-0.006	0.0058	-0.017	0.006	0.953	1	0.329
		LEAN [kg]	11.752	2.5533	6.748	16.756	21.185	1	0.000
		FAT [kg]	8.223	1.3397	5.597	10.849	37.675	1	0.000
		REE [kcal/h]	0.573	0.1041	0.369	0.777	30.309	1	0.000
		XTYT24 [Cnts]	2.942E-05	1.7892E-06	2.592E-05	3.293E-05	270.444	1	0.000
		Scale	0.003						
	HFD+S	Intercept	0.228	0.0332	0.163	0.293	47.280	1	0.000
	(Scale:	KO	-0.025	0.0046	-0.034	-0.016	30.740	1	0.000
	0.002)	HET	-0.002	0.0059	-0.014	0.009	0.151	1	0.697
		LEAN [kg]	-5.643	2.1374	-9.832	-1.454	6.970	1	0.008
		FAT [kg]	4.449	1.7298	1.059	7.840	6.616	1	0.010
		REE [kcal/h]	0.799	0.1004	0.602	0.995	63.257	1	0.000
		XTYT24 [Cnts]	3.526E-05	2.0637E-06	3.122E-05	3.931E-05	291.967	1	0.000

ON	**NCD**	Intercept	-0.084	0.0774	-0.236	0.067	1.187	1	0.276
		KO	-0.010	0.0125	-0.034	0.014	0.647	1	0.421
		HET	0.007	0.0150	-0.022	0.037	0.232	1	0.630
		LEAN [kg]	10.649	4.0929	2.627	18.671	6.770	1	0.009
		FAT [kg]	-1.434	5.8641	-12.927	10.060	0.060	1	0.807
		REE [kcal/h]	0.881	0.1357	0.615	1.147	42.125	1	0.000
		XTYT24 [Cnts]	-5.044E-09	2.1917E-07	-4.346E-07	4.245E-07	0.001	1	0.982
		Scale	0.005						
	HFD	Intercept	-0.044	0.0172	-0.078	-0.011	6.690	1	0.010
		KO	0.008	0.0048	-0.001	0.018	2.932	1	0.087
		HET	-0.008	0.0035	-0.015	-0.001	5.630	1	0.018
		LEAN [kg]	8.494	1.5629	5.430	11.557	29.535	1	0.000
		FAT [kg]	6.696	0.8605	5.009	8.382	60.547	1	0.000
		REE [kcal/h]	0.698	0.0609	0.579	0.818	131.306	1	0.000
		XTYT24 [Cnts]	2.899E-05	2.0184E-06	2.503E-05	3.294E-05	206.224	1	0.000
		Scale	0.001						
	HFD+S	Intercept	0.099	0.0165	0.067	0.132	36.213	1	0.000
		KO	-0.012	0.0025	-0.017	-0.007	24.428	1	0.000
		HET	-0.004	0.0023	-0.009	0.000	3.203	1	0.074
		LEAN [kg]	0.502	1.1002	-1.654	2.659	0.208	1	0.648
		FAT [kg]	4.484	0.8976	2.724	6.243	24.953	1	0.000
		REE [kcal/h]	0.757	0.0514	0.657	0.858	217.317	1	0.000
		XTYT24 [Cnts]	3.632E-05	3.2475E-06	2.996E-05	4.269E-05	125.103	1	0.000
		Scale	0.001						
OFF	**NCD**	Intercept	0.133	0.0831	-0.030	0.296	2.560	1	0.110
		KO	-0.011	0.0123	-0.035	0.013	0.819	1	0.365
		HET	-0.002	0.0139	-0.030	0.025	0.030	1	0.863
		LEAN [kg]	17.609	4.9315	7.943	27.274	12.750	1	0.000
		FAT [kg]	-8.676	7.7882	-23.940	6.589	1.241	1	0.265
		REE [kcal/h]	0.306	0.1420	0.027	0.584	4.628	1	0.031
		XTYT24 [Cnts]	-1.926E-07	2.5966E-07	-7.015E-07	3.163E-07	0.550	1	0.458
		Scale	0.006						
	HFD	Intercept	0.001	0.0403	-0.078	0.080	0.001	1	0.972
		KO	0.021	0.0087	0.004	0.038	5.697	1	0.017
		HET	-0.003	0.0094	-0.021	0.016	0.085	1	0.771
		LEAN [kg]	14.917	3.6909	7.683	22.151	16.334	1	0.000
		FAT [kg]	7.870	1.8579	4.229	11.511	17.945	1	0.000
		REE [kcal/h]	0.423	0.1415	0.145	0.700	8.924	1	0.003
		XTYT24 [Cnts]	2.089E-05	1.4733E-06	1.800E-05	2.377E-05	200.968	1	0.000
		Scale	0.002						
	HFD+S	Intercept	0.412	0.0811	0.253	0.571	25.799	1	0.000
		KO	-0.049	0.0121	-0.073	-0.026	16.671	1	0.000
		HET	0.000	0.0138	-0.027	0.027	0.000	1	0.991
		LEAN [kg]	-16.547	5.0263	-26.398	-6.695	10.838	1	0.001
		FAT [kg]	6.069	3.9073	-1.589	13.727	2.413	1	0.120
		REE [kcal/h]	0.874	0.2100	0.462	1.286	17.325	1	0.000
		XTYT24 [Cnts]	3.753E-05	3.2466E-06	3.116E-05	4.389E-05	133.606	1	0.000
		Scale	0.002						

v. Hyperinsulinemic-euglycemic clamp

In HE-clamp experiments, LINKO mice did not show an altered glucose infusion rate (GIR) or blood glucose concentration, as assessed through a GEE with logarithmic link function including baseline blood glucose concentration as covariate (**Figure 11**). While a trend towards lower blood glucose concentration and higher GIR in LINKO mice relative to WT controls was observed, it did not reach statistical significance (**Table 11**).

We observed differential glucose metabolism between the genotypes: Clamp glucose clearance and glycogen synthesis were elevated in LINKO mice relative to WT controls, while glycolysis was significantly suppressed, pointing toward a stronger anabolic response to hyperinsulinemia in LINKO mice. Meanwhile, no significant differences in baseline blood glucose clamp blood glucose, basal glucose clearance, and hepatic glucose output parameters between the genotypes were identified using one-way ANOVA and Holm-Sidak correction (**Figure 12, Table 12**). Tissue uptake of 2-DG, plasma insulin level, and plasma FFA level did not differ significantly between the genotypes (**Figure 13, Table 12**).

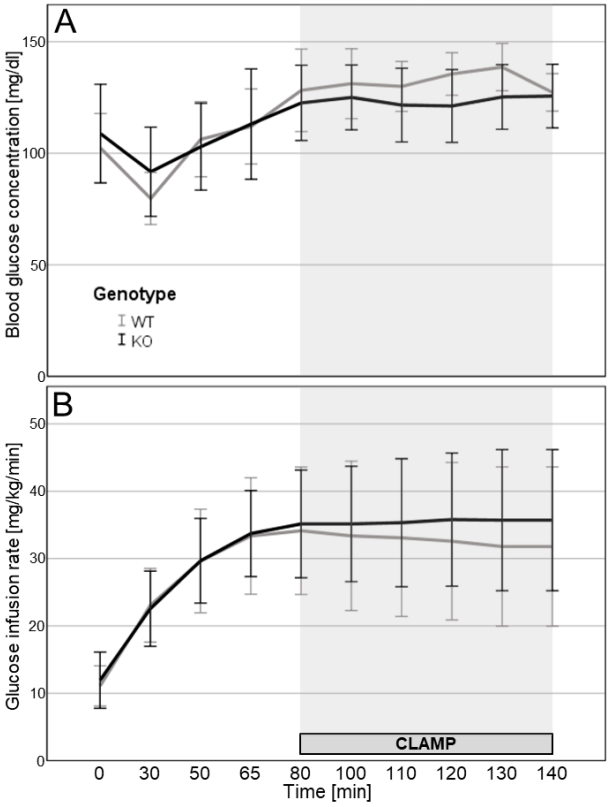

Figure 11: HE-clamp. **A:** Blood glucose concentration over time. **B:** Glucose infusion rate over time. KO: n = 7. WT: n = 8.

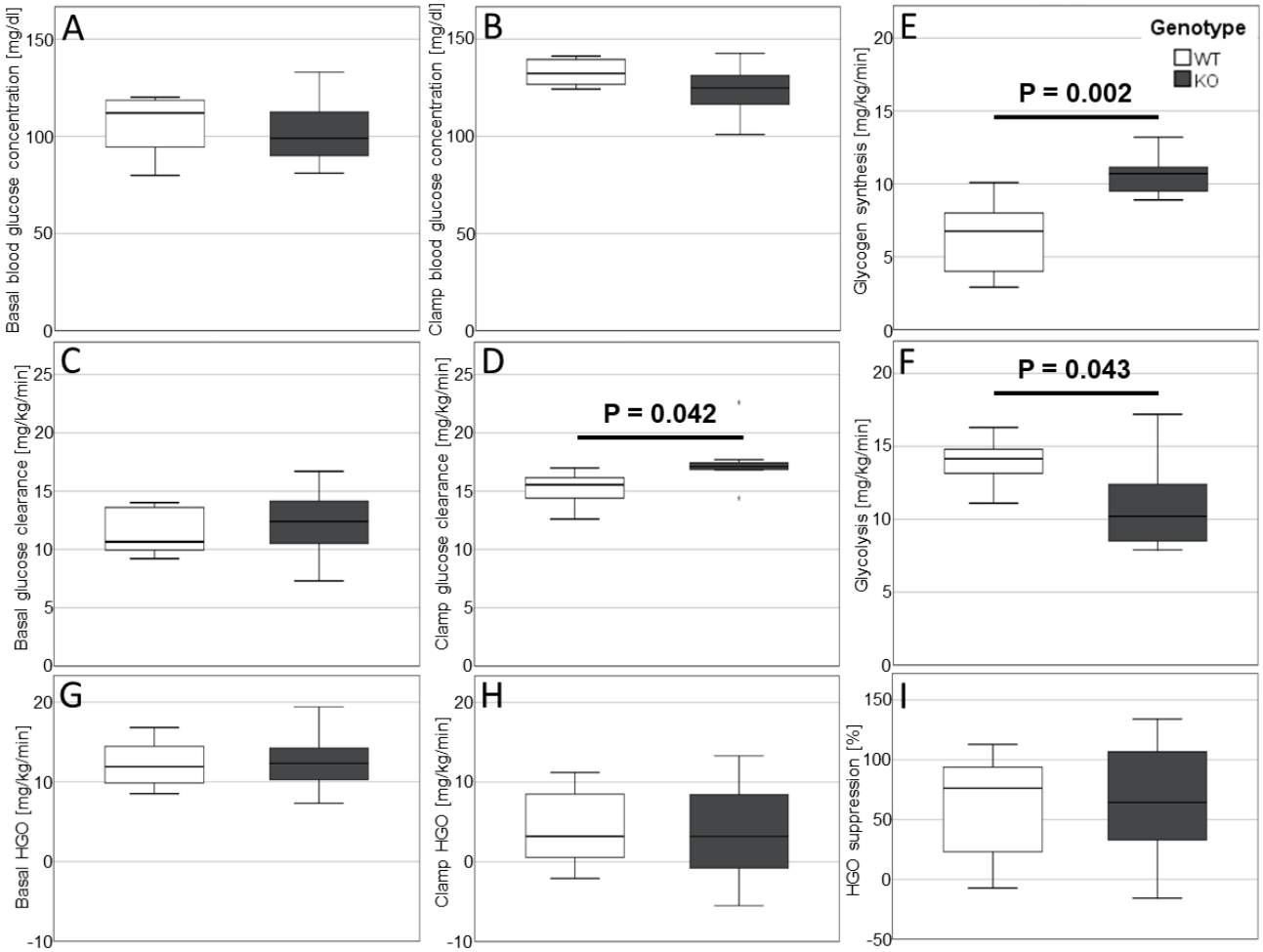

Figure 12: HE-clamp: Glucose metabolism after infusion of [3-H]-D-Glucose. **A:** Baseline blood glucose. **B:** Clamp blood glucose. **C:** Basal glucose clearance. **D:** Clamp glucose clearance. **E:** Glycogen synthesis. **F:** Glycolysis. **G:** Basal hepatic glucose output. **H:** Clamp hepatic glucose output. **I:** Hepatic glucose output suppression. KO: n = 7. WT: n = 8.

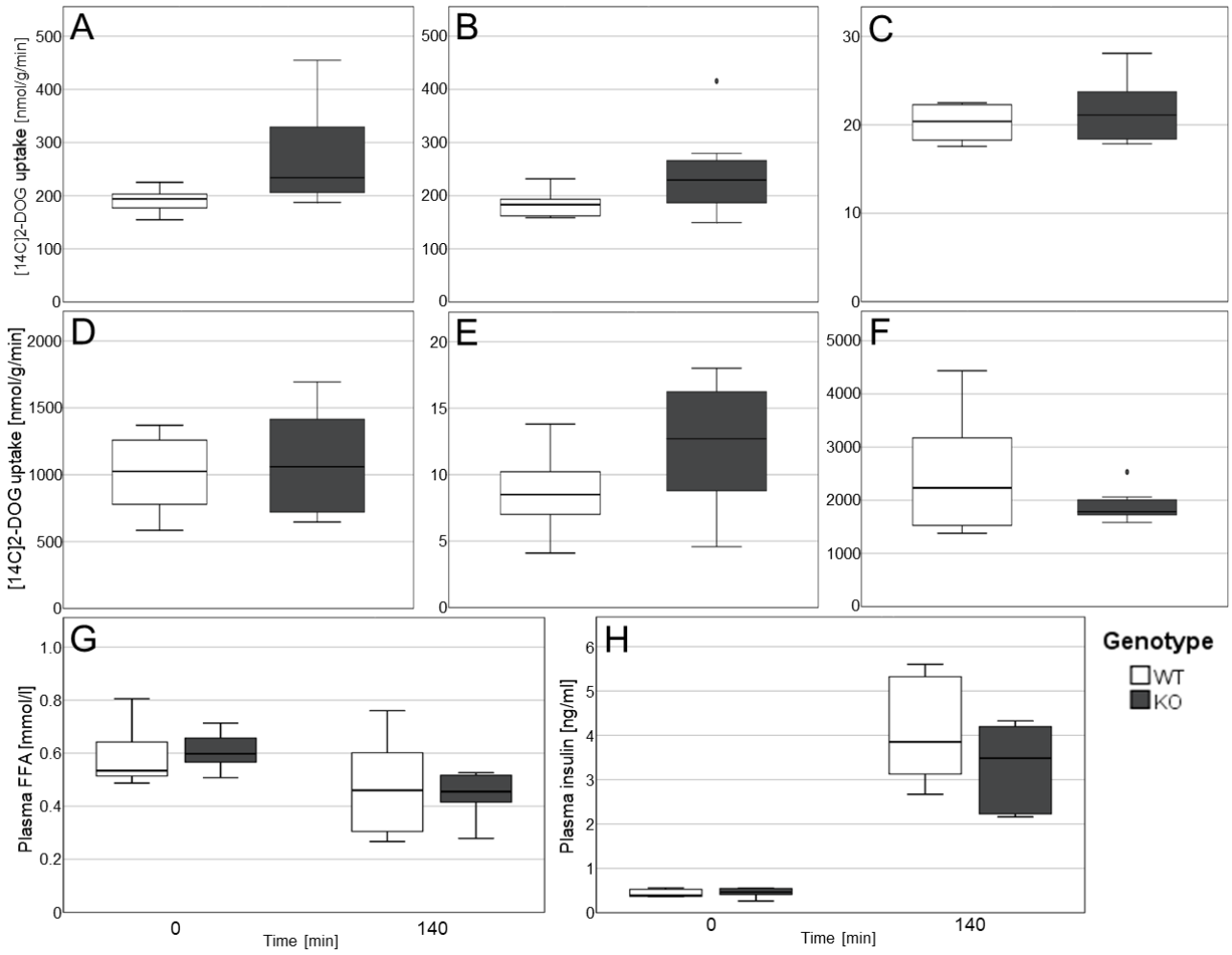

Figure 13: HE-clamp: Uptake of 2-DG, plasma FFA and plasma insulin levels. **A:** M. quadriceps femoris. **B:** M. gastrocnemius. **C:** Liver. **D:** Heart. **E:** Visceral adipose tissue. **F:** Brown adipose tissue. **G:** Plasma free fatty acid concentration. **H:** Plasma insulin concentration. KO: N = 6-7. WT: N = 8.

Table 11: HE-clamp: GEE parameter estimates for blood glucose and GIR. Logarithmic link function.

				95% Wald CI		Hypothesis Test		
Measure	**Parameter**	**B**	**SE**	**Lower**	**Upper**	**Wald χ^2**	**df**	**Sig.**
Blood glucose	Intercept	4.969	0.1429	4.689	5.249	1209.771	1	0.000
	KO	-0.068	0.0398	-0.146	0.010	2.930	1	0.087
	Glc-Basal [mg/dl]	-0.001	0.0013	-0.003	1.748E-03	0.393	1	0.531
	Scale	0.012						
GIR	Intercept	3.235	0.4947	2.265	4.204	42.753	1	0.000
	KO	0.088	0.1464	-0.199	0.375	0.361	1	0.548
	Glc-Basal [mg/dl]	0.002	0.0044	-0.006	0.011	0.293	1	0.588
	Scale	0.087						

Table 12: HE-clamp: Statistics for covariates, glucose metabolism and tissue uptake. One-way ANOVA or Welch test.

Measure	Genotype	N	Mean	SD	95% CI		ANOVA	
					Lower	Upper	F	P
Body weight [g]	KO	7	28.6429	3.18792	25.6945	31.5912	1.545	0.236
	WT	8	30.7625	3.38397	27.9334	33.5916		
Baseline blood glucose [mg/dl]	KO	7	102.5714	19.38089	84.6471	120.4958	0.165	0.691
	WT	8	106.2500	15.73667	93.0938	119.4062		
Insulin 0min [ng/ml]	KO	7	0.4576	0.10642	0.3591	0.5560	0.075	0.789
	WT	7	0.4431	0.09009	0.3598	0.5265		
Insulin 140min [ng/ml]	KO	6	3.3122	0.93687	2.3290	4.2953	1.861	0.197
	WT	8	4.1083	1.17223	3.1282	5.0883		
FFA 0min [mmol/l]	KO	6	0.6067	0.07310	0.5300	0.6834	0.196	0.666
	WT	8	0.5840	0.10777	0.4939	0.6741		
FFA 140min [mmol/l]	KO	7	0.4464	0.08913	0.3640	0.5289	0.098	0.750 Welch
	WT	8	0.4700	0.17978	0.3197	0.6203		
Basal HGO [mg/kg/min]	KO	7	12.5714	4.08563	8.7929	16.3500	0.039	0.846
	WT	8	12.2125	2.91079	9.7790	14.6460		
Clamp HGO [mg/kg/min]	KO	7	3.7571	6.83419	-2.5634	10.0777	0.021	0.886
	WT	8	4.2000	4.83470	0.1581	8.2419		
HGO suppression [%]	KO	7	66.0114	53.16158	16.8452	115.1777	0.032	0.862
	WT	8	61.4900	45.37376	23.5566	99.4234		
Hepatic glucose uptake [mg/kg/min]	KO	7	21.6157	3.79310	18.1077	25.1237	0.783	0.392
	WT	8	20.2375	2.12043	18.4648	22.0102		
Glycolysis [mg/kg/min]	KO	7	11.0143	3.29668	7.9654	14.0632	5.031	**0.043**
	WT	8	13.9500	1.60089	12.6116	15.2884		
Gycogen synthesis [mg/kg/min]	KO	7	10.5857	1.46564	9.2302	11.9412	15.748	**0.002**
	WT	8	6.3125	2.48966	4.2311	8.3939		
Basal glc clearance [mg/kg/min]	KO	7	12.2429	3.13042	9.3477	15.1380	0.352	0.563
	WT	8	11.4500	1.99141	9.7851	13.1149		
Clamp glc clearance [mg/kg/min]	KO	7	17.5286	2.47502	15.2396	19.8176	5.101	**0.042**
	WT	8	15.2250	1.40077	14.0539	16.3961		
Uptake Quadriceps [nmol/g/min]	KO	6	191.3333	23.71216	166.4489	216.2177	3.437	0.066 Welch
	WT	8	272.5250	104.26248	185.3594	359.6906		
Uptake Gastrocne-mius [nmol/g/min]	KO	6	185.3667	26.54059	157.5140	213.2193	2.493	0.140
	WT	8	241.2750	82.86239	172.0003	310.5497		
Uptake Tibial muscle [nmol/g/min]	KO	7	115.1857	29.97540	87.4631	142.9083	0.873	0.367
	WT	8	132.4175	39.83920	99.1111	165.7239		
Uptake WAT [nmol/g/min]	KO	6	8.6867	3.23802	5.2886	12.0848	2.424	0.145
	WT	8	12.2538	4.83409	8.2123	16.2952		
Uptake BAT [nmol/g/min]	KO	7	2493.2143	1236.17434	1349.9437	3636.4849	1.461	0.267 Welch
	WT	7	1910.1429	316.73736	1617.2097	2203.0761		
Uptake Heart [nmol/g/min]	KO	6	1007.0167	292.41985	700.1409	1313.8925	0.188	0.672
	WT	8	1091.1500	400.26356	756.5213	1425.7787		

b. Glucose production in LINKO primary hepatocytes

After starvation and stimulation through different glucose production media, LINKO primary hepatocytes showed a trend towards higher capacity for glucose production relative to WT controls under all conditions including fasted state (O), which reached statistical significance under the condition of maximum substrate stimulation (GGP) (**Figure 14**, **Table 13**).

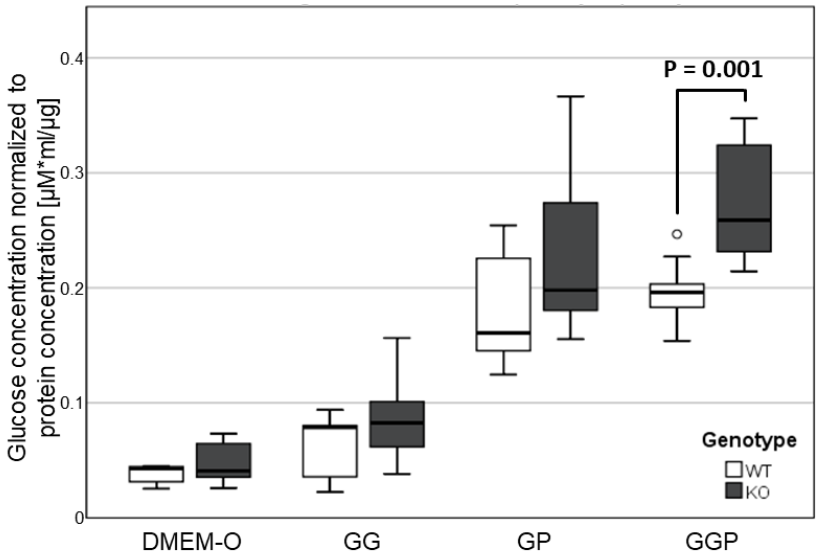

Figure 14: Glucose production in LINKO primary hepatocytes. DMEM-O: Starvation medium. GG: DMEM-O + glucagon + glutamic acid. GP: DMEM-O + glucagon + pyruvic acid. GGP: DMEM-O + glucagon + glutamic acid + pyruvic acid. N = 3.

Table 13: Glucose production in LINKO primary hepatocytes: Statistics. One-way ANOVA. N = 3.

				95% CI		ANOVA	
Medium	Genotype	Mean	SD	**Lower Bound**	**Upper Bound**	**F**	**P**
DMEM-O	KO	0.047	0.018	0.034	0.061	1.814	0.197
	WT	0.039	0.008	0.033	0.045		
GGP	KO	0.272	0.050	0.233	0.311	15.340	0.001
	WT	0.195	0.030	0.173	0.218		
GG	KO	0.085	0.036	0.057	0.112	1.664	0.215
	WT	0.065	0.028	0.044	0.086		
GP	KO	0.226	0.069	0.173	0.279	2.550	0.130
	WT	0.181	0.050	0.142	0.219		

c. Gene expression in LINKO liver samples

In liver samples from HFD-fed LINKO mice, several genes involved in mitochondrial function were significantly or near-significantly upregulated in the livers of LINKO mice relative to WT controls (**Figure 15**, **Table 14**): Nuclear respiratory factor 1 / NRF1 (23.3%, p =0.013), carnitine palmitoyl transferase I / CPT1A (25.5%, p = 0.051), Sirtuin 1 / SIRT1 (30.4%, p = 0.053) and medium-chain acyl-CoA dehydrogenase / ACADM (27.8%, p = 0.071). Significant or near-significant upregulation was also found in two markers of ER stress: DnaJ Heat Shock Protein Family (Hsp40) Member B9 / DNAJB9 (23.3%, p = 0.038) and X-box binding protein 1 / XBP1 (74.7%, p = 0.072). Genes involved in glucose and lipid metabolism as well as inflammation were not differentially expressed in LINKO mice relative to WT controls. The expression of $_{m}$INDY was suppressed by 99.1% ($p < 0.001$), suggesting complete recombination in hepatocytes. Its functionally closest family member, SLC13A3, was not differentially expressed.

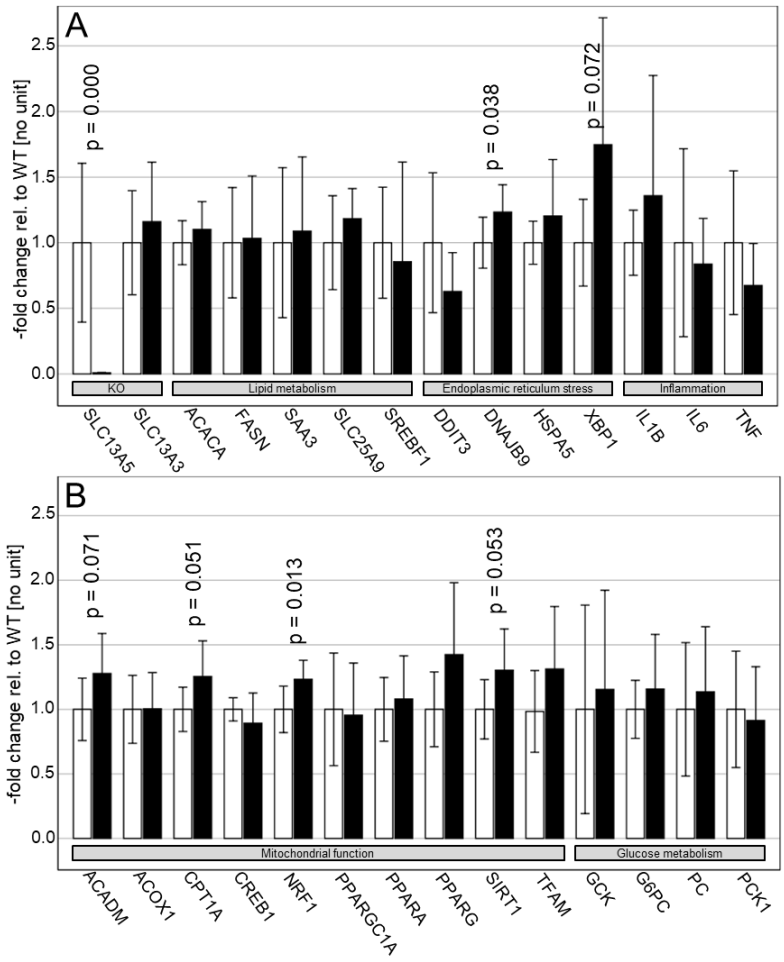

Figure 15 A and B: Gene expression in LINKO liver samples (n = 9) relative to WT (n = 7), grouped by physiological function (grey boxes). ACACA: Acetyl-CoA carboxylase. ACADM: Medium-chain-acyl-CoA-dehydrogenase. ACOX: Acetyl-CoA oxidase 1. CPT1A: Carnitine palmitoyltransferase 1. CREB1: cAMP response element-binding protein. DDIT3: DNA damage inducible transcript 3. DNAJ B9: DnaJ heat shock protein family (HSP40) member B9. FASN: Fatty acid synthase. G6PC: Glucose-6-phosphatase, catalytic subunit. GCK: Glucokinase. HSPA5: Heat shock protein family A (Hsp70) member 5. IL1B: Interleukin 1 beta. IL6: Interleukin 6. NRF1: Nuclear respiratory factor 1. PC: Pyruvate carboxylase. PCK1: Phosphoenolpyruvate carboxykinase 1. PPARA: Peroxisome proliferator activated receptor alpha.PPARG: Peroxisome proliferator activated receptor gamma. PPARGC1A: Peroxisome proliferator-activated receptor gamma coactivator 1-alpha (PGC1A). SAA3: Serum amyloid A-3 protein. SIRT1: Sirtuin-1. SLC13A3: Solute carrier family 13 member 3. SLC13A5: Solute carrier family 13 member 5. SLC25A20: Solute carrier family 25 member 20. SREBF1: Sterol regulatory element binding transcription factor 1. TFAM: Mitochondrial transcription factor A. TNF: Tumor necrosis factor alpha. XBP1: X-box binding protein 1.

Table 14: Gene expression in LINKO liver samples: Statistics. One-way ANOVA. KO: N = 9. WT: N = 7.

Function	Gene	Genotype	Mean -fold change (ΔΔCt)	SD	P
Mitochondrial Function	**ACADM**	WT	1.026	0.248	0.071
		KO	1.311	0.317	
	ACOX1	WT	1.014	0.171	0.139
		KO	0.897	0.122	
	CPT1A	WT	1.013	0.174	**0.051**
		KO	1.271	0.279	
	CREB1	WT	1.003	0.090	0.248
		KO	0.897	0.234	
	NRF1	WT	1.013	0.182	**0.013**
		KO	1.249	0.150	
	PPARGC1A	WT	1.083	0.473	0.835
		KO	1.035	0.437	
	PPARA	WT	1.027	0.254	0.605
		KO	1.110	0.344	
	PPARG	WT	1.035	0.300	0.090
		KO	1.474	0.576	
	SIRT1	WT	1.023	0.235	**0.053**
		KO	1.334	0.327	
	TFAM	WT	1.038	0.303	0.096
		KO	1.427	0.507	
Lipid Metabolism	**ACACA**	WT	1.012	0.170	0.319
		KO	1.115	0.215	
	SLC25A20	WT	1.052	0.376	0.235
		KO	1.244	0.242	
	FASN	WT	1.075	0.452	0.885
		KO	1.111	0.510	
	SAA3	WT	1.119	0.639	0.768
		KO	1.218	0.632	
	SREBF1	WT	1.072	0.454	0.659
		KO	0.917	0.814	
Glucose Metabolism	**GCK**	WT	1.222	0.987	0.703
		KO	1.410	0.939	
	G6PC	WT	1.025	0.230	0.388
		KO	1.187	0.433	
	PC	WT	1.094	0.565	0.607
		KO	1.242	0.552	
	PCK1	WT	1.097	0.494	0.698
		KO	1.002	0.456	
ER-stress	**DNAJ B9**	WT	1.016	0.197	**0.038**
		KO	1.253	0.212	
	DDIT3	WT	1.108	0.591	0.113
		KO	0.696	0.328	
	HSPA5	WT	1.013	0.166	0.256
		KO	1.220	0.435	
	XBP1	WT	1.045	0.345	0.072
		KO	1.826	1.011	

Inflammation	**IL1B**	WT	1.030	0.255	0.334
		KO	1.399	0.943	
	IL6	WT	1.242	0.890	0.572
		KO	1.040	0.433	
	TNF	WT	1.099	0.602	0.157
		KO	0.741	0.351	
Carboxylate transport	**SLC13A5**	WT	1.156	0.645	**<0.001**
		KO	0.010	0.014	
	SLC13A3	WT	1.060	0.421	0.471
		KO	1.231	0.481	

6. Discussion

a. Summary

To evaluate the role of the liver in the beneficial metabolic effects seen after complete knockout of the mammalian INDY orthologue (mINDY) in mice, we established a liver-specific conditional knockout mouse model of mINDY using the Cre-loxP system. We compared LINKO mice to their wild type controls under three diets of differing caloric density and performed comprehensive metabolic phenotyping. This included body weight, size, and composition, ipGTT, indirect calorimetry, and HE-clamp. Additionally, we established an *in vitro*-assay of glucagon-stimulated glucose production capacity in LINKO primary hepatocytes and screened for gene expression changes in liver samples of LINKO mice by qPCR. We did not observe differences in body weight and size, body composition, and glucose metabolism during ipGTT. Indirect calorimetry led to slightly increased EE and RER in HFD-fed mice only. The HE-clamp unveiled an antiglycolytic effect in LINKO mice. In line with this observation, LINKO primary hepatocytes showed a higher capacity for glucose production upon starvation. Lastly, we observed an increase in the expression of some genes involved in mitochondrial respiration, oxidative capacity, and ER-stress in LINKO mice, together pointing towards a more efficient counter-regulation against the hypercaloric challenge.

b. Methodical considerations

i. Transgenic mice

To create a mouse model of DIO for this study, we selected the C57Bl/6J strain, with housing, husbandry and feeding conditions implemented according to standard protocols. This mouse strain has been widely used in metabolic research due to its susceptibility to DIO and disturbances in glucose homeostasis, and represents the most thoroughly established model for these conditions.[53] All metabolic phenotyping was conducted after week 12, based on the assumption that by the completed third month, mice have reached maturity.[54] A metabolic phenotype of this model should be visible at this timepoint, as was the case in previous experiments on INKO mice.[27]

For liver-specific conditional mIndy recombination, we used the Cre-loxP system, which similarly has been widely validated in transgenic research across fields.[55] The insertion of

lox sites around the mINDY gene was established earlier with no known phenotype reported.[27] In the creation of the albumin-Cre mouse, the transgene is inserted into chromosome 13, causing a small deletion in Speer6-ps1 (spermatogenesis associated glutamate (E)-rich protein 6, pseudogene 1). This albumin-Cre mouse shows no reported phenotype and can be used as homo- or heterozygote due to its high recombination efficiency.[56] Even if unspecific phenotypes should exist due to the two genomic alterations, we minimized genetic differences between the experimental groups by using mice with genotype fl/fl, Cre- as our WT control.

At present, the Cre-loxP technology is a standard for tissue-specific conditional knockout due to its high specificity and effectiveness, although developments towards using the procedurally more efficient CRISPR/Cas9 system are underway.[57] Also, posttranscriptional approaches such as through siRNA or ASOs represent interventional options to target mINDY, with varying remaining gene activity representing an important caveat.[58,59]

ii. Diets

To model DIO in rodents, different dietary interventions of increased caloric density are commonly used.[60–62] With previous experiments on INKO mice having shown a marked metabolic phenotype upon adipogenic stress through a HFD intervention, we used different adipogenic diets to dissect whether the liver-specific mINDY knockout mediates a protective phenotype against DIO, and whether a modelled Western diet of even higher caloric density may cause greater exacerbation of DIO and thus further carve out a possible protective phenotype in LINKO mice.[27,63]

While this negative-controlled paradigm of three differing dietary interventions is one strength of our study, the *ad libitum*-fed experimental setting precluded the possibility to measure the exact caloric intake of each animal. Our own mechanistic insights into phenotypic differences between the dietary groups where therefore limited to assumptions about gross caloric intake. Other studies mimicking a Western diet in mouse models exacerbated the intervention further, e.g. by additionally increasing the relative content of saturated fatty acids or by limiting physical activity.[64] While exacerbation along these lines might indeed have represented a viable fourth experimental group, we chose our approach in order to keep the number of altered variables between the groups at a minimum.

iii. Body weight, size and composition

While non-invasive body mass and body composition measurements took place repeatedly along the experimental schedule, we did not measure body length *in vivo*, which would be possible only under anesthesia*;* instead, we conducted a single measurement of body length after mice were sacrificed at 16 weeks in order to minimize strain and possible behavioral or metabolic effects of repeated anesthesia on the animals as reported elsewhere.[65–68]

Several methods are available to determine body composition, the most notable being dissection and subsequent chemical analysis, dual x-ray absorptiometry (DXA), and ^{1}H-NMR. We selected the latter, as it allows for non-invasive and radiation-free measurements of body compartments (i.e. fat, free fluid and lean mass) without the need to anesthetize or sacrifice the animal and is therefore ideal for longitudinal experiments. Also, it has been demonstrated to estimate especially the body fat compartment with higher accuracy than DXA.[69–72] A potential small overestimation of the fat compartment inherent to ^{1}H-NMR could not be ruled out entirely, as we used no other method for validation.[71] However, our controlled and longitudinal experimental setup limited the possibility of an instrument bias towards more obese animals.

iv. Intraperitoneal glucose tolerance test

To screen for impaired glucose homeostasis, we performed ipGTTs. While this method allows to efficiently gauge differences in glucose disposal, conclusions about the pathophysiology regarding tissue-specific effects or insulin secretion and action cannot be drawn. Nevertheless, the GTT represents a standard in orientating metabolic phenotyping.[73–75]

We addressed several variables that can confound the outcomes of GTT experiments: To circumvent artifacts associated with enteral application of glucose, such as the metabolic effects of incretins, we chose the intraperitoneal application route.[74] As routinely practiced, we fasted mice overnight for a duration of 16h, administered glucose at a dosage ratio of 1g/kg, and based our dosage calculations on total body mass. All three factors potentially confound experimental outcomes: A 16h fast is discussed to be disproportionately long in mice, potentially diminishing subtle differences in glucose response.[76,77] Additionally, a

higher glucose dosage of up to 2g/kg BW has been shown to be better able to unveil more subtle differences in glucose tolerance, increasing the experiment's sensitivity.[76] Conversely, administering a glucose dose that has been calculated based on total body mass can positively confound experimental outcomes: Obese mice will receive higher dosages than their non-obese controls, although their lean tissue mass, the main site of glucose disposal, may not differ to a similar degree.[76,78] However, we established experimental conditions mimicking those from the experiments on INKO mice, as a quantifiable comparison between INKO and LINKO mice regarding their metabolic phenotype was necessary to evaluate our hypothesis. Also, INKO mice showed marked effects in GTTs despite the three conditions being present – leading to our understanding that our experiments should not require to be conducted at a higher sensitivity in order to prove an effect, if present.[27] Lastly, the experimental groups showed no mean differences in body composition at the GTT time points, excluding the possibility that this confounder may have influenced our results.

v. Indirect calorimetry

We assessed substrate utilization and EE by performing indirect calorimetry using respirometry chambers. Besides overall EE as derived through the abbreviated Weir formula, this technology enables the calculation of the RER from the rates of oxygen consumption ($\dot{V}O2$) and carbon dioxide production ($\dot{V}CO2$).[48] From this, substrate utilization (i.e., fatty acid vs. carbohydrate catabolism) is estimated, as lipid oxidation and carbohydrate oxidative phosphorylation require different molarities of $\dot{V}O2$ relative to $\dot{V}CO2$. Indirect calorimetry is widely used in metabolic phenotyping, as it generates estimates of these metabolic measures in a continuous and perturbation-free manner.[49,79–81]

Several inherent confounders must be considered. Firstly, while the technology in our experimental setup measures movement, food and water consumption and gas exchange, it omits secretions in the form of urine and feces, thus limiting the accuracy in determining energy uptake as well as protein metabolism. Especially regarding our dietary paradigm, a more detailed analysis of food uptake and waste secretion might have provided mechanistic insight into why the HFD+S diet did not produce the most obese phenotype. Secondly, the system we used provides automated calculations of the variables of interest. While it is standard methodology that these calculations are normalized *a priori* to lean mass by

integrating a fixed exponential term into them, this would have omitted individual differences between the mice; also, other potential confounders such as fat mass, movement, and resting energy expenditure are not taken into account. We therefore used the raw data to calculate RER and EE based on the abbreviated Weir formula and integrated possible confounders into a mathematical model *a posteriori*. This, although the matter of ongoing debate, is regarded an efficient way to reduce bias in this experimental setup.[49]

vi. HE-clamp

We performed HE-clamps, because in addition to a better-controlled experimental setup, this technique allows for estimates of insulin sensitivity, hepatic glucose metabolism, and organ-specific glucose uptake, thus providing a more detailed insight into metabolic function than ipGTT alone.[74,82]

We established the infusion protocol according to current standards;[27,50] however, several possible confounders can be discussed. Firstly, mice underwent a 16 hour-long overnight fast, the metabolic consequences of which are similar to those discussed above (see **7.b.iv.**).[77] Secondly, we used the tail cut for blood sampling in conscious mice, which necessitates increased manipulation of mice compared to sampling through an arterial catheter. Especially when large blood volumes are taken, this approach has been associated with increased catecholamine levels, which we did not measure.[77] Meanwhile, the stress from repeated manipulation under no sedation has to be weighed against reported metabolic effects of anesthesia in mice.[83] The rise in catecholamines can be countered in part by infusion of a blood replacement medium, for which we used an albumin-based artificial plasma. While hypovolemia can be effectively counteracted through this approach, we could not account for a resulting decrease in hematocrit. Also, no methodical comparisons with other options for plasma replacement have been published.

Our insulin infusion rate of 3 mU/kg/min, while widely utilized and proven to be efficient in lean mice, is relatively low compared to other experiments in insulin-resistant mice; an increased dose may have been more efficient at producing metabolic differences between the groups, as some degree of insulin resistance was to be expected in this DIO model.[77] Lastly, we normalized our insulin infusion rates to total body mass instead of lean body mass, possible effects of which are discussed above (see **7.b.iv**).

Lastly, one executional aspect of our HE-clamp may additionally have confounded our findings: During the clamp interval, plasma glucose levels tended to be non-significantly lower in LINKO mice, while the GIR in that group tended to be, also non-significantly, elevated. Compounded, this minute deficit in clamp stringency may have masked a subtle difference in insulin sensitivity as seen by others.[59] While the above-mentioned variables can confound results of HE-clamp experiments, we adhered to current standards to ensure maximal comparability between our findings and those in INKO mice.[27,84]

vii. Glucose production in LINKO primary hepatocytes

We established an assay for glucose production capacity in LINKO primary hepatocytes by stimulating fasted cells with glucagon and gluconeogenesis substrates and measuring glucose concentration in the supernatant. Comparable assays have been used for questions regarding glucose production in different models, as they allow for more stringent control of factors influencing cellular metabolism compared to *in vivo*-experiments, but at the same time maintain closer functional connection to the organ the culture is based on, as compared to cell line-based *in vitro*-experiments.[85,86] We are the first to assess glucose production in LINKO primary hepatocytes.

While the assay is carried out under standard tissue culture conditions and disturbances of the plated cells are minimized, the necessary incidents of cell handling, i.e. extraction, plating, cultivation, transfer, starvation, washing and stimulation, all introduce levels of artificiality into the observation. Also, as commonly observed in primary cell cultures, we cannot completely exclude contamination through cell types other than hepatocytes and similarly cannot account for eventual changes in differentiation over time in culture. While we followed good cell culture practice, used cells quickly and controlled the experiment by using negative controls from WT mice, a negative medium control, as well as true biological triplicates, the above-mentioned factors introduce inherent biases that cannot completely be accounted for.

Another limitation of this experiment lies in the fact that through the selected stimulants alone, we could not differentiate whether enzymatic processes in the common final path of gluconeogenesis and/or TCA cycle processes are responsible for differences between LINKO and WT hepatocytes. To dissect mechanistically which enzymes in the TCA cycle

and gluconeogenesis path show increased activity, this preliminary assay must be supported by additional gene expression analysis and more detailed cellular studies using selective enzyme inhibitors. These further steps, however, were beyond the scope of this work.

viii. Gene expression in LINKO primary hepatocytes

In order to screen for changes in transcriptional regulatory pathways akin to those reported in INKO mice[27], we performed a RealTime-qPCR based expression analysis of genes involved in the regulation of mitochondrial function, glucose and lipid metabolism, endoplasmic reticulum stress and inflammation in liver samples obtained from LINKO and WT mice on HFD. We also analyzed mRNA expression of $_m$INDY and its functionally closest family member, SLC13A3, in order to assess the efficiency of the knockout model as well as a potential compensatory upregulation of SLC13A3.

RealTime qPCR has been exhaustively discussed regarding the varying reproducibility of its results, leading to the establishment of “Minimum Information for Publication of Quantitative Real-Time PCR Experiments” (MIQE) guidelines delivering a path towards better standardization.[87] While we adhered to MIQE criteria in almost all aspects of the qPCR experiments, our internal controls and quantitative analysis did not meet these standards. With two reference genes used and quantification of differential expression levels calculated using the $\Delta\Delta$Ct method, we adhered to established standards which are regarded insufficient in the MIQE framework. Although our strong biological replication supports our findings, there is room for better internal controlling in future experiments.

In terms of target pre-selection, our method through its limited number of pre-determined mRNA targets carries a stronger selection bias than other screening approaches, such as the microarray-based gene set enrichment analysis conducted in INKO mice, or transcriptomic analysis through next-generation sequencing (RNAseq), which has been developed in recent years to be applied to cell-type specific questions through specific translating ribosome affinity purification (TRAP).[27,88–90] However, considering the limited metabolic phenotype observed in our *in vivo* experiments, we used this well-stablished approach for a first orientating overview over genetic categories previously seen to be differentially regulated in INKO mice.[27]

ix. Statistics

We established regression models using GEEs to analyze longitudinal observations. This approach is considered to more accurately represent the information contained within this type of data than parametric testing between grouped means. This is because the latter a) is sensitive against violations of the basic assumptions of normality and homoscedasticity, b) when applied to longitudinal data, underrepresents variance, and c) does not account for higher correlation structures through possible additional levels of clustering within the data, such as by timepoint.[91–93]

In our case, the use of GEEs unveiled a difference in blood glucose during HE-clamp which would have evaded testing through ANOVA; also, subtle differences in EE and RER did not appear statistically significant using standard parametric testing but did so under the use of GEEs, supporting their higher sensitivity in these types of data. While statistically more sensitive, this approach was limited by the fact that we could test only for main effects of the independent variable and covariates, as adding interaction terms to the models would have required larger datasets to accommodate for additional degrees of freedom. Nevertheless, in consultations with the Charité Institute of Biometry and Clinical Epidemiology, we tested and confirmed the validity of this approach.

c. Discussion of results

i. Our findings

Weight, size, body composition: We did not observe differences in body weight, size or composition in LINKO mice compared to WT controls. However, heterozygous mice fed a HFD displayed a slightly but significantly reduced body weight, a finding which may correspond to the more pronounced phenotypes observed in other studies using a knockdown approach and therefore not reaching complete recombination of $_{m}$INDY in the liver (see **7.c.ii**). However, dissecting this surprising phenotype specifically in heterozygous mice further was beyond the scope of this work.

Our DIO model resembled DIO models from comparable studies in its effectiveness: While Birkenfeld and colleagues reported their 12-week-old control mice at ~37g after 6 weeks on HFD, and Brachs and colleagues reported theirs to have reached ~32g at the same age but

4 weeks on HFD+S, our mice on HFD weighed ~35g after 9 weeks on HFD.[27,59] While the onset and duration of the HFD interventions varied, it is surprising to observe that despite a more severe dietary intervention, our mice did not surpass the DIO phenotype observed in the INKO study. Several factors may have caused this difference: Least likely is a differing susceptibility to DIO in the C57Bl/6J strains used in these experiments, as mice were derived from the same provider and backcrossed frequently.[27,59] Another option is that the colony was contaminated with intestinal nematode parasites, which have been reported to carry a potential to attenuate obesity.[94] However, the colony was tested regularly with no infections reported. Lastly, differences in the genetic model may have come into play, although the $_{m}$INDY fl/fl mouse that constituted our WT control was the same as in the study on INKO mice, and even non-floxed wildtype controls reached a more pronounced DIO than our mice.[27,59] This attenuation in BW gain may have masked metabolic effects which possibly could have been more pronounced if mice had reached a stronger DIO phenotype more rapidly.

Surprisingly, the diet with the highest caloric density (HFD+S) did not produce the most pronounced DIO phenotype: In terms of body weight, body composition and indirect calorimetry, this was instead caused by the HFD regimen. A type I error suggesting a false positive difference between the two diets appears unlikely due to the longitudinal stability and statistical strength of this finding. It could be hypothesized that increased caloric content in the drinking water may lead to decreased food consumption and thus cause a smaller total caloric intake than through HFD alone. Also, the knockout model may react more strongly to adipogenic stress when caloric intake consists predominantly of lipid, not carbohydrate sources. While a small number of studies have addressed the differing adipogenicity of HFD and HFD+S, a full mechanistic picture does not exist yet.[95,96] Additionally, no further studies exist to answer this question in liver-specific $_{m}$INDY knockout models, as we are the first to examine this phenotype. This observation therefore warrants additional efforts to confirm its reproducibility and assess its mechanism.

ipGTT: The ipGTT did not unveil differences in glucose excursion, insulin secretion, and HOMA-IR between experimental groups on NCD, HFD and HFD+S. This finding opposes the marked difference in glucose disposal seen in INKO mice, a difference that may have

been influenced by genotype and DIO phenotype: Our mice underwent ipGTTs at week 12 and a body weight of ~34 g, whilst INKO mice were tested at the same time point but weighing ~37 g.[27] In the siRNA-based knockdown approach using wildtype C57Bl/6J mice as controls, mice underwent ipGTTs at the same age weighing just ~31 g, and showed no phenotype, mirroring our results.[59] A liver-specific approach to suppress mINDY thus appears to be less relevant to glucose disposal than a full-body knockout, independently of timepoint or genotype. in addition, the effectiveness of the DIO intervention cannot be assessed here but is likely relevant, because even in control mice, baseline glucose levels as well as glucose excursions were higher in the INKO study than in our experiment (~150 mg/dL baseline and ~300 mg/dL excursion in INKO controls vs. ~130 mg/dL baseline and ~200 mg/dL excursion in our study).[27] Possible reasons for such systemic differences under similar experimental conditions include unknown confounders, such as small differences in housing conditions or slight genetic shifts within mouse strains.

Indirect calorimetry: In indirect calorimetry, we observed modestly increased RER and EE in LINKO mice on HFD with strongest statistical effects during the lights off-period, pointing towards an increase in carbohydrate metabolism and overall gas exchange. LINKO mice in the HFD+S cohort, however, displayed a decreased EE relative to controls. Meanwhile, all covariates, most notably locomotion, did not differ between the groups. By contrast, INKO mice displayed strongly increased gas exchange rates alongside an elevated EE, but no alterations in RER.[27] While these effects appeared markedly even in a small sample of INKO mice (n = 5), our outcomes were subtle and, in the case of EE, contradictory between the HFD and the HFD+S cohort. Based on this, it can be argued that the highly sensitive statistical model pointed out significance where a substantial phenotypic difference was absent, even though we used a larger sample than others.[27] At last, the effects observed in our sample were too subtle to translate to a whole-body phenotype in body weight and composition, an outcome closely mirrored by the siRNA-mediated knockdown model used by Brachs and colleagues.[59] This goes in line with a long-ongoing discussion about the value of statistical significance, which must be regarded in the context of apparent effect size in order to circumvent type I errors.[97–99]

It remains to be discussed whether the contradictory EE outcomes between the HFD and the HFD+S cohort may be caused by differences inherent to these diets or the level of DIO. While no studies to our knowledge address this question directly, leaner mice have been associated with higher EE, adding onto the notion that this subtle and contradictory finding may be an artifact. In this context, one should also take into account the extensive debate focusing on the indirect derivation of the EE from gas exchange parameters and its normalization to different body metrics.[27,49,100] In our case, replication in a better-powered experiment would bring more clarity.

HE-Clamp: The HE-clamp in mice on HFD did not reveal a difference in insulin sensitivity between LINKO mice and WT controls, as approximated through the GIR. Contrasting this, INKO mice as well as mice undergoing siRNA-mediated $_{m}$INDY knockdown and rats with an ASO-based $_{m}$INDY-knockdown showed elevated insulin sensitivity relative to their respective controls.[27,58,59] While we did not observe a similarly marked effect of our knockdown on insulin sensitivity, our finding of significantly elevated glucose clearance and glycogen anabolism during the clamp interval in LINKO mice indicates a stronger response to hyperinsulinemia in LINKO mice at least in some measures. Meanwhile, we did not observe suppressed endogenous glucose production as reported by others.[27,58,59] In line with Brachs and colleagues, we also did not observe significant differences in tissue-specific uptake of 2-DG or differences in plasma levels of free fatty acids, contrasting strongly the marked phenotype reported in INKO mice.[27,59]

Taken together, LINKO mice showed an elevated response to hyperinsulinemia in some parameters, but the least pronounced comprehensive phenotype when compared to the other published models. Possible reasons for this might be inherent to the chosen models: as discussed in more detail below (chapter ii6.c.ii), phenotypic differences between knockout and knockdown approaches can be attributed at least partly to differentially regulated mechanisms of compensation and are affected by the timing and completeness of the respective intervention.

Specifically in the case of endogenous glucose production, a likely compensatory role of other organs should be discussed, as especially the kidney is also capable of gluconeogenesis. Consecutively, in the HE-clamp, endogenous glucose production is a

composite of hepatic and extrahepatic glucose synthesis, where hepatic production is generally accountable for more than 70% of total production.[101–103] We can therefore hypothesize that in our model, a compensatory increase of extrahepatic glucose production may have led to a less pronounced suppression of overall endogenous glucose production than in the INKO model. While assessing liver-specific glucose output *in vivo* was beyond the scope of our HE-clamp setup, we conducted a pilot experiment *in vitro* to assess hepatocytes specifically.

Glucose production in LINKO primary hepatocytes: In addition to measurements of glucose production *in vivo*, we determined for the first time glucose production in primary hepatocytes from HFD-fed LINKO mice. INDY has been described to be a downstream mediator of glucagon signaling through the transcription factors CREBP and PPARGC1A, which both modulate gluconeogenesis.[27,44,85,104,105] Thus, measuring glucose production directly in hepatocytes serves to elucidate an apparent contradiction between suppressed HGO as measured in other published models or unaffected HGO as observed in our model, but increased expression of pro-gluconeogenic transcription factors under reduced function of mINDY.

In both experimental groups, glucose production was highest in cells stimulated with pyruvate and glutamate as substrates, the effect being driven by pyruvate. This difference goes in line with the number of enzymatic steps involved, as glutamate requires deamination as well as processing through the TCA cycle, while pyruvate requires only one enzymatic step to be transformed into oxaloacetate, which is then used as substrate for gluconeogenesis in the cytosol – leading to a higher degree of rate control by pyruvate.[106]

Surprisingly, our *in vitro*-assay showed an increased capacity for glucose production in LINKO primary hepatocytes upon stimulation with glucagon, contrasting the observations from our own and other published HE-clamp experiments.[27,58,59] On a cellular level, the *in vitro* controlled conditions may have unmasked an effect that was overridden in the animal models: Intracellular abundance of citrate plays a role in regulating gluconeogenesis, citrate being an activator of the rate-limiting enzyme, fructose-1,6-bisphosphatase.[107] After an overnight fast, WT animals are likely better able to supplement cytosolic citrate levels from blood plasma than their KO counterparts, as has been suggested by reduced *in vitro* uptake

of [^{14}C]-labeled citrate in $_{m}$INDY-knockdown HEK-293 cells, as well as decreased capacity for fatty acid synthesis in INKO mice.[27,36,59] Following this paradigm, INKO animals may have to rely more heavily on intracellular citrate synthesis from substrates derived from lipid and/or protein degradation, thereby connecting intracellular citrate abundance to the cellular, not whole-body, state of nutrition.[107] With INKO mice consistently displaying lower concentrations of intrahepatic lipid stores, it would therefore come as no surprise that their tendency towards gluconeogenesis is lowered as well.[27,36]

In absence of citrate *in vitro*, however, the higher levels of glucose production in LINKO primary hepatocytes may be due to compensatory upregulation of anabolic and/or transport processes, especially those that increase intracellular citrate production from TCA cycle intermediates – such as pyruvate carboxylase activity, leading to more efficient utilization of metabolites contained in the culture medium for gluconeogenesis. As reported elsewhere, increased capacity for glucose production correlates with improved mitochondrial oxidative function - an aspect we could hypothesize to hold true in our setting as well, especially as INKO livers showed markedly elevated oxidative capacity in mitochondria.[27,108] In this pilot experiment, we could not assess gene expression in the plated cells to address these differences more thoroughly; this aspect clearly needs to be elucidated further, alongside substrate-specific uptake studies in INKO and LINKO primary hepatocytes.

Gene expression: We observed near-complete suppression of $_{m}$INDY expression in liver samples of HFD-fed LINKO mice. The remaining mRNA signal can be attributed to cells within the liver that suppress the albumin promotor and are thus not affected by an albumin-Cre mediated knockout, such as endothelium, Kupffer or bile duct cells.[109] In line with the findings by Birkenfeld and colleagues, SLC13A3 showed no upregulation in HFD mice. The closest member of the carboxylate transporter family, SLC13A3, was upregulated in INKO mice under NCD, but not under HFD conditions.[27]

In our gene expression panel, we observed several genes differentially expressed: NRF1 is a regulatory peptide involved in mitochondrial respiration and has been shown to exert protective effects against NAFLD, NASH and hepatic neoplasia in mice.[110,111] CPT1A, a downstream mediator of PPARGC-1A, is a key rate-limiting enzyme of fatty acid oxidation, inducible through physical activity and again protective of NAFLD.[112] ACADM, a

dehydrogenase also involved in fatty acid oxidation, exerts an important role in energy homeostasis in a catabolic state and under caloric challenge.[113] SIRT1, a deacetylase, has been associated with protective functions against oxidative and inflammatory stress, mediating a life-prolonging effect akin to caloric restriction.[114,115] DNAJB9 acts as cochaperone within the endoplasmic reticulum, suppressing proapoptotic signaling in the unfolded-protein response.[116,117] The transcription factor XBP1 is also activated as part of the UPR and exerts a multitude of functions, including increased insulin sensitivity, aiming to maintain intracellular homeostasis.[118–120] Taken together, while only delivering a broad image, these findings point towards a broadly hepatoprotective effect of the LINKO model against hypercaloric stress, even in the absence of a strong metabolic phenotype.

ii. Comparable studies

During and after our research, several studies have targeted $_{m}$INDY in mice and rats pharmacologically. Out of these, two approaches were liver-specific and thus apply for direct comparison with our conditional knockout approach.

A 4-week-long treatment course with 2′-O-methoxyethyl chimeric antisense oligonucleotides (ASOs) in rats fed on HFD suppressed hepatic $_{m}$INDY expression by 91%. Similar to our study, no effects on body weight could be observed; however, plasma markers indicated a beneficial metabolic phenotype: Fasting plasma insulin and triglyceride levels were reduced by 74% and 35%, respectively, in ASO-treated rats. In HE-clamp experiments, both hepatic triglyceride content and hepatic glucose production were markedly suppressed by 25%. While fasting plasma glucose concentration also tended to be lower in knockdown animals, the effect did not reach statistical significance. To summarize, rats receiving the liver-specific ASOs showed a phenotype of elevated insulin sensitivity and protection against hepatic steatosis.[58]

Another study subjected HFD-fed mice to an 8-week course of liver-selective anti-$_{m}$INDY small inhibitory RNA (siRNA) injections.[59] While the knockdown in this study was less effective (61%), it still produced a metabolic phenotype. In accordance with our study, no differences in body weight and body composition were observed. In indirect calorimetry, energy expenditure, RER, locomotor activity and caloric intake showed no significant differences; this contrasts our findings with slightly but significantly increased energy

expenditure and RER in LINKO mice on HFD. Also, similarly to our findings, ipGTT produced no differences in blood glucose and insulin levels, and HOMA-IR after an overnight fast was similar between the groups. HE-clamp experiments showed a suppressed endogenous glucose production and a non-significant trend towards higher GIR in the siRNA group, with all uptake parameters not differing between the groups. This closely mirrors our findings. Lastly, the study showed lower liver lipid concentrations and a 10% lower liver weight, again indicating a protective effect of mINDY knockdown against hepatic steatosis in two measures outside of our work's scope.[59]

Taken together, these findings suggest that liver-targeted approaches to suppress mINDY cause a protective phenotype against some liver-related metabolic pathologies, while not reproducing the striking metabolic phenotype seen in the whole-body INKO model. However, differences between these studies and ours should be highlighted: The model by Pesta and colleagues was based on rats instead of mice and used larger experimental groups.[58] Additionally, in both interventional studies, mice were subjected to their respective diet intervention and mINDY knockdown at a higher degree of maturity (400g body weight in rats and 8 weeks of age in mice, respectively), while our study increasingly suppressed mINDY from the time at which the albumin promotor gains activity during the fetal stage.[58,59] More precisely, recombination via albumin-Cre was reported to be 40% efficient at birth, 75% efficient after 3 weeks and complete by 6 weeks of age.[109,121]

Comparing the findings from these studies with our own, we observed that liver-specific targeting of mINDY through a knockout progressively effective from birth caused a more subtle metabolic phenotype than posttranscriptional knockdown interventions at later points of life. This observation, while surprising, is in accordance with a line of evidence of genetic compensation in mammals, in which knockdowns, despite targeting the same gene loci, yielded more pronounced phenotypes than knockouts.[122–124] With several mechanisms proposed, the common threads are that a) genetic expression changes tend to be triggered through mutated DNA (and thus, knockout) rather than through knockdown, which occurs further downstream at the mRNA level; and b) there may be off-target, uncharacterized effects of the mutant mRNA as well as the molecules used for knockdown (e.g. siRNA, ASOs).[125] In our case, compensatory regulation for mINDY's lost transport capacity might

involve other membrane carboxylate transporters with lower affinities for citrate such as SLC13A3; also, mINDY itself may be upregulated in other tissues for compensation, which was not a possibility in the INKO model.[27] While we assessed mINDY expression in different organs (data not shown), we could not find any statistically significant upregulations, leaving the possibility that a more subtle compensatory upregulation throughout several organs may have evaded the sensitivity of our RealTime-qPCR-based approach. Possible ectopic functions of mutant mRNA and system effects of knockdown mediators were controlled for, but not characterized in the above-mentioned studies related to liver-specific mINDY inhibition.[58,59]

The fact that all approaches of liver-specific suppression of mINDY to date did not fully replicate the INKO metabolic phenotype, but recreated some aspects of it under the condition of diet-induced obesity, indicates clearly that the transporter mediates its effects only partly through the liver but has yet uncharacterized metabolic functions in other organs. Such a network effect of citrate metabolism with relevance for the whole-body metabolic phenotype might involve citrate's known role as an intermediary metabolite, as well as a likely, but largely unstudied role in neuronal metabolism: mINDY is known to be highly expressed in some parts of the central nervous system including the cerebral cortex, hypothalamus, cerebellum, olfactory bulb and possibly glia, but its role in CNS physiology and metabolic regulation has not yet been characterized.[25,30,34]

While a more detailed assessment of biochemistry and molecular metabolism was not within the scope of this work, a fuller picture with regard to the other liver-specific interventional studies would have resulted from including plasma and liver lipid analyses, comprehensive quantitative expression studies of mINDY and related transporters using next-generation sequencing, as well as uptake studies using [^{14}C]-labelled citrate, and ex-vivo metabolic assessments of different organs. Also, current efforts are directed towards dissecting mINDY's role in the central nervous system.

In summary, our approach to target mINDY specifically in the liver yielded less pronounced metabolic outcomes than the comparable studies discussed above. Also, all liver-targeted approaches could not replicate the metabolic phenotype caused by a full-body knockout of mINDY. However, even the mild effects associated with liver-specific targeting of mINDY

warrant current efforts of translation into humans: increased insulin sensitivity and protection from hepatic steatosis are, if they translate to humans, of great interest in the prevention or treatment of T2DM and NASH. Recently, loss-of-function mutations in human SLC13A5 were associated with a form of neonatal epileptic encephalopathy.[126] While it is to be confirmed whether a pharmacological targeting of mINDY in humans would also carry an epileptogenic potential, a liver-specific approach may be especially tempting in order to harvest this promising target's benefits while circumventing its potential risks.

7. Summary

Background: To counter the fast-growing global prevalence of type 2 diabetes mellitus (T2DM) and metabolic disease more effectively, increased preventive efforts as well as the development of novel therapeutic strategies are needed. In the search of new pharmacological targets, monogenic modulators of whole-body energy homeostasis are especially promising. A decreased expression of the carboxylate transporter SLC13A5 (INDY, I'm not dead yet) and its orthologues is associated with a beneficial metabolic phenotype and prolonged life-expectancy across species, including *C. elegans, D. melanogaster* and mice: In a pioneering study, a whole-body knockout of the mammalian INDY orthologue ($_m$INDY) in mice was observed to cause a metabolic phenotype comparable to caloric restriction, leading to an increase in life expectancy as well as protection from obesity, insulin resistance and hepatic steatosis; several studies have since underlined these findings, making $_m$INDY a putative target for future pharmacological interventions against metabolic disease.[24,26–29] To date, however, INDY's molecular mechanism has not been fully elucidated, and a main effector organ for its physiological role in metabolism, if existent, is yet to be found. High expression of the $_m$INDY transcript in liver tissue provides ground for the hypothesis that its contribution to energy homeostasis may be caused by a physiological role in hepatocyte intermediary metabolism.

Research Question: To what extent is the protective effect of reduced $_m$INDY function on murine whole-body metabolism mediated by its expression in the liver?

Hypothesis: A liver-specific conditional knockout of $_m$INDY in mice contributes to beneficial metabolic effects akin to those observed in whole-body knockout models of $_m$INDY.

Methods: We generated a liver-specific conditional $_m$INDY knockout (LINKO) mouse and performed metabolic phenotyping including body composition, glucose tolerance tests, indirect calorimetry, and hyperinsulinemic-euglycemic clamp over a 16-week period across three dietary conditions of differing caloric content. We assessed capacity for glucose production in primary hepatocytes derived from LINKO mice and screened for gene expression changes in LINKO liver samples.

Results: There were no differences in body weight or length between LINKO homozygotes and WT controls under all three diet conditions. No differences between genotypes were observed in body composition and intraperitoneal glucose tolerance tests. In hyperinsulinemic-euglycemic clamps, LINKO mice showed no difference in GIR. However, increases in clamp glucose clearance and glycogen synthesis, as well as a decrease in glycolysis were observed. Indirect calorimetry yielded conflicting results, with LINKO homozygotes in the HFD group showing an increased energy expenditure, but LINKO homozygotes in the HFD+S group showing a decreased energy expenditure relative to the respective wildtype groups, after adjustment for covariates. Respiratory exchange ratio was slightly, but significantly higher in LINKO homozygotes compared to wildtype controls in the HFD group and nearing significance in the HFD+S group, suggesting a slight shift towards carbohydrate catabolism. In cultured primary hepatocytes, LINKO homozygous samples displayed increased capacity for glucose production by 39.1%, as measured by glucose in supernatant normalized to protein count. Gene expression analysis yielded increased expression of genes implicated in mitochondrial function and unfolded protein response, but no differences in genes related to lipid or glucose metabolism and inflammation.

Conclusion: We showed that a liver-specific conditional knockout of the mammalian INDY orthologue in mice (LINKO) produced a mild protective metabolic phenotype in diet-induced obesity, but did not sufficiently replicate the phenotype seen in full-body knockout models, suggesting that the interorgan crosstalk between liver and other organs, such as skeletal muscle, adipose tissue, brain and kidney seems to be required to generate the complete beneficial phenotype. As recent studies targeting hepatic $_{m}$INDY by different interventions yielded stronger phenotypes, interventional, liver-specific antagonism of $_{m}$INDY may, nevertheless, represent an attractive target for pharmacological interventions. However, more studies in different organ systems, especially the central nervous system, are needed for a comprehensive understanding of $_{m}$INDY's role in metabolism and in order to pave the way towards $_{m}$INDY's use for the treatment and/or prevention of diabetes and NAFLD.

8. References

1. Skyler JS, Bakris GL, Bonifacio E, Darsow T, Eckel RH, Groop L, Groop PH, Handelsman Y, Insel RA, Mathieu C, McElvaine AT, Palmer JP, Pugliese A, Schatz DA, Sosenko JM, Wilding JPH, Ratner RE. Differentiation of diabetes by pathophysiology, natural history, and prognosis. *Diabetes*. 2017;66(2):241-255. doi:10.2337/db16-0806

2. Forbes JM, Fotheringham AK. Vascular complications in diabetes: old messages, new thoughts. *Diabetologia*. 2017;60(11):2129-2138. doi:10.1007/s00125-017-4360-x

3. GLOBAL REPORT ON DIABETES*. WHO Library* 2016;1:20-31. ISBN 978 92 4 156525

4. Zheng Y, Ley SH, Hu FB. Global aetiology and epidemiology of type 2 diabetes mellitus and its complications. *Nat Rev Endocrinol*. 2017;14(2):88-98. doi:10.1038/nrendo.2017.151

5. Gassaway BM, Petersen MC, Surovtseva Y V., Barber KW, Sheetz JB, Aerni HR, Merkel JS, Samuel VT, Shulman GI, Rinehart J. PKCε contributes to lipid-induced insulin resistance through cross talk with p70S6K and through previously unknown regulators of insulin signaling. *Proc Natl Acad Sci U S A*. 2018;115(38):E8996-E9005. doi:10.1073/pnas.1804379115

6. ter Horst KW, Gilijamse PW, Versteeg RI, Ackermans MT, Nederveen AJ, la Fleur SE, Romijn JA, Nieuwdorp M, Zhang D, Samuel VT, Vatner DF, Petersen KF, Shulman GI, Serlie MJ. Hepatic Diacylglycerol-Associated Protein Kinase Cε Translocation Links Hepatic Steatosis to Hepatic Insulin Resistance in Humans. *Cell Rep*. 2017;19(10):1997-2004. doi:10.1016/j.celrep.2017.05.035

7. Samuel VT, Shulman GI. Mechanisms for insulin resistance: common threads and missing links. *Cell*. 2012;148(5):852-871. doi:10.1016/j.cell.2012.02.017

8. Hemmingsen B, Gimenez-Perez G, Mauricio D, Roqué i Figuls M, Metzendorf M-I, Richter B. Diet, physical activity or both for prevention or delay of type 2 diabetes mellitus and its associated complications in people at increased risk of developing type 2 diabetes mellitus. *Cochrane Database Syst Rev*. 2017 Dec 4;12(12):CD003054. doi: 10.1002/14651858.CD003054.pub4.

9. Church TS, Blair SN, Cocreham S, Johannsen N, Johnson W, Kramer K, Mikus CR, Myers V, Nauta M, Rodarte RQ, Sparks L, Thompson A, Earnest CP. Effects of aerobic and resistance training on hemoglobin A1c levels in patients with type 2 diabetes: A randomized controlled trial. *JAMA - J Am Med Assoc*. 2010;304(20):2253-2262. doi:10.1001/jama.2010.1710

10. Balk EM, Earley A, Raman G, Avendano EA, Pittas AG, Remington PL. Combined diet and physical activity promotion programs to prevent type 2 diabetes among persons at increased risk: A systematic review for the community preventive services task force. *Ann Intern Med*. 2015;163(6):437-451. doi:10.7326/M15-0452

11. Sumamo Schellenberg E, Dryden DM, Vandermeer B, Ha C, Korownyk C. Lifestyle interventions for patients with and at risk for type 2 diabetes: A systematic review and meta-analysis. *Ann Intern Med*. 2013;159(8):543-551. doi:10.7326/0003-4819-159-8-201310150-00007

12. Meigs JB, Cupples LA, Wilson PW. Parental transmission of type 2 diabetes: the Framingham Offspring Study. *Diabetes*. 2000;49(12):2201-2207.

13. Poulsen P, Kyvik KO, Vaag A, Beck-Nielsen H. Heritability of type II (non-insulin-dependent) diabetes mellitus and abnormal glucose tolerance--a population-based twin study. *Diabetologia*. 1999;42(2):139-145.

14. Kaprio J, Tuomilehto J, Koskenvuo M, Romanov K, Reunanen A, Eriksson J, Stengård J, Kesäniemi YA. Concordance for type 1 (insulin-dependent) and type 2 (non-insulin-dependent) diabetes mellitus in a population-based cohort of twins in Finland. *Diabetologia*. 1992;35(11):1060-1067.

15. Willemsen G, Ward KJ, Bell CG, Christensen K, Bowden J, Dalgård C, Harris JR, Kaprio J, Lyle R, Magnusson PKE, Mather KA, Ordoňana JR, Perez-Riquelme F, Pedersen NL, Pietiläinen KH, Sachdev PS, Boomsma DI, Spector T. The Concordance and Heritability of Type 2 Diabetes in 34,166 Twin Pairs From International Twin Registers: The Discordant Twin (DISCOTWIN) Consortium. *Twin Res Hum Genet*. 2015;18(06):762-771. doi:10.1017/thg.2015.83

16. Fuchsberger C, Flannick J, Teslovich TM, Mahajan A, Agarwala V, Gaulton KJ, Ma C, Fontanillas P, Moutsianas L, McCarthy DJ, Rivas MA, Perry JRB, Sim X, Blackwell TW, Robertson NR, Rayner NW, Cingolani P, Locke AE, Tajes JF, Highland HM, Dupuis J, Chines PS, Lindgren CM, Hartl C, Jackson AU, Chen H, Huyghe JR, van de Bunt M, Pearson RD, Kumar A, Müller-Nurasyid M, Grarup N, Stringham HM, Gamazon ER, Lee J, Chen Y, Scott RA, Below JE, Chen P, Huang J, Go MJ, Stitzel ML, Pasko D, Parker SCJ, Varga TV, Green T, Beer NL, Day-Williams AG, Ferreira T, Fingerlin T, Horikoshi M, Hu C, Huh I, Ikram MK, Kim BJ, Kim Y, Kim YJ, Kwon MS, Lee J, Lee S, Lin KH, Maxwell TJ, Nagai Y, Wang X, Welch RP, Yoon J, Zhang W, Barzilai N, Voight BF, Han BG, Jenkinson CP, Kuulasmaa T, Kuusisto J, Manning A, Ng MCY, Palmer ND, Balkau B, Stančáková A, Abboud HE, Boeing H, Giedraitis V, Prabhakaran D, Gottesman O, Scott J, Carey J, Kwan P, Grant G, Smith JD, Neale BM, Purcell S, Butterworth AS, Howson JMM, Lee HM, Lu Y, Kwak SH, Zhao W, Danesh J, Lam VKL, Park KS, Saleheen D, So WY, Tam CHT, Afzal U, Aguilar D, Arya R, Aung T, Chan E, Navarro C, Cheng CY, Palli D, Correa A, Curran JE, Rybin D, Farook VS, Fowler SP, Freedman BI, Griswold M, Hale DE, Hicks PJ, Khor CC, Kumar S, Lehne B, Thuillier D, Lim WY, Liu J, van der Schouw YT, Loh M, Musani SK, Puppala S, Scott WR, Yengo L, Tan ST, Taylor HA Jr, Thameem F, Wilson G Sr, Wong TY, Njølstad PR, Levy JC, Mangino M, Bonnycastle LL, Schwarzmayr T, Fadista J, Surdulescu GL, Herder C, Groves CJ, Wieland T, Bork-Jensen J, Brandslund I, Christensen C, Koistinen HA, Doney ASF, Kinnunen L, Esko T, Farmer AJ, Hakaste L, Hodgkiss D, Kravic J, Lyssenko V, Hollensted M, Jørgensen ME, Jørgensen T, Ladenvall C, Justesen JM, Käräjämäki A, Kriebel J, Rathmann W, Lannfelt L, Lauritzen T, Narisu N, Linneberg A, Melander O, Milani L, Neville M, Orho-Melander M, Qi L, Qi Q, Roden M, Rolandsson O, Swift A,

Rosengren AH, Stirrups K, Wood AR, Mihailov E, Blancher C, Carneiro MO, Maguire J, Poplin R, Shakir K, Fennell T, DePristo M, de Angelis MH, Deloukas P, Gjesing AP, Jun G, Nilsson P, Murphy J, Onofrio R, Thorand B, Hansen T, Meisinger C, Hu FB, Isomaa B, Karpe F, Liang L, Peters A, Huth C, O'Rahilly SP, Palmer CNA, Pedersen O, Rauramaa R, Tuomilehto J, Salomaa V, Watanabe RM, Syvänen AC, Bergman RN, Bharadwaj D, Bottinger EP, Cho YS, Chandak GR, Chan JCN, Chia KS, Daly MJ, Ebrahim SB, Langenberg C, Elliott P, Jablonski KA, Lehman DM, Jia W, Ma RCW, Pollin TI, Sandhu M, Tandon N, Froguel P, Barroso I, Teo YY, Zeggini E, Loos RJF, Small KS, Ried JS, DeFronzo RA, Grallert H, Glaser B, Metspalu A, Wareham NJ, Walker M, Banks E, Gieger C, Ingelsson E, Im HK, Illig T, Franks PW, Buck G, Trakalo J, Buck D, Prokopenko I, Mägi R, Lind L, Farjoun Y, Owen KR, Gloyn AL, Strauch K, Tuomi T, Kooner JS, Lee JY, Park T, Donnelly P, Morris AD, Hattersley AT, Bowden DW, Collins FS, Atzmon G, Chambers JC, Spector TD, Laakso M, Strom TM, Bell GI, Blangero J, Duggirala R, Tai ES, McVean G, Hanis CL, Wilson JG, Seielstad M, Frayling TM, Meigs JB, Cox NJ, Sladek R, Lander ES, Gabriel S, Burtt NP, Mohlke KL, Meitinger T, Groop L, Abecasis G, Florez JC, Scott LJ, Morris AP, Kang HM, Boehnke M, Altshuler D, McCarthy MI. The genetic architecture of type 2 diabetes. *Nature*. 2016;536(7614):41-47. doi:10.1038/nature18642

17. Steinthorsdottir V, Thorleifsson G, Sulem P, Helgason H, Grarup N, Sigurdsson A, Helgadottir HT, Johannsdottir H, Magnusson OT, Gudjonsson SA, Justesen JM, Harder MN, Jørgensen ME, Christensen C, Brandslund I, Sandbæk A, Lauritzen T, Vestergaard H, Linneberg A, Jørgensen T, Hansen T, Daneshpour MS, Fallah MS, Hreidarsson AB, Sigurdsson G, Azizi F, Benediktsson R, Masson G, Helgason A, Kong A, Gudbjartsson DF, Pedersen O, Thorsteinsdottir U, Stefansson K. Identification of low-frequency and rare sequence variants associated with elevated or reduced risk of type 2 diabetes. *Nat Genet*. 2014;46(3):294-298. doi:10.1038/ng.2882

18. Manning A, Highland HM, Gasser J, Sim X, Tukiainen T, Fontanillas P, Grarup N, Rivas MA, Mahajan A, Locke AE, Cingolani P, Pers TH, Viñuela A, Brown AA, Wu Y, Flannick J, Fuchsberger C, Gamazon ER, Gaulton KJ, Im HK, Teslovich TM, Blackwell TW, Bork-Jensen J, Burtt NP, Chen Y, Green T, Hartl C, Kang HM, Kumar A, Ladenvall C, Ma C, Moutsianas L, Pearson RD, Perry JRB, Rayner NW, Robertson NR, Scott LJ, van de Bunt M, Eriksson JG, Jula A, Koskinen S, Lehtimäki T, Palotie A, Raitakari OT, Jacobs SBR, Wessel J, Chu AY, Scott RA, Goodarzi MO, Blancher C, Buck G, Buck D, Chines PS, Gabriel S, Gjesing AP, Groves CJ, Hollensted M, Huyghe JR, Jackson AU, Jun G, Justesen JM, Mangino M, Murphy J, Neville M, Onofrio R, Small KS, Stringham HM, Trakalo J, Banks E, Carey J, Carneiro MO, DePristo M, Farjoun Y, Fennell T, Goldstein JI, Grant G, Hrabé de Angelis M, Maguire J, Neale BM, Poplin R, Purcell S, Schwarzmayr T, Shakir K, Smith JD, Strom TM, Wieland T, Lindstrom J, Brandslund I, Christensen C, Surdulescu GL, Lakka TA, Doney ASF, Nilsson P, Wareham NJ, Langenberg C, Varga TV, Franks PW, Rolandsson O, Rosengren AH, Farook VS, Thameem F, Puppala S, Kumar S, Lehman DM, Jenkinson CP, Curran JE, Hale DE, Fowler SP, Arya R, DeFronzo RA, Abboud HE, Syvänen AC, Hicks PJ, Palmer ND, Ng MCY,

Bowden DW, Freedman BI, Esko T, Mägi R, Milani L, Mihailov E, Metspalu A, Narisu N, Kinnunen L, Bonnycastle LL, Swift A, Pasko D, Wood AR, Fadista J, Pollin TI, Barzilai N, Atzmon G, Glaser B, Thorand B, Strauch K, Peters A, Roden M, Müller-Nurasyid M, Liang L, Kriebel J, Illig T, Grallert H, Gieger C, Meisinger C, Lannfelt L, Musani SK, Griswold M, Taylor HA Jr, Wilson G Sr, Correa A, Oksa H, Scott WR, Afzal U, Tan ST, Loh M, Chambers JC, Sehmi J, Kooner JS, Lehne B, Cho YS, Lee JY, Han BG, Käräjämäki A, Qi Q, Qi L, Huang J, Hu FB, Melander O, Orho-Melander M, Below JE, Aguilar D, Wong TY, Liu J, Khor CC, Chia KS, Lim WY, Cheng CY, Chan E, Tai ES, Aung T, Linneberg A, Isomaa B, Meitinger T, Tuomi T, Hakaste L, Kravic J, Jørgensen ME, Lauritzen T, Deloukas P, Stirrups KE, Owen KR, Farmer AJ, Frayling TM, O'Rahilly SP, Walker M, Levy JC, Hodgkiss D, Hattersley AT, Kuulasmaa T, Stančáková A, Barroso I, Bharadwaj D, Chan J, Chandak GR, Daly MJ, Donnelly PJ, Ebrahim SB, Elliott P, Fingerlin T, Froguel P, Hu C, Jia W, Ma RCW, McVean G, Park T, Prabhakaran D, Sandhu M, Scott J, Sladek R, Tandon N, Teo YY, Zeggini E, Watanabe RM, Koistinen HA, Kesaniemi YA, Uusitupa M, Spector TD, Salomaa V, Rauramaa R, Palmer CNA, Prokopenko I, Morris AD, Bergman RN, Collins FS, Lind L, Ingelsson E, Tuomilehto J, Karpe F, Groop L, Jørgensen T, Hansen T, Pedersen O, Kuusisto J, Abecasis G, Bell GI, Blangero J, Cox NJ, Duggirala R, Seielstad M, Wilson JG, Dupuis J, Ripatti S, Hanis CL, Florez JC, Mohlke KL, Meigs JB, Laakso M, Morris AP, Boehnke M, Altshuler D, McCarthy MI, Gloyn AL, Lindgren CM. A Low-Frequency Inactivating AKT2 Variant Enriched in the Finnish Population Is Associated With Fasting Insulin Levels and Type 2 Diabetes Risk. *Diabetes*. 2017;66(7):2019-2032. doi:10.2337/db16-1329

19. Hivert M-F, Vassy JL, Meigs JB. Susceptibility to type 2 diabetes mellitus--from genes to prevention. *Nat Rev Endocrinol*. 2014;10(4):198-205. doi:10.1038/nrendo.2014.11

20. McCarthy MI. Biological and translational insights from T2DM genetics. *Nat Rev Endocrinol*. 2017;13(2):71-72. doi:10.1038/nrendo.2016.212

21. Visscher PM, Wray NR, Zhang Q, Sklar P, McCarthy MI, Brown MA, Yang J. 10 Years of GWAS Discovery: Biology, Function, and Translation. *Am J Hum Genet*. 2017;101(1):5-22. doi:10.1016/j.ajhg.2017.06.005

22. White JR. A brief history of the development of diabetes medications. *Diabetes Spectr*. 2014;27(2):82-86. doi:10.2337/diaspect.27.2.82

23. Daniels MA, Kan C, Willmes DM, Ismail K, Pistrosch F, Hopkins D, Mingrone G, Bornstein SR, Birkenfeld AL. Pharmacogenomics in type 2 diabetes: oral antidiabetic drugs. *Pharmacogenomics J*. 2016;16(5):399-410. doi:10.1038/tpj.2016.54

24. Rogina B, Reenan RA, Nilsen SP, Helfand SL. Extended life-span conferred by cotransporter gene mutations in Drosophila. *Science (80-)*. 2000;290(5499):2137-2140.

25. A. Hediger M, Bergeron MJ, Clémençon B, Hediger MA, Markovich D. SLC13 family of Na+-coupled di- and tri-carboxylate/sulfate transporters. *Mol Aspects Med*. 2013;34(2):299-312.

26. Wang P-Y, Neretti N, Whitaker R, Hosier S, Chang C, Lu D, Rogina B, Helfand SL. Long-lived Indy and calorie restriction interact to extend life span. *Proc Natl Acad Sci U S A*. 2009;106(23):9262-9267. doi:10.1073/pnas.0904115106

27. Birkenfeld AL, Lee HY, Guebre-Egziabher F, Alves TC, Jurczak MJ, Jornayvaz FR, Zhang D, Hsiao JJ, Martin-Montalvo A, Fischer-Rosinsky A, Spranger J, Pfeiffer AF, Jordan J, Fromm MF, König J, Lieske S, Carmean CM, Frederick DW, Weismann D, Knauf F, Irusta PM, De Cabo R, Helfand SL, Samuel VT, Shulman GI. Deletion of the Mammalian INDY Homolog Mimics Aspects of Dietary Restriction and Protects against Adiposity and Insulin Resistance in Mice. *Cell Metab.* 2011;5:184-195. doi:10.1016/j.cmet.2011.06.009

28. Anderson RM, Weindruch R. The caloric restriction paradigm: implications for healthy human aging. *Am J Hum Biol*. 2012;24(2):101-106. doi:10.1002/ajhb.22243

29. Schwarz F, Karadeniz Z, Fischer-Rosinsky A, Willmes DM, Spranger J, Birkenfeld AL. Knockdown of Indy/CeNac2 extends Caenorhabditis elegans life span by inducing AMPK/aak-2. *Aging (Albany NY)*. 2015;7(8):553-567. doi:10.18632/aging.100791

30. Inoue K, Zhuang L, Maddox DM, Smith SB, Ganapathy V. Structure, function, and expression pattern of a novel sodium-coupled citrate transporter (NaCT) cloned from mammalian brain. *J Biol Chem*. 2002;277(42):39469-39476.

31. Inoue K, Zhuang L, Ganapathy V. Human Na+-coupled citrate transporter: Primary structure, genomic organization, and transport function. *Biochem Biophys Res Commun*. 2002;299(3):465-471.

32. Inoue K, Fei Y-J, Zhuang L, Gopal E, Miyauchi S, Ganapathy V. Functional features and genomic organization of mouse NaCT, a sodium-coupled transporter for tricarboxylic acid cycle intermediates. *Biochem J*. 2004;378(3):949-957.

33. Pajor AM. Molecular properties of the SLC13 family of dicarboxylate and sulfate transporters. *Pflugers Arch Eur J Physiol*. 2006;451(5):597-605.

34. Willmes DM, Kurzbach A, Henke C, Schumann T, Zahn G, Heifetz A, Jordan J, Helfand SL, Birkenfeld AL. The longevity gene INDY (I'm Not Dead Yet) in metabolic control: Potential as pharmacological target. *Pharmacol Ther*. 2018;185:1-11. doi:10.1016/J.PHARMTHERA.2017.10.003

35. Markovich D, Murer H. The SLC13 gene family of sodium sulphate/carboxylate cotransporters. *Pflugers Arch Eur J Physiol*. 2004;447(5):594-602.

36. Mancusso R, Gregorio GG, Liu Q, Wang D-N. Structure and mechanism of a bacterial sodium-dependent dicarboxylate transporter. *Nature*. 2012;491(7425):622-626.

37. Zhang FF, Pajor AM. Topology of the Na(+)/dicarboxylate cotransporter: the N-terminus and hydrophilic loop 4 are located intracellularly. *Biochim Biophys Acta*. 2001;1511(1):80-89. doi:10.1016/s0005-2736(00)00385-0

38. Pajor AM. Sodium-coupled dicarboxylate and citrate transporters from the SLC13 family. *Pflugers Arch*. 2014 Jan;466(1):119-30. doi: 10.1007/s00424-013-1369-y.

39. Gopal E, Miyauchi S, Martin PM, Ananth S, Srinivas SR, Smith SB, Prasad PD, Ganapathy V. Expression and functional features of NaCT, a sodium-coupled citrate transporter, in human and rat livers and cell lines. *Am J Physiol Gastrointest Liver Physiol*. 2007;292(1):G402-8. doi:10.1152/ajpgi.00371.2006

40. Gopal E, Miyauchi S, Martin PM, Ananth S, Srinivas SR, Smith SB, Prasad PD, Ganapathy V. Expression and functional features of NaCT, a sodium-coupled citrate transporter, in human and rat livers and cell lines. *Am J Physiol - Gastrointest Liver Physiol*. 2007;292(1):G402-G408.

41. Yodoya E, Wada M, Shimada A, Katsukawa H, Okada N, Yamamoto A, Ganapathy V, Fujita T. Functional and molecular identification of sodium-coupled dicarboxylate transporters in rat primary cultured cerebrocortical astrocytes and neurons. *J Neurochem*. 2006;97(1):162-173.

42. Kekuda R, Wang H, Huang W, Pajor AM, Leibach FH, Devoe LD, Prasad PD, Ganapathy V. Primary structure and functional characteristics of a mammalian sodium-coupled high affinity dicarboxylate transporter. *J Biol Chem*. 1999;274(6):3422-3429.

43. Wang P-Y, Neretti N, Whitaker R, Hosier S, Chang C, Lu D, Rogina B, Helfand SL. Long-lived Indy and calorie restriction interact to extend life span. *Proc Natl Acad Sci U S A*. 2009;106(23):9262-9267. doi:10.1073/pnas.0904115106.

44. Neuschäfer-Rube F, Lieske S, Kuna M, Henkel J, Perry RJ, Erion DM, Pesta D, Willmes DM, Brachs S, von Loeffelholz C, Tolkachov A, Schupp M, Pathe-Neuschäfer-Rube A, Pfeiffer AFH, Shulman GI, Püschel GP, Birkenfeld AL. The mammalian INDY homolog is induced by CREB in a rat model of type 2 diabetes. *Diabetes*. 2014;63(3):1048-1057. doi:10.2337/db13-0749

45. Von Loeffelholz C, Lieske S, Neuschäfer-Rube F, Willmes DM, Raschzok N, Sauer IM, König J, Fromm MF, Horn P, Chatzigeorgiou A, Pathe-Neuschäfer-Rube A, Jordan J, Pfeiffer AFH, Mingrone G, Bornstein SR, Stroehle P, Harms C, Wunderlich FT, Helfand SL, Bernier M, de Cabo R, Shulman GI, Chavakis T, Püschel GP, Birkenfeld AL. The Human Longevity Gene Homolog INDY and Interleukin-6 Interact in Hepatic Lipid Metabolism. *Hepatology*. 2017;66(2):616-630. doi:10.1002/hep.29089

46. Harford KA, Reynolds CM, McGillicuddy FC, Roche HM. Fats, inflammation and insulin resistance: insights to the role of macrophage and T-cell accumulation in adipose tissue. *Proc Nutr Soc*. 2011;70(4):408-417. doi:10.1017/S0029665111000565

47. Berglund ED, Li CY, Poffenberger G, Ayala JE, Fueger PT, Willis SE, Jewell MM, Powers AC, Wasserman DH. Glucose metabolism in vivo in four commonly used inbred mouse strains. *Diabetes*. 2008;57(7):1790-1799. doi:10.2337/db07-1615

48. Weir JBDB. New methods for calculating metabolic rate with special reference to

protein metabolism. *J Physiol*. 1949;109(1-2):1-9. doi:10.1113/jphysiol.1949.sp004363

49. Tschöp MH, Speakman JR, Arch JR, Auwerx J, Brüning JC, Chan L, Eckel RH, Farese RV Jr, Galgani JE, Hambly C, Herman MA, Horvath TL, Kahn BB, Kozma SC, Maratos-Flier E, Müller TD, Münzberg H, Pfluger PT, Plum L, Reitman ML, Rahmouni K, Shulman GI, Thomas G, Kahn CR, Ravussin E. A guide to analysis of mouse energy metabolism. *Nat Methods.* 2011 Dec 28;9(1):57-63. doi: 10.1038/nmeth.1806.

50. Camporez JPG, Jornayvaz FR, Lee H-Y, Kanda S, Guigni BA, Kahn M, Samuel VT, Carvalho CRO, Petersen KF, Jurczak MJ, Shulman GI. Cellular Mechanism by Which Estradiol Protects Female Ovariectomized Mice From High-Fat Diet-Induced Hepatic and Muscle Insulin Resistance. *Endocrinology*. 2013;154(3):1021-1028. doi:10.1210/en.2012-1989

51. Brawerman G, Mendecki J, Lee SY. A procedure for the isolation of mammalian messenger ribonucleic acid. *Biochemistry*. 1972;11(4):637-641.

52. Rio DC, Ares M, Hannon GJ, Nilsen TW. Purification of RNA using TRIzol (TRI reagent). *Cold Spring Harb Protoc*. 2010;2010(6):pdb.prot5439. doi:10.1101/pdb.prot5439

53. Surwit RS, Kuhn CM, Cochrane C, McCubbin JA, Feinglos MN. Diet-induced type II diabetes in C57BL/6J mice. *Diabetes*. 1988;37(9):1163-1167. doi:10.2337/diab.37.9.1163

54. Flurkey K, Currer J, Harrison D. Mouse models in aging research. *American College of Laboratory Animal Medicine Volume III, 2007, 637-672.* https://doi.org/10.1016/B978-012369454-6/50074-1

55. Kim H, Kim M, Im S-K, Fang S. Mouse Cre-LoxP system: general principles to determine tissue-specific roles of target genes. *Lab Anim Res*. 2018;34(4):147-159. doi:10.5625/lar.2018.34.4.147

56. Postic C, Shiota M, Niswender KD, Jetton TL, Chen Y, Moates JM, Shelton KD, Lindner J, Cherrington AD, Magnuson MA. Dual roles for glucokinase in glucose homeostasis as determined by liver and pancreatic beta cell-specific gene knock-outs using Cre recombinase. *J Biol Chem*. 1999;274(1):305-315. doi:10.1074/jbc.274.1.305

57. Miyasaka Y, Uno Y, Yoshimi K, Kunihiro Y, Yoshimura T, Tanaka T, Ishikubo H, Hiraoka Y, Takemoto N, Tanaka T, Ooguchi Y, Skehel P, Aida T, Takeda J, Mashimo T. CLICK: one-step generation of conditional knockout mice. *BMC Genomics*. 2018;19(1):318. doi:10.1186/s12864-018-4713-y

58. Pesta DH, Perry RJ, Guebre-Egziabher F, Zhang D, Jurczak M, Fischer-Rosinsky A, Daniels MA, Willmes DM, Bhanot S, Bornstein SR, Knauf F, Samuel VT, Shulman GI, Birkenfeld AL. Prevention of diet-induced hepatic steatosis and hepatic insulin resistance by second generation antisense oligonucleotides targeted to the longevity gene mIndy (Slc13a5). *Aging (Albany NY)*. 2015;7(12):1086-1093. doi:10.18632/aging.100854

59. Brachs S, Winkel AF, Tang H, Birkenfeld AL, Brunner B, Jahn-Hofmann K, Margerie D, Ruetten H, Schmoll D, Spranger J. Inhibition of citrate cotransporter Slc13a5/mINDY by RNAi improves hepatic insulin sensitivity and prevents diet-induced non-alcoholic fatty liver disease in mice. *Mol Metab*. 2016;5(11):1072-1082. doi:10.1016/J.MOLMET.2016.08.004

60. Thibault L. Animal Models of Dietary-Induced Obesity. *Anim Model Study Hum Dis*. Published online January 1, 2013:277-303. doi:10.1016/B978-0-12-415894-8.00013-0

61. Heydemann A. An Overview of Murine High Fat Diet as a Model for Type 2 Diabetes Mellitus. *J Diabetes Res*. 2016;2016. doi:10.1155/2016/2902351

62. Ito M, Suzuki J, Tsujioka S, Sasaki M, Gomori A, Shirakura T, Hirose H, Ito M, Ishihara A, Iwaasa H, Kanatani A. Longitudinal analysis of murine steatohepatitis model induced by chronic exposure to high-fat diet. *Hepatol Res*. 2007;37(1):50-57. doi:10.1111/j.1872-034X.2007.00008.x

63. Ishimoto T, Lanaspa MA, Rivard CJ, Roncal-Jimenez CA, Orlicky DJ, Cicerchi C, McMahan RH, Abdelmalek MF, Rosen HR, Jackman MR, MacLean PS, Diggle CP, Asipu A, Inaba S, Kosugi T, Sato W, Maruyama S, Sánchez-Lozada LG, Sautin YY, Hill JO, Bonthron DT, Johnson RJ. High-fat and high-sucrose (western) diet induces steatohepatitis that is dependent on fructokinase. *Hepatology*. 2013 Nov;58(5):1632-43. doi: 10.1002/hep.26594.

64. Tetri LH, Basaranoglu M, Brunt EM, Yerian LM, Neuschwander-Tetri BA. Severe NAFLD with hepatic necroinflammatory changes in mice fed trans fats and a high-fructose corn syrup equivalent. *Am J Physiol - Gastrointest Liver Physiol*. 2008;295(5). doi:10.1152/ajpgi.90272.2008

65. Hohlbaum K, Bert B, Dietze S, Palme R, Fink H, Thöne-Reineke C. Impact of repeated anesthesia with ketamine and xylazine on the well-being of C57BL/6JRj mice. *PLoS One*. 2018;13(9):e0203559. doi:10.1371/journal.pone.0203559

66. Hohlbaum K, Bert B, Dietze S, Palme R, Fink H, Thöne-Reineke C. Severity classification of repeated isoflurane anesthesia in C57BL/6JRj mice-Assessing the degree of distress. *PLoS One*. 2017;12(6):e0179588. doi:10.1371/journal.pone.0179588

67. Kikuchi T, Tan H, Mihara T, Uchimoto K, Mitsushima D, Takase K, Morita S, Goto T, Andoh T, Kamiya Y. Effects of volatile anesthetics on the circadian rhythms of rat hippocampal acetylcholine release and locomotor activity. *Neuroscience*. 2013;237:151-160. doi:10.1016/J.NEUROSCIENCE.2013.01.062

68. Yonezaki K, Uchimoto K, Miyazaki T, Asakura A, Kobayashi A, Takase K, Goto T. Postanesthetic effects of isoflurane on behavioral phenotypes of adult male C57BL/6J mice. *PLoS One*. 2015;10(3):e0122118. doi:10.1371/journal.pone.0122118

69. Li M, Vassiliou CC, Colucci LA, Cima MJ. ^{1}H nuclear magnetic resonance (NMR) as a tool to measure dehydration in mice. *NMR Biomed*. 2015;28(8):1031-1039. doi:10.1002/nbm.3334

70. Bakermans AJ, Abdurrachim D, Moonen RPM, Motaal AG, Prompers JJ, Strijkers GJ, Vandoorne K, Nicolay K. Small animal cardiovascular MR imaging and spectroscopy. *Prog Nucl Magn Reson Spectrosc*. 2015;88-89:1-47. doi:10.1016/J.PNMRS.2015.03.001

71. Halldorsdottir S, Carmody J, Boozer CN, Leduc CA, Leibel RL. Reproducibility and accuracy of body composition assessments in mice by dual energy x-ray absorptiometry and time domain nuclear magnetic resonance. *Int J Body Compos Res*. 2009;7(4):147-154.

72. Tinsley FC, Taicher GZ, Heiman ML. Evaluation of a Quantitative Magnetic Resonance Method for Mouse Whole Body Composition Analysis. *Obes Res*. 2004;12(1):150-160. doi:10.1038/oby.2004.20

73. Toye AA, Lippiat JD, Proks P, Shimomura K, Bentley L, Hugill A, Mijat V, Goldsworthy M, Moir L, Haynes A, Quarterman J, Freeman HC, Ashcroft FM, Cox RD. A genetic and physiological study of impaired glucose homeostasis control in C57BL/6J mice. *Diabetologia*. 2005;48(4):675-686. doi:10.1007/s00125-005-1680-z

74. Muniyappa R, Lee S, Chen H, Quon MJ. Current approaches for assessing insulin sensitivity and resistance in vivo: advantages, limitations, and appropriate usage. *Am J Physiol Endocrinol Metab*. 2008;294:15-26. doi:10.1152/ajpendo.00645.2007.-Insulin

75. Samuel VT, Obici S, Croniger CM, Shulman GI, McGuinness OP, Morton GJ, Wasserman DH, Ayala JE. Standard operating procedures for describing and performing metabolic tests of glucose homeostasis in mice. *Dis Model Mech*. 2010;3(9-10):525-534. doi:10.1242/dmm.006239

76. Andrikopoulos S, Blair AR, Deluca N, Fam BC, Proietto J. Evaluating the glucose tolerance test in mice. *Am J Physiol Metab*. 2008;295(6):E1323-E1332. doi:10.1152/ajpendo.90617.2008

77. Ayala JE, Bracy DP, McGuinness OP, Wasserman DH. Considerations in the design of hyperinsulinemic-euglycemic clamps in the conscious mouse. *Diabetes*. 2006;55(2):390-397. doi:10.2337/diabetes.55.02.06.db05-0686

78. McGuinness OP, Ayala JE, Laughlin MR, Wasserman DH. NIH experiment in centralized mouse phenotyping: The Vanderbilt experience and recommendations for evaluating glucose homeostasis in the mouse. *Am J Physiol - Endocrinol Metab*. 2009;297(4). doi:10.1152/ajpendo.90996.2008

79. Melanson EL, Ingebrigtsen JP, Bergouignan A, Ohkawara K, Kohrt WM, Lighton JRB. A new approach for flow-through respirometry measurements in humans. *Am J Physiol Regul Integr Comp Physiol*. 2010;298(6):R1571-9. doi:10.1152/ajpregu.00055.2010

80. Frayn KN. Calculation of substrate oxidation rates in vivo from gaseous exchange. *J Appl Physiol Respir Environ Exerc Physiol.* 1983;55(2):628-634. doi:10.1152/jappl.1983.55.2.628

81. Even PC, Mokhtarian A, Pele A. Practical aspects of indirect calorimetry in laboratory animals. *Neurosci Biobehav Rev.* 1994;18(3):435-447. doi:10.1016/0149-7634(94)90056-6

82. DeFronzo RA, Tobin JD, Andres R. Glucose clamp technique: a method for quantifying insulin secretion and resistance. *Am J Physiol*. 1979;237(3):E214-23. doi:10.1152/ajpendo.1979.237.3.E214

83. Brown ET, Umino Y, Loi T, Solessio E, Barlow R. Anesthesia can cause sustained hyperglycemia in C57/BL6J mice. *Vis Neurosci*. 2005;22(5):615-618. doi:10.1017/S0952523805225105

84. Jurczak MJ, Lee HY, Birkenfeld AL, et al. SGLT2 deletion improves glucose homeostasis and preserves pancreatic beta-cell function. *Diabetes.* 2011;60(3):890-898. doi:10.2337/db10-1328

85. Herzig S, Long F, Jhala US, Hedrick S, Quinn R, Bauer A, Rudolph D, Schutz G, Yoon C, Puigserver P, Spiegelman B, Montminy M. CREB regulates hepatic gluconeogenesis through the coactivator PGC-1. *Nature*. 2001;413(6852):179-183. doi:10.1038/35093131

86. Taddeo EP, Hargett SR, Lahiri S, Nelson ME, Liao JA, Li C, Slack-Davis JK, Tomsig JL, Lynch KR, Yan Z, Harris TE, Hoehn KL. Lysophosphatidic acid counteracts glucagon-induced hepatocyte glucose production via STAT3. *Sci Rep*. 2017;7(1). doi:10.1038/s41598-017-00210-y

87. Bustin SA, Benes V, Garson JA, Hellemans J, Huggett J, Kubista M, Mueller R, Nolan T, Pfaffl MW, Shipley GL, Vandesompele J, Wittwer CT. The MIQE guidelines: Minimum information for publication of quantitative real-time PCR experiments. *Clin Chem*. 2009;55(4):611-622. doi:10.1373/clinchem.2008.112797

88. Hupe M, Li MX, Gertow Gillner K, Adams RH, Stenman JM. Evaluation of TRAP-sequencing technology with a versatile conditional mouse model. *Nucleic Acids Res*. 2014;42(2). doi:10.1093/nar/gkt995

89. Heiman M, Kulicke R, Fenster RJ, Greengard P, Heintz N. Cell type-specific mRNA purification by translating ribosome affinity purification (TRAP). *Nat Protoc*. 2014;9(6):1282-1291. doi:10.1038/nprot.2014.085

90. Wang AW, Wangensteen KJ, Wang YJ, Zahm AM, Moss NG, Erez N, Kaestner KH. TRAP-seq identifies cystine/glutamate antiporter as a driver of recovery from liver injury. *J Clin Invest*. 2018;128(6):2297-2309. doi:10.1172/JCI95120

91. Ballinger GA. Using Generalized Estimating Equations for Longitudinal Data Analysis. *Organ Res Methods*. 2004;7(2):127-150. doi:10.1177/1094428104263672

92. Zeger SL, Liang KY. Longitudinal data analysis for discrete and continuous outcomes. *Biometrics.* 1986 Mar;42(1):121-30. PMID: 3719049.

93. Zeger SL, Liang KY, Albert PS. Models for longitudinal data: a generalized estimating equation approach. *Biometrics.* 1988 Dec;44(4):1049-60. Erratum in: Biometrics 1989 Mar;45(1):347. PMID: 3233245.

94. Su CW, Chen CY, Li Y, Long SR, Massey W, Kumar DV, Walker WA, Shi HN. Helminth infection protects against high fat diet-induced obesity via induction of alternatively activated macrophages. *Sci Rep*. 2018;8(1):4607. doi:10.1038/s41598-018-22920-7

95. Heinonen I, Rinne P, Ruohonen ST, Ruohonen S, Ahotupa M, Savontaus E. The effects of equal caloric high fat and western diet on metabolic syndrome, oxidative stress and vascular endothelial function in mice. *Acta Physiol*. 2014;211(3):515-527. doi:10.1111/apha.12253

96. Hu S, Wang L, Yang D, Li L, Togo J, Wu Y, Liu Q, Li B, Li M, Wang G, Zhang X, Niu C, Li J, Xu Y, Couper E, Whittington-Davies A, Mazidi M, Luo L, Wang S, Douglas A, Speakman JR. Dietary Fat, but Not Protein or Carbohydrate, Regulates Energy Intake and Causes Adiposity in Mice. *Cell Metab.* 2018 Sep 4;28(3):415-431.e4. doi: 10.1016/j.cmet.2018.06.010.

97. Schober P, Bossers SM, Schwarte LA. Statistical significance versus clinical importance of observed effect sizes: What do p values and confidence intervals really represent? *Anesth Analg*. 2018;126(3):1068-1072. doi:10.1213/ANE.0000000000002798

98. Van Calster B, Steyerberg EW, Collins GS, Smits T. Consequences of relying on statistical significance: Some illustrations. *Eur J Clin Invest*. 2018;48(5). doi:10.1111/eci.12912

99. Lytsy P. P in the right place: Revisiting the evidential value of P-values. *J Evid Based Med*. 2018;11(4):288-291. doi:10.1111/jebm.12319

100. Watson E, Fargali S, Okamoto H, Sadahiro M, Gordon RE, Chakraborty T, Sleeman MW, Salton SR. Analysis of knockout mice suggests a role for VGF in the control of fat storage and energy expenditure. *BMC Physiol*. 2009;9(1). doi:10.1186/1472-6793-9-19

101. Cersosimo E, Garlick P, Ferretti J. Renal glucose production during insulin-induced hypoglycemia in humans. *Diabetes*. 1999;48(2):261-266. doi:10.2337/diabetes.48.2.261

102. Kaneko K, Soty M, Zitoun C, Duchampt A, Silva M, Philippe E, Gautier-Stein A, Rajas F, Mithieux G. The role of kidney in the inter-organ coordination of endogenous glucose production during fasting. *Mol Metab*. 2018;16:203-212. doi:10.1016/j.molmet.2018.06.010

103. Stumvoll M, Chintalapudi U, Perriello G, Welle S, Gutierrez O, Gerich J. Uptake and release of glucose by the human kidney: Postabsorptive rates and responses to epinephrine. *J Clin Invest*. 1995;96(5):2528-2533. doi:10.1172/JCI118314

104. Puigserver P, Rhee J, Donovan J, Walkey CJ, Yoon JC, Oriente F, Kitamura Y, Altomonte J, Dong H, Accili D, Spiegelman BM. Insulin-regulated hepatic gluconeogenesis through FOXO1–PGC-1α interaction. *Nature*. 2003;423(6939):550-555. doi:10.1038/nature01667

105. Oh K-J, Han H-S, Kim M-J, Koo S-H. CREB and FoxO1: two transcription factors for the regulation of hepatic gluconeogenesis. *BMB Rep*. 2013;46(12):567. doi:10.5483/BMBREP.2013.46.12.248

106. Yang D, Brunengraber H. Glutamate, a Window on Liver Intermediary Metabolism. *J Nutr*. 2000;130(4):991S-994S. doi:10.1093/jn/130.4.991s

107. Iacobazzi V, Infantino V. Citrate – new functions for an old metabolite. *Biol Chem*. 2014;395(4):387-399. doi:10.1515/hsz-2013-0271

108. Sunny NE, Parks EJ, Browning JD, Burgess SC. Excessive hepatic mitochondrial TCA cycle and gluconeogenesis in humans with nonalcoholic fatty liver disease. *Cell Metab*. 2011;14(6):804-810. doi:10.1016/j.cmet.2011.11.004

109. Weisend CM, Kundert JA, Suvorova ES, Prigge JR, Schmidt EE. Cre activity in fetal albCre mouse hepatocytes: Utility for developmental studies. *Genesis*. 2009;47(12):789-792. doi:10.1002/dvg.20568

110. Parola M, Novo E. Nrf1 gene expression in the liver: A single gene linking oxidative stress to NAFLD, NASH and hepatic tumours. *J Hepatol*. 2005;43(6):1096-1097. doi:10.1016/j.jhep.2005.09.008

111. Xu Z, Chen L, Leung L, Yen TSB, Lee C, Chan JY. Liver-specific inactivation of the Nrf1 gene in adult mouse leads to nonalcoholic steatohepatitis and hepatic neoplasia. *Proc Natl Acad Sci*. 2005;102(11):4120-4125. doi:10.1073/pnas.0500660102

112. Pereira RM, Rodrigues KC da C, Anaruma CP, Sant'Ana MR, de Campos TDP, Gaspar RS, Canciglieri R dos S, de Melo DG, Mekary RA, da Silva ASR, Cintra DE, Ropelle ER, Pauli JR, de Moura LP. Short-term strength training reduces gluconeogenesis and NAFLD in obese mice. *J Endocrinol*. 2019;241(1):59-70. doi:10.1530/JOE-18-0567

113. Frier BC, Jacobs RL, Wright DC. Interactions between the consumption of a high-fat diet and fasting in the regulation of fatty acid oxidation enzyme gene expression: an evaluation of potential mechanisms. *Am J Physiol Integr Comp Physiol*. 2011;300(2):R212-R221. doi:10.1152/ajpregu.00367.2010

114. Kitada M, Ogura Y, Monno I, Koya D. Sirtuins and Type 2 Diabetes: Role in Inflammation, Oxidative Stress, and Mitochondrial Function. *Front Endocrinol (Lausanne)*. 2019;10:187. doi:10.3389/fendo.2019.00187

115. Wagner GR, Hirschey MD. Nonenzymatic Protein Acylation as a Carbon Stress Regulated by Sirtuin Deacylases. *Mol Cell*. 2014;54(1):5-16. doi:10.1016/j.molcel.2014.03.027

116. Amin-Wetzel N, Saunders RA, Kamphuis MJ, Rato C, Preissler S, Harding HP, Ron D. A J-Protein Co-chaperone Recruits BiP to Monomerize IRE1 and Repress the Unfolded Protein Response. *Cell*. 2017;171(7):1625-1637.e13. doi:10.1016/j.cell.2017.10.040

117. Lee HJ, Kim JM, Kim KH, Heo JI, Kwak SJ, Han JA. Genotoxic stress/p53-induced DNAJB9 inhibits the pro-apoptotic function of p53. *Cell Death Differ*. 2015;22(1):86-95. doi:10.1038/cdd.2014.116

118. Yang J, Wu X, Wu X, Zhou D, Lin T, Ding S, Zhang Y, Xue J, Zhuge Q. The Multiple Roles of XBP1 in Regulation of Glucose and Lipid Metabolism. *Curr Protein Pept Sci*. 2017;18(6):630-635. doi:10.2174/1389203717666160627085011

119. Cho YM, Kim DH, Lee KH, Jeong S-W, Kwon O-J. The IRE1α-XBP1s pathway promotes insulin-stimulated glucose uptake in adipocytes by increasing PPARγ activity. *Exp Mol Med*. 2018;50(8):102. doi:10.1038/s12276-018-0131-0

120. Wu R, Zhang Q-H, Lu Y-J, Ren K, Yi G-H. Involvement of the IRE1α-XBP1 Pathway and XBP1s-Dependent Transcriptional Reprogramming in Metabolic Diseases. *DNA Cell Biol*. 2015;34(1):6. doi:10.1089/DNA.2014.2552

121. Postic C, Magnuson MA. DNA excision in liver by an albumin-Cre transgene occurs progressively with age. *genesis*. 2000;26(2):149-150. doi:10.1002/(SICI)1526-968X(200002)26:2<149::AID-GENE16>3.0.CO;2-V

122. Daude N, Wohlgemuth S, Brown R, Pitstick R, Gapeshina H, Yang J, Carlson GA, Westaway D. Knockout of the prion protein (PrP)-like Sprn gene does not produce embryonic lethality in combination with PrP C-deficiency. *PNAS*. 2012;109(23):9035-9040. doi:10.1073/pnas.1202130109

123. De Souza AT, Dai X, Spencer AG, Reppen T, Menzie A, Roesch PL, He Y, Caguyong MJ, Bloomer S, Herweijer H, Wolff JA, Hagstrom JE, Lewis DL, Linsley PS, Ulrich RG. Transcriptional and phenotypic comparisons of Ppara knockout and siRNA knockdown mice. *Nucleic Acids Res*. 2006;34(16):4486-4494. doi:10.1093/nar/gkl609

124. Young R, Passet B, Vilotte M, Cribiu EP, Béringue V, Le Provost F, Laude H, Vilotte J-L. The prion or the related Shadoo protein is required for early mouse embryogenesis. *FEBS Lett*. 2009;583(19):3296-3300. doi:10.1016/j.febslet.2009.09.027

125. El-Brolosy MA, Stainier DYR. Genetic compensation: A phenomenon in search of mechanisms. Moens C, ed. *PLOS Genet*. 2017;13(7):e1006780. doi:10.1371/journal.pgen.1006780

126. Bhutia Y, Kopel J, Lawrence J, Neugebauer V, Ganapathy V, Bhutia YD, Kopel JJ, Lawrence JJ, Neugebauer V, Ganapathy V. Plasma Membrane Na+-Coupled Citrate Transporter (SLC13A5) and Neonatal Epileptic Encephalopathy. *Molecules*. 2017;22(3):378. doi:10.3390/molecules22030378

9. Statutory Declaration

“I, Martin Daniels, by personally signing this document in lieu of an oath, hereby affirm that I prepared the submitted dissertation on the topic *The mammalian citrate transporter mINDY (I’m not dead yet) and its protective role in hepatic metabolism / Protektive Rolle des Zitrattransporters mINDY (I’m not dead yet) im murinen Leberstoffwechsel*, independently and without the support of third parties, and that I used no other sources and aids than those stated.
All parts which are based on the publications or presentations of other authors, either in letter or in spirit, are specified as such in accordance with the citing guidelines. The sections on methodology (in particular regarding practical work, laboratory regulations, statistical processing) and results (in particular regarding figures, charts and tables) are exclusively my responsibility.

Furthermore, I declare that I have correctly marked all of the data, the analyses, and the conclusions generated from data obtained in collaboration with other persons, and that I have correctly marked my own contribution and the contributions of other persons (cf. declaration of contribution). I have correctly marked all texts or parts of texts that were generated in collaboration with other persons.

My contributions to any publications to this dissertation correspond to those stated in the below joint declaration made together with the supervisor. All publications created within the scope of the dissertation comply with the guidelines of the ICMJE (International Committee of Medical Journal Editors; www.icmje.org) on authorship. In addition, I declare that I shall comply with the regulations of Charité – Universitätsmedizin Berlin on ensuring good scientific practice.

I declare that I have not yet submitted this dissertation in identical or similar form to another Faculty.

The significance of this statutory declaration and the consequences of a false statutory declaration under criminal law (Sections 156, 161 of the German Criminal Code) are known to me.”

Date Signature

10. Curriculum vitae

Mein Lebenslauf wird aus datenschutzrechtlichen Gründen in der elektronischen Version meiner Arbeit nicht veröffentlicht.

11. Publications

- Willmes DM, Daniels MA, Lieske S, et al. The longevity gene mINDY (I'm not dead yet) affects blood pressure through sympathoadrenal mechanisms. JCI Insight 2020, accepted for publication.
- Tabansky I, Liang Y, Frankfurt M, et al. Molecular profiling of reticular gigantocellularis neurons indicates that eNOS modulates environmentally-dependent levels of arousal. PNAS Jul 2018, 115 (29) E6900-E6909.
- Willmes DM, Schumann T, Henke C, et al. The longevity gene mINDY (I'm not dead, yet) affects blood pressure through sympathoadrenal mechanisms (Poster). J. Am. Coll. Cardiol. 2018 Mar, 71 (11 Supplement) A1813.
- Daniels MA, Kan C, Willmes DM, et al. Pharmacogenomics in type 2 diabetes: oral antidiabetic drugs. Pharmacogenomics J. 2016 Jul 19. doi: 10.1038/tpj.2016.54.
- Jordan J, Fischer-Posovszky P, Reinke J, et al. A novel heart-adipose tissue axis: Atrial natriuretic peptide and leptin interactions in man. Diabetologie und Stoffwechsel 2016; 11 - LB8.
- Pesta DH, Perry RJ, Guebre-Egziabher F, et al. Prevention of diet-induced hepatic steatosis and hepatic insulin resistance by second generation antisense oligonucleotides targeted to the longevity gene mIndy (Slc13a5). Aging (Albany NY). 2015 Dec;7(12):1086-93 .
- Haufe S, Kaminski J, Utz W, et al. Differential response of the natriuretic peptide system to weight loss and exercise in overweight or obese patients. J Hypertens. 2015 Jul;33(7):1458-64.

12. Acknowledgements

I would like to extend my heartfelt gratitude to all who contributed to this work's completion. Especially:

Prof. Dr. Andreas Birkenfeld, for kindly and cooperatively accepting me into his research group and allowing me to work on this fascinating project, as much as for his continuous support of my first steps in Science and Medicine.

Prof. Dr. Joachim Spranger, for his support of this doctorate as second adviser and for granting me the possibility to carry out my research at his institute.

Dr. Diana Willmes, for guiding me through this doctorate and for many shared hours at the laboratory.

Prof. Donald Pfaff, for accepting me into his laboratory and granting me the possibility to extend my scientific horizon. Dr. Inna Tabansky, Dr. Lee Ming Kow, Dr. Sebastian Brachs, Dr. Anica Kurzbach, Diana Woellner, and Heide Lück, for scientific insight, genial collaboration, and invaluable support.

Paula-Carlotta Johannsen, Merle Müller-Knapp, Annika Wolfsberger, Philip Bischoff, Jan-Frederik Fischer, Jonas Fritzsching, Stephen Karam, Dominik Soll, and Mathias Yuan, for countless and invaluable exchanges without which this project would not have seen its completion.

The German Academic Scholarship Foundation (Studienstiftung des deutschen Volkes), the German Research Foundation (DFG), as well as the Boehringer Ingelheim-Fonds for the financial and ideational support that enabled me to carry out this research.

My parents Miriam und Rikus, my siblings Milena, Manuel and Nicolai, as much as my grandmothers Christine and Eleonore, for their unconditional support. In deep gratefulness, I dedicate this work to my family.